



UNIVERSITÀ DEGLI STUDI
DI GENOVA



Università degli Studi di Genova – Fondazione Istituto Italiano di Tecnologia

PhD Course in "Neurosciences" XXXII Cycle

Curriculum "Neurosciences and Neurotechnologies" (CODE-6198)

Academic Years 2016-2019

**Prader Willi locus Snord116 RNA regulates hypothalamic
functions: sleep and temperature**

Supervisor:

Valter Tucci

Ph.D Candidate:

Matteo Falappa

Contents

Abstract	1
Chapter 1 – Introduction	3
1.1 Sleep.....	4
1.1.1 Sleep characterization and sub-stages	4
1.1.2 Sleep functions	6
1.1.3 Hierarchical sleep regulation	8
1.1.4 Genetic control of sleep.....	15
1.2 Epigenetics	16
1.2.1 Genomic imprinting	18
1.2.2 Genomic imprinting defects	18
1.3 Prader-Willi syndrome	19
1.3.1 Genetic background.....	19
1.3.2 Clinical features	21
1.3.3 Sleep alterations and PWS.....	21
1.3.4 Hypothalamus and PWS.....	22
1.3.5 Current treatment	23
Chapter 2 – Aims of the studies	25
2.1 Study I - <i>Snord116</i> may play a role in the hypothalamic formation	26
2.2 Study II - <i>Snord116</i> in the regulation of the macrostructural sleep aspects and in the brain-circuits ...	26
2.3 Study III - New alternative pharmacological approach for PWS	27
Chapter 3 – Materials and methods	28
3.1 Study I	28
3.2 Study II	39
3.3 Study III	43
Chapter 4 – Results	46
4.1 Study I	46
4.1.1 Loss of paternal <i>Snord116</i> alters neuronal dynamics in the LH associated with sleep homeostasis	46
4.1.2 OX putative neurons are reduced in PWS ^{Cr^{m+}/p⁻} mutants compared with controls	47
4.1.3 A high proportion of neurons in the LH do not respond to food intake in PWS ^{Cr^{m+}/p⁻} mutant mice	48
4.1.4 Sleep homeostasis is disrupted in PWS mutant mice	50
4.1.5 Thermoneutrality does not increase REM sleep in mutants	50
4.1.6 Peripheral thermoregulatory responses are absent in PWS mutants	51
4.1.7 Lack of <i>Snord116</i> impairs the OX system in the LH.....	54
4.1.8 Loss of <i>Snord116</i> leads to transcriptional reprogramming in the hypothalamus	55
4.1.9 OX regulation in the hypothalamus depends on two paternally expressed genes, <i>Snord116</i> and <i>Peg3</i>	57
4.2 Study II	60
4.2.1 Paternal <i>Snord116</i> deletion impacts macrostructural sleep aspects in mice	60
4.2.2 Paternal deletion of <i>Snord116</i> alters sleep spindles in PWS mice	61
4.2.3 PWS mutants show increased spontaneous physical activity over the circadian cycle	62
4.2.4 Paternal <i>Snord116</i> deletion leads to dysregulation of norepinephrine	63
4.3 Study III	64
4.3.1 Effect of Pitolisant on the Sleep-wake cycle	64
4.3.2 Effect of Pitolisant on physical activity	69
Chapter 5 – Discussion	70
5.1 The paternally imprinted gene <i>Snord116</i> gene regulate hypothalamic orexin neurons, Study I	71

5.2 The paternally imprinted gene <i>Snord116</i> regulates the macrostructural sleep aspects and cortical neuronal activity, Study II	74
5.3 Effect of Pitolisant on REM sleep alteration in the <i>Snord116</i> mice as model of Prader Willi Syndrome, Study III	78
5.4 Limitations of the thesis and suggestions for future experiment	79
Chapter 6 – Conclusions	80
Appendix A	81
Appendix B	82
Bibliography	83
Supplementary materials	97
Figures	97
Tables.....	105

Abstract

Sleep is a complex behavior and it is hierarchically regulated involving several brain regions, neurotransmitters, and genes that co-operate in building modulatory mechanisms aimed at controlling and maintaining sleep. Specifically, this thesis attempts to address/understand how genomic imprinting, which affect a subset of genes in mammals resulting in a monoallelic expression, may regulate sleep.

One of the main brain regions involved in sleep regulation is the hypothalamus. Within the hypothalamic region imprinted genes are highly expressed. Interestingly, it has been described that hypothalamic insufficiency (notably, the word “insufficiency” referred to the hypothalamus in this thesis always introduces the hypothalamic issues of the PWS) caused by lack of paternal expression of chromosome 15q11-q13, leads to Prader-Willi syndrome (PWS). Specifically, the microdeletion of the small nuclear ribonucleic acid (RNA)-116 (*SNORD116*) cluster within the PWS locus plays a major role in developing the main endophenotypes that characterize this syndrome (i.e. REM sleep dysfunction, hyperphagia and temperature instability). However, what could be the role of the paternally imprinted gene *Snord116* in the hypothalamic function is unknown. Additionally, is still unclear the specific contribution of the *Snord116* gene in developing the PWS symptoms. Since these unresolved points my research has been split into three parts:

In the first part of this research, it has been shown that the paternally imprinted gene *Snord116* plays a crucial role in the formation and organization of the orexin (OX) and melanin concentrating hormone (MCH) systems, the two main neuro-modulatory systems within the lateral hypothalamus (LH). Moreover, a compromised neuronal dynamic in the LH and a sleep-wake regulation of mice with paternal deletion of *Snord116* (*PWScr^{m+/p-}*) is observed. This abnormal neuronal dynamic is accompanied by a significant reduction in OX neurons in the LH of mutant mice. For this reason, it is proposed that the dysregulation of rapid eye movement (REM) sleep, food intake and temperature control observed in PWS mice are potentially due to this imbalance between OX- and MCH-expressing neurons in the LH as observed in mutant mice.

In the second part of this research, it has been investigated the microstructural

electrophysiological components of sleep, such as REM sleep features and sleep spindles during non-REM sleep. Indeed, REM sleep is thought to contribute to neuronal network formation early in brain development, while spindles are markers of thalamocortical processes. In neurodevelopmental disorders both sleep structures (REM and sleep spindles) are often compromised and this influence functional properties of cortical neurons. These results indicate that REM sleep properties and its occurrence (REM sleep episodes classified as short-and long REM sleep episode) throughout the sleep-wake cycles are selectively influenced by the *Snord116* gene in mice. Moreover, the specific abnormalities in sleep spindles in PWS model systems, indicate that these sleep features may be translated as potential biomarkers in human PWS sufferers.

In the third part of this research, it has been proposed a new therapeutic approach for PWS patients aiming to ameliorate the sleep phenotypes that significantly compromise the quality of life of these patients. Pitolisant (a wake-promoting drug) was orally administrated in mice carrying the paternal deletion of the *Snord116* gene that are affected by REM sleep alteration coupled with a reduction of the OX neurons.

Overall the results of this research show that Pitolisant ameliorates the REM sleep alteration in these mice, although other studies are needed to clarify whether this drug may be easily translated/used in clinics.

In conclusion, this thesis provides support for the important role of *Snord116* in the regulation of REM sleep and its propensity and its regulatory mechanisms in the hypothalamus. Finally, a new pharmacological approach for PWS by using Pitolisant has been proposed to ameliorate the sleep alteration that significantly affects the PWS patients.

Chapter 1

Introduction

Sleep is a universal and physiological phenomenon which is extremely important to keep our brain and body healthy. Indeed, sleep alterations are implicated in several human diseases, however, how sleep is regulated is not completely understood.

The recognition of sleep behavior across multiple lines of the animal kingdom strongly suggests the presence of a shared or universal function. Sleep is also characterized by a homeostatic regulatory capacity that includes compensation with increased sleep intensity or duration after loss [1], in all species that have been systematically examined so far [2]–[5]. Sleep is usually defined in most animal species by behavioral criteria [6]. These criteria include species-specific posture, behavioral quiescence and elevated arousal threshold. Sleep can also be defined as reduced responsiveness to external stimuli and relative inactivity with loss of consciousness [7]. Since sleep is a complex behavior it is regulated in a hierarchical way, that goes from a more general (biological and homeostatic) to a more complex and specific organization represented by genetic and epigenetic regulations of sleep. Specifically, in this thesis we investigated how an epigenetic phenomenon, namely genomic imprinting, may regulate sleep.

Since one of the most important epigenetic dysfunctions in humans is represented by Prader Willi Syndrome (PWS), where approximately 76% of PWS patients exhibit abnormal sleep [8], we used this model to understand the role of the imprinted genes in the regulation of sleep.

Overall, I believe that the results of this thesis may bring a new understanding of how genomic imprinting may play a crucial role in the regulation of sleep, therefore opening the way for new interventional approaches for sleep disorders.

1.1 Sleep

1.1.1 Sleep characterization and sub-stages

Sleep is characterized by precise physiological and behavioral features; indeed, using electroencephalography (EEG) combined with electromyography (EMG) and electrooculogram (EOG) It is possible to identify different sleep states. The vast majority of endothermic (warm-blooded) birds and mammals exhibit three distinct type of sleep states: non-rapid eye movement sleep (non-REM) and rapid eye movement sleep (REM) and wakefulness that alternate cyclically over the 24-hour. These three sleep-wake states have specific characteristics; including variation in brain waveforms, eye movements and muscle tone. These three stages are very similar between humans and rodents although some differences have been described. See Box 1 for more details between humans and rodent sleep. Notably, in this thesis all experiments were performed on mice.

The three main sleep stages and how they are defined are detailed below.

Non-REM state

Both in humans and rodents the non-REM state is characterized by generalized immobility, a reduced muscle activity, regular respiration and heart rate, and typically by a decrease of faster components of EEG, a state of cortical EEG slowing, often with high amplitude EEG slow waves [9], [10]. The EEG shows predominantly frequency of 4 to 7 Hz activity and irregularly spaced bursts of slow waves [11]. These regular occurrences of local and global slow cortical oscillations include bursts of oscillatory brain activity in the sigma frequency (12 – 15 Hz) named sleep spindles. Usually these events are isolated and appear both spontaneously as well as on the application of alerting stimuli at irregular intervals. Sleep spindles are bursts of activity usually last from 0.5 and 2 seconds. They are characteristic transient features of the EEG sleep (spindles represent an EEG graphoelement typical of sleep) [12]. Dysregulation of spindle properties is a sensitive indicator of thalamocortical and neuromodulator dysfunction in many diseases, including neurodevelopmental disorders [13]. Non-REM sleep also includes K-complex waveforms (frequency between 0.1 and 1 Hz) and high – amplitude slow-wave activity (SWA at around 0.5 – 4.5 Hz) [14]. Non-REM sleep in humans, accounting for about 80% of sleep time, and it has a greater depth during the early stage of sleep and then decreases in

intensity and duration across time [7].

Non-REM sleep is usually divided into three stages [7] in humans, while this classification in rodents is difficult to see. However, for differences in the sleep architecture between humans and rodents see Box 1. The three stages of non-REM sleep in humans represent the following characteristics: Stage I represents a transition from wakefulness and it occupies 5 to 10% of normal sleep. Stage II is characterized by the repetitive presence of distinctive sleep spindles and K-complex waveforms [7]. Stage III is the deepest state of non-REM sleep and it is characterized by SWA. In this stage it is most difficult to awaken people. Interestingly, SWA is considered as a marker for sleep intensity and pressure [10], [15]. Indeed, the longer a subject has been awake the higher the spectral power in the slow wave range of the EEG in subsequent sleep, which declines during the course of sleep [16]. This increase of SWA is accompanied by a decrease in regional cerebral blood flow and heart rate and a reduction in cerebral glucose utilization, indicating a lower metabolic demand [17]. For this reason it has been suggested that SWA plays a role in the restorative process of sleep [10], [15], [18].

REM state

REM sleep is also known as paradoxical sleep, it qualifies as a sleep stage (as well as a behavioral state) and occurs for about 20% of total sleep time. It only occurs after period of non-REM sleep and in humans it becomes more intensive and extensive towards the end of the sleep period [7]. Even though the REM state is characterized by desynchronized brain waves (low-voltage, high-frequency) and cortical EEG activation resembling wakefulness, it differs from the wake state by the presence of a generalized skeletal muscle atonia with intermittent muscle twitches of the distal extremities, penile or clitoral erections and increased respiratory and heart rate variability [19]. During REM sleep, there is also the presence of vivid dreams in humans [20], [21], loss of thermoregulatory defense and the appearance of rapid eye movements [22]. For this reason, REM sleep is concisely defined as a highly activated brain in a paralyzed body [23]. The electrophysiological features of the REM state show oscillation in the range of theta frequencies (5 – 8 Hz) and slow alpha activity that arises mostly from the hippocampus. However, these theta oscillations have been found in cortical structures too, but none of these have been able to generate a generalized theta activity [24]. The role of the REM

state is still not clear, but many studies conducted to date indicate that it has a possible role in memory consolidation [25]–[27].

Wake state

The wake state is characterized by consciousness with consequent activation of muscle tone [28]. This is a behavioral active phase with interaction with the external environment. From an electrophysiological point of view, during the wake state neurons in the cerebral cortex fire irregularly and EEG recordings display low-amplitude, high-frequency fluctuations.

1.1.2 Sleep functions

Sleep is a complex and highly regulated behavior that occurs in all the animal species that have been studied so far. This suggests that sleep has one or more fundamental functions, such as energy conservation [29], body or brain restoration [30], [31], maintaining neuronal plasticity [15], [32] and memory consolidation [33]. All these categories imply that sleep has a critical role in promoting and maintaining health. Indeed, totally sleep-deprived rats were dead or sacrificed when death appears imminent within 11-32 days as shown by Rechtschaffen [34] meaning a crucial role of sleep in maintain health.

Energy conservation and body restoration

Since wakefulness accounts for the metabolic active period in the brain, as glycogen decreases over the period of wakefulness, the consequent increase of extracellular adenosine leads to energy reduction. Thus, it has been suggested that sleep is necessary to replenish energy stores in the brain [35] ; sleep may accounts for recovery of energy stores and thus restoration of energy balance. Moreover, according to Borbely and Achermann [36] delta power during sleep is influenced by this metabolic change. In particular, NREM sleep is associated with significant reductions in blood flow and metabolism, while total blood flow and metabolism in REM sleep is comparable to wakefulness[37]. However, metabolism and blood flow increase in certain brain regions during REM sleep, compared to wakefulness, such as the limbic system (which is involved with emotions), and visual association areas [38]. Additionally REM sleep requires more energy form the other sleep stages because during this stage rapid eye movement, muscle

twitches and penile or clitoral erections [39] are usually observed. Since REM sleep requires a metabolic increase, it is expected that other systems will be diminished or inhibited to allow the redistribution of energy [22]. For this reason, as described above, the REM state is characterized by muscle atonia and loss of thermoregulatory defense [40] increasing sensitivity to ambient temperature [41]. All these findings indicate that the deterioration of tissue integrity associated with wakefulness is restored during sleep.

Neuronal plasticity

As the brain is able to change and reorganize its neuronal network it is thought that sleep can play a role in neuronal plasticity [42]. Indeed, neuronal plasticity continues throughout life even if the nervous system is most plastic in early ontogenetic development [43]. The idea that sleep may in some way facilitate synaptic plasticity has long been supported by a predominant occurrence of sleep in the human new-born occupying two-thirds of the time, with REM sleep occupying half of the total sleep time of entire 24-hour period [42]. The percentage of total sleep as well as REM sleep, declines rapidly in the early childhood so that by approximately age 10 the adult percentage of REM sleep is reached, which is 20% of the total sleep. This evidence clearly indicates that sleep and particularly REM sleep in the early stage of life plays an important function in promoting nervous system growth and development [42], [44]. Moreover the importance of sleep in facilitating neuronal plasticity has been theorized by the following “homeostatic synaptic plasticity” hypothesis [15], [45]–[47]. This hypothesis claims that during wakefulness the brain is able to acquire new information, and then tends to be saturated at the end of waking time where the synaptic strength is high. Consequently, during the sleep period, the acquired information (accounting for synaptic strength) is processed and the strength of each synapse decreases until reaching the baseline level. The downscaling of the synaptic strength is driven by SWA, which reinforces connections between strongly correlated neurons, while others may be eliminated in order to allow the organism to learn afresh the next day.

Taken together, these findings suggest that sleep may facilitate or even is involved in synaptic plasticity. Recent studies have provided evidence showing impaired consolidation of learned responses following sleep deprivation [48]. Other studies nicely described how local SWA that local SWA induction is triggered by learning tasks suggesting

that local plastic changes occur following learning and may be driven by SWA. Indeed, they indicate that local SWA homeostasis is strongly correlated with improved performance in the task after sleep [3].

Memory consolidation

McGaugh defined “memory consolidation” as the time dependent process which converts labile memory into a more permanent form [33]. In particular this process allows the strengthening and consolidation of the information acquired during wakefulness. Both sleep stages, non-REM and REM, are involved in memory-related functions, although they act on different types of memory. Indeed, non-REM seems to be involved in declarative memory (i.e. explicit memory, event explicitly stored and consciously recalled or "declared.") [49], [50], while REM sleep is involved in non-declarative memory (i.e. memory learned without awareness) [50]. Interestingly, according to the sequential hypothesis non-REM operates the first step of the memory process consisting of the weakening of non-adaptive memory traces, then the remaining memory traces are stored again in a better configuration during the REM [51].

Moreover, it has been shown that the duration of REM sleep increases after learning [25] and memory formation can be impaired after REM state deprivation [52].

1.1.3 Hierarchical sleep regulation

Sleep is a complex behavior that has a hierarchical regulation (see Figure 1). At the basis of this regulation, there are the biological and homeostatic control of sleep that cooperates with each-other to maintain the sleep-wake cycle. These two processes are also regulated by genetic and epigenetic factors. Here are the three classifications of the main hierarchical processes of sleep. (see Figure 1):

- Biological and homeostatic control of sleep;
- Molecular control of sleep;
- Genetic and epigenetic control of sleep.

Specifically, in this thesis attention is focused on the epigenetic mechanisms of sleep, which is also the main focus of research of Dr. Tucci’s laboratory.

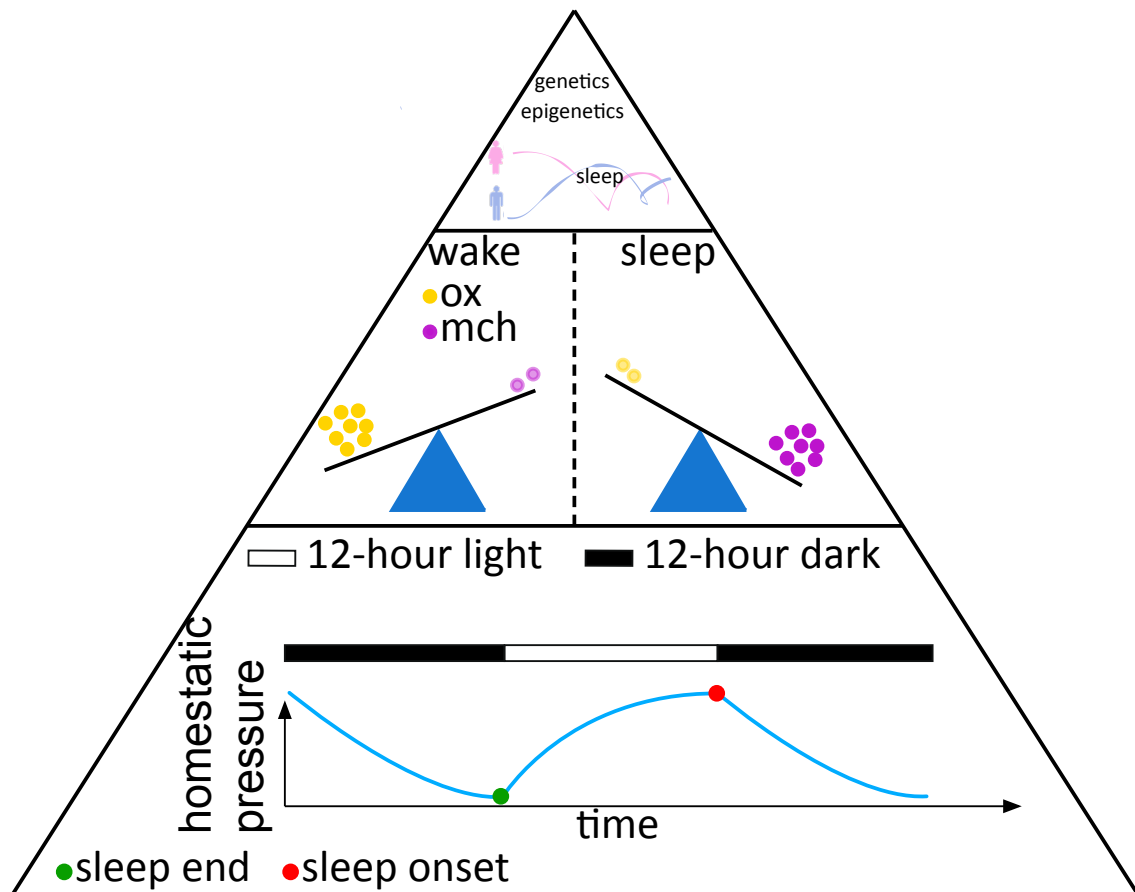


Figure 1 - Hierarchical sleep regulation.

At the lowest level there is the self-sustained homeostatic control of sleep; in the middle, acting on the homeostatic control of sleep, the molecular process (i.e. as the interplay between ox and mch). At the top level the genetic and epigenetic changes acting on sleep phenotype.

Biological and homeostatic control of sleep

Two separate but interacting biological mechanisms play a dominant role in sleep regulation: a sleep-dependent process (S Process) and a sleep-independent circadian process (C Process) [53].

The S process is a biochemical system that accumulates sleep-inducing substances in the brain. Indeed, after a prolonged period of wakefulness it generates the need to sleep, reminding the body to sleep. The *S process* is homeostatically regulated and depended by previous wake. This process peaks just before bedtime at night and dissipates throughout the night as the need for sleep. This means that a prolonged wakefulness results in more intense SWA, which is considered as marker is usually used as a marker of non-REM sleep

intensity and for sleep pressure [10], [15]. For instance, the longer a subject has been awake the higher the spectral power in the slow wave range of the EEG in subsequent sleep, which declines during the course of sleep [16]. To date a large body of evidence clearly describe that the Process S describes the process of synaptic homeostasis. Specifically, the hypothesis claims [15] that, under normal conditions, total synaptic strength increases during wakefulness and reaches a maximum just before going to sleep. Then, as soon as sleep ensues, total synaptic strength begins to decrease, and reaches a baseline level by the time sleep ends. The SWA play a crucial role in this process because they are not only considered as an epiphenomenon of the increased synaptic strength but have a role to play. The repeated sequences of depolarization—hyperpolarization cause the down- scaling of the synapses impinging on each neuron, which means that they all decrease in strength proportionally. This means during sleep the strength of each synapse would decrease by a proportional amount, until the total amount of synaptic weight impinging on each neuron returns to a baseline level.

Moreover, it has been proposed that SWA is mainly involved in the restorative processes of sleep [10], [15], [18]. Indeed, neuroimaging data shows a decrease in absolute levels of brain metabolism after sleep that is also consistent with the hypothesis that synaptic strength is downscaled during sleep [54].

The C process conversely reflects how sleep propensity changes over 24-hours, and its function is to restrict sleep to a time of day that is ecologically appropriate. Notably, the C process is independent of prior sleep-wake history. This process coordinates the light – dark cycle of day and night; which controls; sleep timing, feeding patterns, core body temperature, brain activity and hormone production over a 24-hour period. The oscillatory pattern of circadian activity has a period of approximately 24-hour. In mammals, the suprachiasmatic nucleus (SCN) of the hypothalamus is responsible for the circadian rhythm which is the main circadian pacemaker. These oscillations are driven by the SCN that also co- coordinates the activity of the peripheral clocks of other organs to control all biological rhythms within the body [55]. This circadian oscillation is generated by a network of clock genes, transcription factors able to regulate other gene expression [56]. The SCN is strongly influenced by light entering the eye [57] and, to a lesser extent,

by other time cues such as temperature. Temperature is one of the major signals achieving the coordination of all the clocks around the body. Indeed, temperature changes can be the results of the influence of the SCN over the sympathetic nervous system. However, there isn't a direct coordination of the peripheral clocks by the master clock. Moreover, after SCN lesions sleep is no longer consolidated in one major phase (i.e. in rodents during the day, flies and humans during the night), but occurs in short episodes throughout the 24-hour period [58]. See Box 1 for further differences between humans and rodent's circadian rhythm.

The sleep-wake cycle is balanced through these two processes. Indeed, experiments on human subjects scheduled for a 28-hour rest-activity cycle revealed the uncoupling of the sleep-wake cycle from circadian rhythms supporting the two-state model for sleep regulation [59].

During the sleep period the homeostatic need rapidly dissipates while circadian-regulated melatonin is produced. After a prolonged sleep period, usually in the morning, melatonin secretion stops, and the circadian alerting system begins. This triggers the body to wake up. The homeostatic regulation typically increases throughout the day even if is countered and moderated by the C process for arousal, at least until the night when the automatic circadian clock begins producing melatonin again and the need to sleep increases significantly.

BOX 1

There are some differences in the sleep architecture between humans and rodents. Specifically, the sleep-wake cycle is in the opposite phase in rodents compared to humans. Indeed, rodents are nocturnal animals, they are awake during the night while they sleep during the day. Moreover, human sleep is monophasic, meaning that sleep occurs only once during a 24-hour period (usually at night), while rodents' sleep is polyphasic and relatively fragmented [148], [221]. For instance, in humans the non-REM / REM cycle is repeated from 4 to 6 times per night; these sleep cycles have a fairly constant period, with a duration of around 90 minutes [222]. In rodents the non-REM / REM cycle is shorter lasting around 5 or 12 minutes in mice and rats respectively [44], [148].

Molecular control of sleep

Although sleep is regulated by two main processes, the C process and the S process, in these processes many neurotransmitters, molecular pathways and different brain structures are involved. Specifically, the hypothalamus and brain stem are the main brain regions playing a pivotal role in sleep regulation [60]. To date there are four models describing the major mechanisms that play a crucial role in the regulation of sleep and its transition into wakefulness (See Figure 2 for schematic representation of these models).

The Flip-Flop Model

The main neuropeptides playing a main role in the transitions between sleep and wakefulness are the melanin concentrating hormone (MCH) and orexin/hypocretin (OX) (see Box 2 for Physiological roles of Melanin-Concentrating Hormone and Orexin). MCH neurons also release Gamma-aminobutyrate (GABA: inhibitory neurotransmitter in the brain) and are more active during sleep, in particular during REM sleep [61]. Conversely, OX neurons are more active during wakefulness [62], [63]. These two neuropeptides are the main constituents of the “Flip-Flop Switch Model” [60] (Figure 2A). According to the flip-flop model the balance between the two neuropeptides the OX and MCH model enable the transition between sleep and wakefulness avoiding intermediate states. This model allows an organism to be clearly awake or asleep with only brief periods spent in transition between these states. Since the OX and MCH neuropeptides are located in the lateral hypothalamus (LH), it has been thought that the hypothalamus represents the regulatory center for the sleep switch. Specifically, the OX neurons are considered to be the wake promoters by reinforcing the monoaminergic tone that directly inhibits the ventrolateral preoptic nucleus (VLPO), as VLPO neurons do not have any OX receptors. Conversely MCH neurons and GABAergic nuclei in the VLPO are more active during sleep and inhibit the monoaminergic cell groups as well as OX neurons, further preventing monoaminergic activation that might interrupt sleep [60], [64]. Notably, among all models that are discussed in this section, we seeking to investigate the role of epigenetics in modeling/regulating the flip-flop model paying more attention to the MCH and OX systems.

Reciprocal Inhibition Model

In the brainstem the reciprocal monoaminergic–cholinergic interactions seem to control sleep states like non-REM to REM transitions [65]. In this model, named the “Reciprocal Inhibition Model”, the brainstem has a different response depending on the occurrence of the sleep or wake. This transition between the different sleep stages is given by the synchronization and desynchronization of thalamocortical circuits [65], [66]. In this model, during wakefulness the serotonergic (raphe nuclei, RN), adrenergic (locus coeruleus, LC) and histaminergic (tuberomammillary nucleus, TMN) neurons are activated, while are silenced during non-REM sleep [67] (Figure 2B). During the onset of REM sleep, the aminergic and cholinergic neurons are activated while other outputs are inhibited. However, cholinergic activity in the brainstem also fire during wakefulness [65].

Thalamo-cortical loop.

Thalamocortical processes are oscillatory activity between thalamus and cortical brain region. These oscillation act as between different cortical regions of the brain [68]. Normal oscillatory activities include slow and fast activities. The fast activities may be present in various states of vigilance and frequently coexist with slower rhythms [69]. There are two main classes of this oscillatory rhythms in the thalamocortical system: intrinsic, from a single neuron and extrinsic, from the interaction within a neuronal population (e.g. spindle oscillation) [70]. Extrinsic rhythms are typically observed during the early stages of sleep. In vivo and in vitro studies suggest that spindle oscillations can be generated by the thalamic reticular nucleus although cortical inputs may contribute by initiating or amplifying spindle oscillations [71], [72]. This suggests excitatory and inhibitory connections between cortical and thalamic reticular cells generating the cortical feedback loop. It is this thalamocortical cycle that generates the EEG features from deep sleep to high alert [73].

GABA-Glutamate control of sleep.

Neurons contain either gamma-amino-butyric acid (GABA) or glutamate are important populations of arousal-promoting system [74], [75].

GABAergic mechanisms in sleep regulation are important. However, due to the widespread nature of GABAergic transmission in the brain it is difficult to identify specific

sleep circuits. Indeed, inhibition by GABA both facilitates and inhibits REM sleep [65]. It has been shown that there is a GABA-mediated “switch” between wakefulness and REM in the nucleus pontis oralis [76] and there is a direct inhibition of the mesopontine cholinergic neurons from GABA in the period right before rapid REM sleep. Glutamate increases the activity in mesopontine and pontine reticular in correspondence with the onset of REM state [65] (Figure 2D). Moreover, glutamatergic cells of the pons excite glycinergic inhibit somatic motor neurons to produce REM sleep atonia [65].

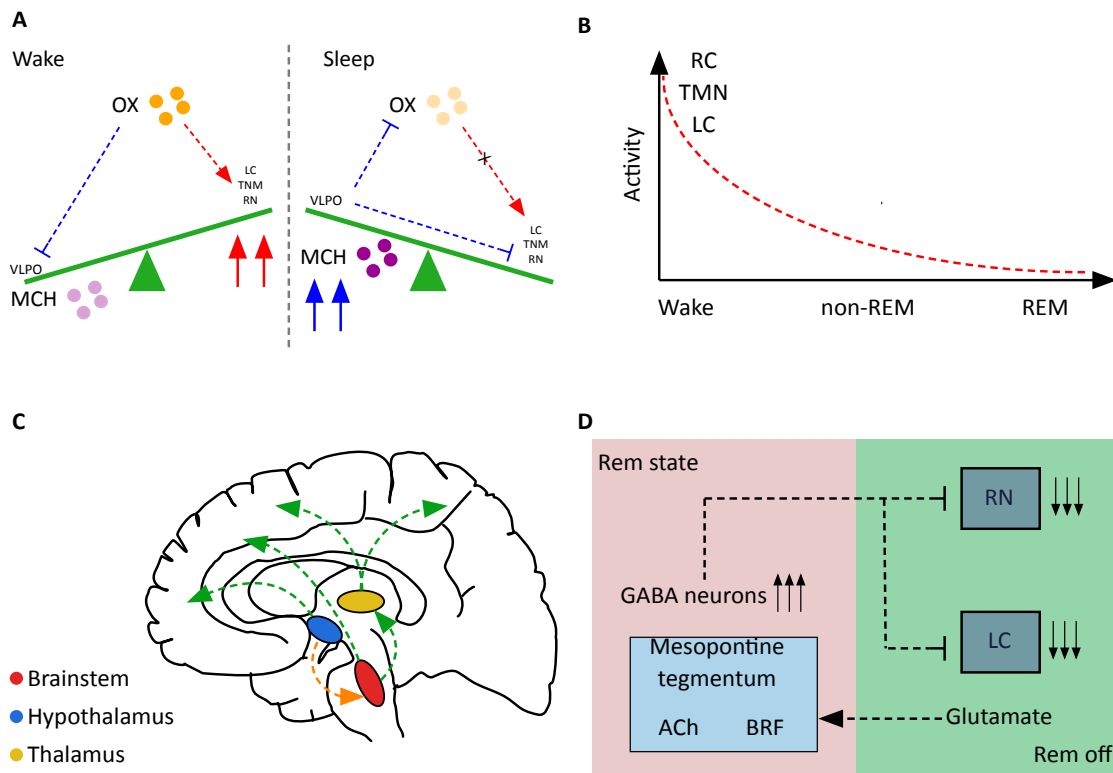


Figure 2, Sleep models

- A- The flip/flop switch model; OX inhibits VLPO and MCH activity decreases promoting wakefulness; During sleep state, VLPO inhibits the monoaminergic cell groups as well as OX while MCH activity increases.
- B- The monoaminergic cell groups decrease activity from wakefulness to non-REM state and it is almost silent during REM.
- C- The brainstem ascending cortical activation and REM / non-REM transitions. This activity is highly correlated with the thalamus activity controlling cortical activation, sleep spindle and EEG synchronizations. Hypothalamus is the regulatory center.
- D- GABA-Glutamate control of sleep; inhibition by GABA both facilitates and inhibits REM sleep while Glutamatergic cells excite GABA-containing neurons inhibiting somatic motor neurons to produce

BOX 2

Neurons containing OX or MCH are the main neural population in the lateral hypothalamus. These two separate and distinct neuronal population projects to similar brain regions.

Two different neuropeptides are synthesized from OX neurons: orexin A (OXA) and orexin B (OXB), which binds two different orexin receptors, the orexin Receptor-1 (OX1R) and orexin Receptor-2 (OX2R). OXA binds both OX1R and OX2R, while OXB signals mainly act through OX2R.

The OX physiological functions are expressed in wakefulness stabilization, energy expenditure, food reward and addiction behavior and increased food intake. Moreover, it has been observed that low glucose levels stimulate OXA release; while high glucose levels inhibit OXA release. Furthermore, it has been shown that cardiovascular and thermoregulatory regulation are also mediated through OXA, as well as it is acting on inflammation, suggesting an anti-inflammatory function in neuro-inflammation diseases and it also inhibits apoptosis.

MCH exerts its action through the MCH1 receptor (Mchr1) and MCH2 receptor (Mchr2), although the latter is not functional in rodents. MCH neurons play opposite roles in respect of OX in sleep-wake regulation. Indeed, MCH particularly fires during REM; MCH activation is regulated by high glucose levels.

Finally, MCH, as well as OX, are orexigenic peptides, meaning that both are involved in food intake stimulation and promotion of palatable or calorific food consumption.

1.1.4 Genetic control of sleep

A bidirectional relationship between sleep and genetic factors has been described, while it has been shown that several mutations affect sleep, it has also been recognized that sleep affects the expression of genes.

The first observation of sleep under genetic control was first described in a study with twins in the 1930's [77]. This data has also been confirmed by animal studies showing that sleep quality and quantity are influenced by genes, observed in more than 70 mutant mice lines [78], [79]. Additionally, several human sleep disorders have been identified as having a genetic basis. An example of a human disease that has been linked to a genetic alteration of the hypocretin/orexin system is narcolepsy, investigated by performing genetic studies in dogs and mice [80]. As given above sleep also influences the expression of certain gene. Indeed, whole-genome transcriptomic studies have revealed that the brains of sleeping and awake animals also differ at the molecular level. In rats, mice, hundreds of brain transcripts change their level of expression between sleep and wakefulness [81]. In rats and mice, these changes occur mainly in the cerebral cortex, cerebellum and hypothalamus, but can also occur in other areas of the brain. It has been observed that sleep-and wakefulness-related transcripts belong to different functional

categories, suggesting that the two behavioral states may favor different cellular processes. Overall, it has been observed that neurons are more hyperpolarized during sleep than during wakefulness, and mutations/gene alterations can significantly change the resting membrane potential, the balance between inhibitory and excitatory neurotransmission, and/or the overall neuronal excitability of large sets of neurons which are likely to affect the quantity and quality of sleep.

Additionally, a growing corpus of data indicates that epigenetic mechanisms regulate sleep. In particular the role of genomic imprinting, an epigenetic mechanism that regulates parent-of-origin effects in mammals and which is involved in the control of sleep and in particular of REM sleep is discussed and investigated.

1.2 Epigenetics

... *“the branch of biology which studies the causal interactions between genes and their products, which bring the phenotype into being”* ... (Conrad Waddington, 1905-1975)

The term epigenetic means what is beside genetics and is defined as the study of heritable changes in gene expression without a change in DNA sequence i.e. changing the phenotype without changing the genotype. Epigenetic mechanisms can influence the gene expression by switching genes on “active gene” or off “inactive gene” but also influence gene activity at the transcriptional and post-transcriptional levels. These modifications do not change the DNA sequence but instead they affect how cells “read” genes. The main epigenetic mechanisms through which tissue-specific gene-expression patterns and global gene silencing are established and maintained are the DNA methylation and the histone modifications.

DNA methylation

DNA methylation is the most frequent modification in eukaryotic cells and it is known as a silencing epigenetic mechanism [82], [83]. DNA methylation consists of a chemical process of adding a methyl group to the carbon at position 5 of the cytosine ring. Since DNA methylation is involved in many important biological processes such as X chromosome inactivation, genomic imprinting, and defense against exogenous parasitic

DNAs, these patterns must be properly established and maintained. Two components regulate the mammalian DNA methylation system:

- the DNA methyltransferases (DNMTs), with the function of establishing and maintain DNA methylation patterns;
- the methyl-CpG binding proteins (MBDs), involved in “reading” methylation marks.

These DNMTs are essential for embryonic development as demonstrated by Li and Okano [84], [85]. The DNMTs can be involved in the recognition of DNA damage, DNA recombination and mutation repair [86]. MBDs have a role in the interpretation of the methylation signal, through the recruitment of chromatin remodeling protein complexes involving histone deacetylases (HDACs), histone methyltransferases (HMTs) and chromatin-modifying proteins [87].

Histone modifications

Histone modification is a covalent post-translational modification of histone proteins. Histone modifications occur mostly in the histone amino-terminal tails jutting from the nucleosome surface as well as in the globular core region [88]. It has been suggested that histone modifications could affect chromosome function through at least two distinct mechanisms that have led to the “histone code” hypothesis [89]:

- the electrostatic charge of the histone may be altered leading to structural change in histones or DNA binding;
- the binding sites for protein recognition modules.

The acetylation of histones usually marks active, transcriptionally competent regions, while hypoacetylated histones are found in transcriptionally inactive euchromatic or heterochromatic regions. Modifications such as acetylation and phosphorylation, are reversible and dynamic, while modifications such as methylation are more stable and are involved in the long-term maintenance of region-status expression of the genome.

1.2.1 Genomic imprinting

Genomic imprinting is an epigenetic phenomenon that causes genes to be expressed in a parent-of-origin-specific manner and as a fundamental concept of genomic imprinting it is the core of this thesis. People inherit two copies of their genes one from the mother and the other from the father. Usually both copies of each gene are active, in cells. However, in some cases, only one of the two copies are normally active, depending on the parent of origin: some genes are normally active only when they are inherited from the father; others are active only when inherited from the mother. The methylation process (see section 1.2) is the main mechanism of genomic imprinting which enables the marking, or “stamping,” of the gene. Notably, the genomic imprinting is a process implicated in the development and function of the brain [90].

To date only a small percentage of all human and mice genes undergo genomic imprinting. Approximately 165 and 197 imprinted genes have been identified in humans and mice (see supplementary Table 1 for detailed list). These imprinted genes tend to cluster together in the same regions of chromosomes. Two major clusters of imprinted genes have been identified in humans, one of the short (p) arm of chromosome 11 (at position 11p15) and another on the long (q) arm of chromosome 15 (in the region 15q11 to 15q13). In particular, in this thesis, I focused on investigating the cluster of genes located in chromosome 15q11.2-q13, which is responsible for developing the PWS (see Figure 3).

1.2.2 Genomic imprinting defects

Monoallelic expression of imprinted genes regulated by complex epigenetic mechanisms are susceptible to dysregulation at multiple levels. Therefore, defectively imprinted regions correlate with several diseases, neurobehavioral and developmental disorders resulting from impaired regulation. Single epigenetic alterations can lead to deregulation of many genes resulting in the formation of multiple disorders [91]. Parental origin of mutations or epigenetic alterations in the gene cluster thus play a critical role in all imprinting disorders.

Imprinting and uniparental disomies (UPDs)

UPDs are the simplest and most frequent type of genetic or epigenetic alterations in imprinting syndromes. UPD occurs when a person receives two copies of a chromosome,

or part of a chromosome, from one parent and no copies from the other parent. UPD can occur as a random event during the formation of egg or sperm cells or may happen in early fetal development. In many cases, UPD may have no effect on health or development because most genes are not imprinted. However, should UPD involve chromosomes where genes are imprinted, such as chromosome 15 this could/may/will lead to several genetic disorders such as either PWS or AS. This thesis focuses only on the PWS, as the research laboratory has published several research articles in this field and one of the mice models of PWS is currently available in the Italian Institute of Technology (IIT).

1.3 Prader-Willi syndrome

PWS is a neurodevelopmental disorder caused by an imprinting defect. PWS is a rare neurologic disease with an estimated prevalence of 1:10,000 – 1:30,000 [92]. PWS is a complex genetic multisystem disorder that shows great variability, with changing clinical features throughout a patient's life. Based on the extreme variability of the genetic background the clinical endophenotypes are greatly mutable between PWS subjects. In the following sections the genetic background and the clinical aspect of this syndrome.

1.3.1 Genetic background

PWS occurs as the result of the absence of expression of paternal genes from chromosome 15q11.2-q13. This genetic defect is defined heterogeneously across patients; indeed, in the 70 – 75% of cases, PWS is determined by a deletion in the paternally derived chromosome 15, while for the remaining 20 – 25% it is caused by maternal uniparental disomy. Rarely, PWS can also be caused by a chromosomal rearrangement called a translocation, or by a mutation or other defect that abnormally inactivates genes on the paternal chromosome 15 [93].

In the PWS regions there are several paternally expressed protein-coding genes implicated; MKRN3, MAGEL2, NDN, NPAP1 and SNURF-SNRPN and a family of paternally expressed small nucleolar RNA (snoRNA) genes or clusters. The latter are molecules that have a variety of functions, including helping to regulate other types of RNA molecules, which play essential roles in producing proteins and in other cell activities, see Figure 3 for PWS cluster. Among all the genes which are compromised in the PWS locus, to date it

is unknown what could be the main candidate genes which play a pivotal role in this syndrome. Moreover, the literature is not helpful because several papers are giving conflicting results. For instance, Kanber and colleagues [94] suggest that the *MAGEL2* gene may not be considered as one of the best candidates for PWS, while Schaaf et al. [95] suggest the opposite. Nevertheless, recent studies suggest [96] that PWS is potentially associated to a disruption of the small nucleolar ribonucleic acid (RNA)-116 (*SNORD116*, also called *HBII-85*) gene. These studies suggest that the loss of a particular group of *SNORD116* cluster [97], may play a major role in causing the signs and symptoms of PWS. In addition, a preclinical study performed in mice carrying the paternal deletion of the *Snord116* shows that the paternal imprinted gene plays a crucial role in developing the major endophenotypes of this syndrome. Indeed, this animal model reproduces hyperphagia and sleep-wake alterations observed in PWS patients [98]–[100]. These findings suggest that *SNORD116* may play a crucial role in PWS and it could be considered as a potential target for new intervention. However, not all aspects of the PWS phenotype have been reproduced with deletions of *Snord116*. Indeed, the hypothalamic congenital deletions of this gene don't lead to hyperphagia and obesity, while adult-onset deletion of *Snord116* in the hypothalamus leads to hyperphagia suggesting an important role of this gene in the regulation of metabolism not only during the development but also during the life span.

However, it is not completely understood how a missing *SNORD116* cluster could contribute to the main features of the disorder. This Ph.D. attempts to fill this gap in the literature by investigating the role of this gene in the PWS. In particular focusing on the sleep alteration that characterizes this syndrome and which significantly compromises the quality of life of PWS patients. To specifically investigate the role of the *SNORD116* cluster in the PWS as well as in the regulation of sleep, a mice model having the paternal deletion of the *Snord116* gene was used. Notably, the PWS region is extremely conserved between mice and humans.

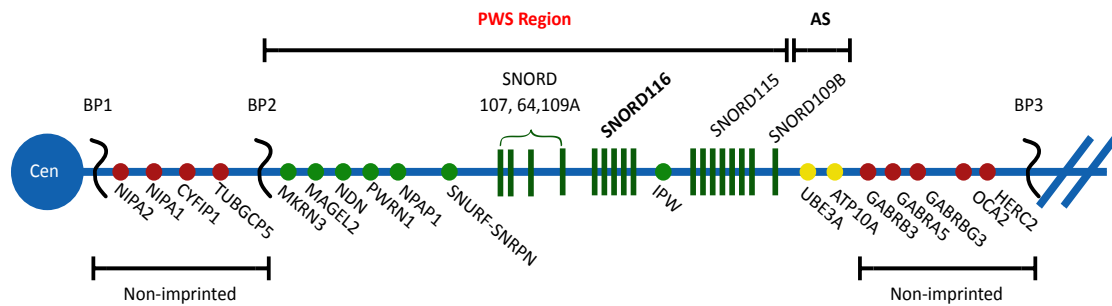


Figure 3 PWS Cluster

Representation of the genetic and expression map of chromosome region 15q11.2-q13. PWS region has five paternal-only expressed unique-copy genes that encode polypeptides (MKRN3, MAGEL2, NDN, and SNURF-SNRPN) and a family of six paternal-only expressed snoRNA genes and IPW, a long non-coding RNA

1.3.2 Clinical features

The clinical picture and the nutritional stages have been classically described as having two phases along their life [101]:

- i. Phase I, also named as the infancy stage, where newborns are characterized by profound hypotonia which can lead to asphyxia, feeding difficulties, including a poor suck, which may lead to failure to thrive.
- ii. Phase II, starting from 2 to 8 years which is characterized by “hyperphagia leading to obesity” [101]. Thus, if obesity is not well controlled it can lead to other related problems such as cardiovascular problems, hypertension, diabetes mellitus, thrombophlebitis, chronic leg edema and respiratory infections [92]. The literature suggests that there is a “switch” between poor feeding and hyperphagia that occurs at approximately 18–36 months in individuals with PWS [102]–[105].

Additionally, PWS patients also have behavioral problems and cognitive impairment, that may be explained by a lower cortical complexity observed in MRI studies [106].

1.3.3 Sleep alterations and PWS

One of the typical features of PWS is the sleep alterations affecting approximately 76% of PWS patients [8], [97]. It has been shown that 90–100% [107] of adults with PWS have excessive daytime sleepiness (EDS) [108] with reduced sleep onset latencies both at nighttime and during the day on the multiple sleep latency test (MSLT) [108]. Previous

studies have reported a complete absence or dysregulation of sleep spindles in PWS patients [109], [110]. One of the predominating endophenotypes of PWS is obesity. Indeed these are several bodies of evidence suggesting that there is a strong relationship between sleep and metabolic disorders [111], [112], suggesting the sleep alteration in the PWS may also exacerbate the metabolic features. Evidence supporting a positive relationship between EDS and body mass index (BMI) has been also described in patients with PWS [108]. Breathing disturbances during sleep, including sleep apnea, may be exacerbated by obesity in individuals with PWS [113], [114]. Additionally, EDS could also be attributed to the level of cerebrospinal fluid (CSF) hypocretin, which was found to be lower than normal in four patients with PWS and the levels correlated with the severity of EDS [115]. Dauvilliers et al. [116] found that one patient with Kleine–Levin syndrome (also affected by PWS) had a two-fold decrease in hypocretin-1 level only during the symptomatic episode, suggesting a possible intermittent alteration of the hypocretin system.

Moreover, sleep disturbances include REM alteration such as a reduction of the REM latency and an increase in the number of REM periods [109]. It has been also shown that PWS patients have altered sleep architecture manifested by a non-REM sleep instability [117]. In some clinical studies PWS patients presented narcoleptic-like symptoms, an EEG profile characterized by the intrusion of REM sleep into the transition between wakefulness and sleep, cataplexy or a transient loss of muscle tone [92], [118].

1.3.4 Hypothalamus and PWS

Hypothalamic dysfunction could be responsible for some of the clinical features of the PWS such as disturbance of energy regulation, temperature instability, short stature, hypogonadism [119], [120], abnormal ventilatory control and in the pathogenesis of EDS [108]. Indeed, the hypothalamus is one of the regions of the brain which plays a crucial role in the control of the sleep-wake cycle and in the regulation of many functions throughout the body, such as feeding, metabolism and temperature, all of which are significantly compromised in PWS.

In supporting the fact that PWS may be linked to hypothalamic insufficiency there is a paper [121] reporting hypothalamic pathology and dysmorphism in postmortem studies of the PWS patients with a highly abnormal structure of the SCN in the hypothalamus.

Moreover, the PWS patients have more sleep cycles per night and more REM periods that have been shown to be controlled by the hypothalamus. Hypothalamic dysfunction in the PWS can also be related to respiratory alterations through obesity, linked with hyperghrelinemia, and hypercapnia suggesting the sleep alteration in the PWS may also exacerbate the metabolic features [122]–[124]. Additionally, it has been shown that some of the paternally imprinted genes (i.e. *Meg3* and *Snord116*) playing a crucial role in the pathophysiology of PWS are highly expressed in the hypothalamic region. Notably, it has been shown in an embryonic chimeric experiment [125] that paternally imprinted genes are extremely important for hypothalamic formation.

1.3.5 Current treatment

Currently, there is no cure for PWS, however, many treatments may allow for better outcomes, especially when provided early. As a main treatment for sleep alterations the first intervention is to improve sleep hygiene by shaping behavior to assure the appropriate amount of sleep and to supplement this with planned naps, if necessary. The second intervention is to treat the source of sleep disruption by using non-invasive intermittent positive pressure ventilation (NIPPV), CPAP, tonsillectomy and adenoidectomy as in the general population. Then, the daytime use of stimulant medication (either methylphenidate or dextroamphetamine derivatives) and/or modafinil (Provigil) is recommended. Modafinil is approved for the treatment of narcolepsy and EDS. Modafinil has been shown to be a safe and effective treatment for EDS and narcolepsy-like phenotype in PWS patients [126]. However, this drug has many side effects, including headaches, anxiety, trouble sleeping, nausea and hallucinations. Currently an alternative to Modafinil is Pitolisant orally active antagonist/inverse agonist of the human histamine H3 receptor. It works by enhancing the histaminergic transmissions in the brain, acetylcholine release in the prefrontal cortex and hippocampus and dopamine release in the prefrontal cortex but not in the striatum. Pitolisant as well as Modafinil is used to enhance wakefulness in patients with EDS and a variety of comorbid neurological diseases: narcolepsy [127], Parkinson's disease and obstructive sleep apnea [128], [129]. However, the use of Pitolisant with PWS patients is under consideration by the scientific community. For this reason, in this thesis, pre-clinical data aimed at clarifying and supporting further clinical studies to understand whether

Pitolisant maybe an alternative approach for PWS patients to ameliorate sleep problems is provided.

Chapter 2

Aims of the studies

Prader-Willi (PWS) is a neurodevelopmental disorder caused by a genomic imprinting defect. In particular, the defect involves the cluster of the paternally imprinted genes located in the chromosome 15 (15q11-13, Figure 3, Chapter 1). Paternally imprinted genes are extremely important for hypothalamic formation as well as for sleep-wake cycle regulation. Among all genes located in the PWS locus, the *Snord116* gene is the main candidate for developing the major endophenotypes of PWS. *Snord116* is also highly expressed in the hypothalamus, which is one of the brain regions involved in sleep regulation. In particular, animal studies suggest that this gene may be involved in the sleep alterations of this syndrome rather than the metabolic alterations. However, it is unclear if *Snord116* plays a role in the hypothalamic function and formation as well as the biological and homeostatic control of sleep.

Based on the above evidences the three aims of this thesis are:

- I. **Study I** to investigate whether *Snord116* may play a role in the hypothalamic formation and in the regulation of the biological and homeostatic control of sleep.
- II. **Study II** to investigate the role of *Snord116* in the regulation of macrostructural sleep aspects and in the brain-circuits involved such as the thalamic reticular nucleus (TRN)/ thalamus circuits or in corticothalamic afferents.
- III. **Study III** to investigate a new alternative pharmacological approach for PWS aimed at ameliorating the sleep disturbances that significantly comprise the quality of life of these patients by using Pitolisant in mice carrying the deletion of the *Snord116* gene.

Notably, most of the data collected in these three studies was analyzed by using Phenopy, a practical user interface for the management of behavioral and sleep analysis developed by me during my PhD. For the published paper see Appendix A.

2.1 Study I

***Snord116* may play a role in the hypothalamic formation and in the regulation of the biological and homeostatic control of sleep**

Imprinted genes are highly expressed in the hypothalamus; however, whether specific imprinted genes affect hypothalamic neuromodulators and their functions is unknown. It has been suggested PWS, a neurodevelopmental disorder caused by lack of paternal expression at chromosome 15q11-q13, is characterised by hypothalamic insufficiency. Here, we investigated the role of the paternally expressed *Snord116* gene within the context of sleep and metabolic abnormalities of PWS, and we reported a novel role of this imprinted gene in the function and organisation of the two main neuromodulatory systems of the lateral hypothalamus (LH), namely, the orexin (OX) and melanin concentrating hormone (MCH) systems. We observed that the dynamics between neuronal discharge in the LH and the sleep-wake states of mice with paternal deletion of *Snord116* (PWScr^{m+/p-}) are compromised. This abnormal state-dependent neuronal activity is paralleled by a significant reduction in OX neurons in the LH of mutants. Therefore, I proposed that an imbalance between OX- and MCH-expressing neurons in the LH of mutants reflects a series of deficits manifested in the PWS, such as dysregulation of rapid eye movement (REM) sleep, food intake and temperature control.

2.2 Study II

***Snord116* in the regulation of the sleep macrostructural aspect and in the brain-circuits**

In the study I, we observed that PWScr^{m+/p-} mice are characterized by REM sleep abnormalities. In this study, we investigated the macrostructural aspect of sleep such as REM sleep features and sleep spindles within non-REM graphoelements sleep. While the former is thought to contribute to neuronal network formation early in brain development, the latter are markers of thalamocortical processes. Both signals are often compromised in neurodevelopmental disorders and influence functional properties of cortical neurons. Thus, we isolated and characterized the intrinsic activity of cortical neurons using *in vitro* microelectrode array (MEA) studies. Regarding the MEA experiment, it was included in another doctoral project and therefore the results will not

be shown. For further information refer to the paper of which I am the first author (sharing authorship) at the following link: <https://doi.org/10.1101/809822>.

These results indicate that the *Snord116* gene in mice selectively influences REM sleep properties, such as theta rhythms and the organization of REM episodes throughout sleep-wake cycles. Moreover, sleep spindles present specific abnormalities in PWS model systems, indicating that these features of sleep may translate as potential biomarkers in human PWS. We observed abnormalities in the synchronization of cortical neuronal activity that are accounted for high levels of norepinephrine.

In conclusion, these results provide support for an important role of *Snord116* in regulating brain activity during sleep and, in particular, cortical neuronal properties, thereby opening new avenues for developing interventions in PWS.

2.3 Study III

New alternative pharmacological approach for PWS

In the Study I and II, we observed that PWS is related to hypothalamic insufficiencies showing also a reduction of orexin neurons. Additionally, they have also sleep-wake cycle alteration, disrupted REM sleep, and temperature instability. The purpose of this study was to investigate the response of $PWScr^{m+/p-}$ mice to acute administration of Pitolisant aimed at improving sleep phenotypes. Pitolisant enhances wakefulness bypassing the orexin system and acting directly on the histamine system. The result of this study confirmed again that $PWScr^{m+/p-}$ mice have an alteration in the macrostructure of sleep affecting only REM sleep, without substantially disrupting any other sleep stages. However, $PWScr^{m+/p-}$ mice exhibited a high propensity to sleep, an inability to maintain wakefulness.

These findings indicate that Pitolisant ameliorates the REM sleep alteration in these mice. However, other studies are needed to investigate whether Pitolisant may also modulate the sleep-wake cycle via temperature.

Chapter 3

Materials and methods

In the following section are described the animal models and methods used for each study.

3.1 Study I

Animal husbandry, breeding, and genotyping

All animals were housed in controlled temperature conditions (22 ± 1 °C) under a 12-hour light/dark cycle (light on 08:00–20:00), with libitum access to food (standard chow diet) and water unless otherwise required by the experimental procedure.

Experiments were performed using adult mice at 15-17 weeks with paternal deletion of the *Snord116* gene and IPW exons A1/A2 B [97] (PWScr^{m+/p-}) and their wild-type littermates as control mice (PWScr^{m+/p+}). To maintain the colony, mice were bred and kept through paternal inheritance on a C57BL/6J background. Genotyping was performed as previously described [100]. Briefly, PCR analysis of genomic DNA from ear punches was performed using the primer pair PWScrF1/PWScrR2 (5'-AGAATCGCTTGAACCCAGGA and 5'-GAGAAGCCCTGTAACATGTCA, respectively). The deletion of PWScr resulted in a PCR product of approximately 300 bp, which was absent in the wild-type genotype.

For experiments in narcoleptic mice, 3 age-matched groups of male and female congenic mice from two different strains (≥ 9 generations of backcrossing) on the C57Bl/6J genetic background were used, as follows:

- I. mice with congenital deficiency of OX gene (Ppox) knockout (KO) [130] (n=11);
- II. mice hemizygous for a transgene (ataxin-3 [Atx] mice), the targeted expression of which causes selective ablation of OX neurons [131] (n=4);
- III. wild-type controls (n= 4). Mouse colonies were maintained in the facilities of the Department of Biomedical and NeuroMotor Sciences at the University of Bologna, Italy.

Mice were housed under a 12-hour light/dark cycle at an ambient temperature of 25°C with free access to water and food (4RF21 diet, Mucedola, Settimo Milanese, Italy).

All animal procedures were approved by the Animal Research Committee and the Veterinary Office of Italy for Istituto Italiano di Tecnologia (IIT) Genova. All efforts were made to minimize the number of animals used and any pain and discomfort according to the principles of the 3Rs [132].

Experimental approach

Neuronal activity in the mouse LH is time-locked with different behavioral and physiological states of the brain.

To identify neuronal populations in the LH that control different physiological behaviors, we adopted a combined experimental approach (Figure 4A) in which I monitored single unit activity (SUA) at the LH in parallel with the cortical state of each animal by means of electroencephalogram and electromyogram (EEG/EMG) recordings. The EEG/EMG information allows the identification of wakefulness, REM sleep and non-REM sleep states in the animal, which represent the three main behavioral states of the mammalian brain. Mice were kept throughout a regular sleep-wake cycle, and EEG/EMG/SUA were recorded during the light-to-dark transition (baseline 1, B1) and during the dark-to-light transition (baseline 2, B2) to test the neuronal responses during the minimum and maximum levels of sleep pressure, respectively (Figure 4B upper panel). Then, each mouse underwent sleep deprivation (SD) to test the homeostatic response following sleep loss (Figure 4B middle panel). A total of 569 well-sorted units were successfully recorded from PWScr^{m+/p+} wild-type mice, and 548 units were recorded from PWScr^{m+/p-} mutant mice across all time points.

Based on the distribution of the firing activity of each unit, we were able to distinguish populations of putative neurons in the LH that were time-locked with the occurrence of specific sleep-wake states (Figures 4C and 4E). In particular, we identified neurons (Figure 4E) associated with sleep (S-max) or wakefulness (W-max). However, we distinguished between non-REM (NR-max), REM (R-max) neurons and neurons firing in both stages (NRR-max) (see supplementary Table 2). We also identified a group of neurons that did not show significant changes in their firing rate across the sleep-wake states, and we called this latter class of neurons “ws” (wake and sleep).

Moreover, to test the other fundamental function of LH, feeding, we food deprived each animal during the 12-hour of darkness of the light/dark cycle, and then, when food was

made available, we evaluated the neuronal responses to food intake (Figure 4B lower panel). In this experiment, a total of 147 units were identified from PWScr^{m+/p+} mice and 74 units from the PWScr^{m+/p-} mice in response to food deprivation.

Following the food deprivation protocol, we also distinguished three different classes of neurons in the LH that respond to food intake. In particular, we defined type I and II neurons as those that fire maximally after or before nose-poking/feeding activity, respectively (Figures 4D and 4F). In this experiment, a third class of neurons, type III neurons, was defined as non-responding neurons.

Experimental protocols

LH neuronal activity recordings. To investigate the neuronal dynamics of the lateral hypothalamus (LH), EEG/EMG and SUA were simultaneously recorded in eight male adult PWScr^{m+/p-} and PWScr^{m+/p+} mice. Animals were individually housed after surgery in their home cages with a food hopper (a hole with an infrared beam) connected to a food dispenser that automatically delivers food pellets after a nose poke (powered by AM-Microsystems [133]). The food used was 20 mg dustless precision pellets (Bioserv). After a 7-day recovery period after surgery, each mouse was connected to a flexible cable and swivel that allowed free movement within the cages; the mice were habituated for 2 days to the cable before SUA and EEG/EMG recordings (Figure 4A). Recordings of EEG/EMG with SUA were acquired at two different baseline (BL) time points (B1 and B2; Figure 4A) for 2-hour according to the C Process and S Process of sleep. Next, to investigate sleep homeostasis, SUA and EEG/EMG were recorded during the first hour of the rebound period (RB, Figure 4A) following 6-hour of total sleep deprivation (SD) and at other two time points over the 18-hour recovery period (SD1 and SD2, Figure 4A).

After a restoration period of 5 days from the previous SD, animals were fasted for 12-hour during the dark period, which corresponds to the active phase of mice. At the beginning of the light period, mice were fed. A few food pellets were initially provided to encourage the mice to eat, and thereafter, food pellets were provided only after nose-poke activity. SUA was continuously recorded for 2-hour after being fed (Figure 4A). EEG/EMG was not recorded during this time.

Homeostatic investigation of sleep.

To investigate the role of the *Snord116* gene in the regulation of the homeostatic component of sleep, we recorded EEG/EMG in ten male adult PWScr^{m+/p-} and PWScr^{m+/p+} mice over 24-hour of baseline (BL) at 22 ± 1°C. The BL recordings began at ZT 0 (the time of light onset in the 12-hour light/dark cycle), and then, mice were sleep deprived during the first 6-hour of the light phase (ZT 0–6) by gentle handling (introduction of novel objects into the cage, tapping on the cage, and, when necessary, delicately touching) and then allowed 18-hour of recovery (ZT 6–24, RB).

Investigation of REM sleep propensity.

To investigate the REM sleep propensity, we housed male adult PWScr^{m+/p-} and PWScr^{m+/p+} mice for five weeks at 30 ± 1°C, which is close to or within the thermoneutral zone (TNZ) of mice [134], [135]. Then, these mice underwent continuous recordings for 24-hour at 30°C ambient temperature while undisturbed and freely moving in their cages.

Surgery

Mice were anaesthetized using 1.5%–2.5% isoflurane in oxygen and placed in a stereotaxic frame (David Kopf Instruments, Tujunga, CA). To assess the sleep-wake cycle, mice were surgically implanted with a telemetric transmitter (volume, 1.9 cm³; total weight, 3.9 g; TL11M2-F20-EET; DSI, St. Paul, MN, USA) connected to electrodes for continuous EEG/EMG recordings. A wireless EEG transmitter/receiver, which also contained a sensor to detect body temperature, was subcutaneously implanted. Specifically, EEG wire electrodes were implanted into the frontal cortex (coordinates: 2 mm posterior to the bregma and 2 mm lateral to the midline in the right parietal skull) and the parietal cortex (coordinates: 3 mm anterior to the lambda and 2 mm lateral to the midline in the right frontal skull). EMG was recorded by two stainless steel wires inserted bilaterally into the neck muscles. Subsequently, to record SUA, a tetrode-based 16-channel micro-wire array (4 x 4, 5.3 mm, 100-200-1250) of silicon probes (NeuroNexus Technologies) was implanted into the LH (coordinates relative to the bregma: –1.45 mm anteroposterior, –1.0 mm mediolateral, and –4.8 mm dorsoventral) of the contralateral hemisphere with respect to the EEG electrodes (Figure 4A). Mice were operated on by performing a small craniotomy, and the dura mater was removed for placement of the tetrodes in the LH. Two screws (1

mm diameter) were used to anchor the implant. One screw placed in the cerebellum was wrapped by the electrode ground. Next, the tetrode and the ground wire were covered with dental acrylic. Following surgery, all animals were administered paracetamol (200 mg/kg; once a day; PO; Tempra) and enrofloxacin (10 mg/kg; once a day; SC; Baytril) for two days.

Histology

At the end of the last recording session, animals were sacrificed, and the locations of the recording electrodes were verified histologically. Mice were anaesthetised using pentobarbital anaesthesia (100 mg/kg, i.p.), and microlesions were made at the tip of one or two microwires by passing a small current (5 mA, 10 s). The animals were transcardially perfused with 10 ml of phosphate-buffered saline (PBS) before infusion of 4% paraformaldehyde (PFA) in PBS. The brains were removed and equilibrated in 30% sucrose, sectioned at 40 μ m on a freezing microtome, mounted onto gelatin-coated slides, air dried, dehydrated in ethanol, stained with Nissl substance, cleared with xylene, and cover slipped with DPX (Figure 4A). Three mice were excluded from the study because the electrode was not correctly placed in the LH (Figure 4A).

Thermal imaging

Surface body temperature was continuously recorded in PWScr^{m+/p-} and PWSc^{rm+/p+} mice for 24-hour at 22°C and 30°C using an infrared thermocamera (FLIR A20). The thermocamera was positioned above the cage where the mice were individually housed. Head (T-head) and tail temperatures (T-tail) were obtained by manually analyzing the recorded video (1 frame/s) using a dedicated software program (Thermocam Research, FLIR). T-head was used to compute the heat loss index (HLI). HLI was calculated by the equation $(T_{\text{head}} - T_a)/(T_{\text{tail}} - T_a)$ [136]. T-head, T-tail and HLI values were collapsed into 2-hour bins and compared between conditions in the two experimental groups.

Additionally, body weight was measured weekly in small groups of both PWSc^{rm+/p-} and PWScr^{m+/p+} mice for 5 weeks at 22°C and at the TNZ (n= 10); the first body weight measurement was recorded at 15 weeks of age. Another group of animals (n=10) born and raised at the TNZ was also investigated. Body weight was assessed from 9 to 20 weeks of age.

A two-way ANOVA with repeated measures on both factors (group x time) was used for the statistical analysis of T-head, T-tail, and HLI over the conditions investigated between the two genotypes (+/+ vs. -/-). A two-way ANOVA was employed for the statistical analysis of body weight (group x time). These data were scored in preliminary analysis by Matteo Cerri from the Dipartimento di Scienze Biomediche e Neuromotorie at University of Bologna.

Real-time quantitative PCR

Thirty PWScr^{m+/p-} and PWScr^{m+/p+} mice were sacrificed by cervical dislocation at three different time points: at ZT 6 (T0), immediately after 6-hour of total SD (T1), and 1-hour after previous SD (ZT 7; T2). Total RNA was extracted from the hypothalamus by the Trizol method (Sigma-Aldrich) according to the manufacturer's instructions [137]. RNA concentrations were then determined by a NanoDrop 2000c spectrophotometer. The complementary DNA was obtained from up to 2 mg of total RNA by using a high-capacity RNA-to-cDNA kit (Invitrogen) and then analyzed with SYBR GREEN qPCR mix. Reactions were performed in three technical replicates using an AB 7900HT fast real-time PCR system (Applied Biosystems). The relative expression levels were quantified according to the previously described $\Delta\Delta$ CT calculation method [138]. Gapdh was used as a reference gene. The specific primer pairs used for the analysis were designed using Primer3 (see supplementary Tables 4). An unpaired t-test was used to compare the differences between the genes investigated in the two genotypes.

Narcoleptic mice were sacrificed between ZT 6 and ZT 7, and the hypothalamus and cortex of the brain were dissected and immediately frozen.

The experiment and the analysis of this part were done in collaboration with my colleagues (Marta Pace and Andrea Freschi) of the Genetics and Epigenetics of Behaviour (GEB).

Perfusion and immunohistochemistry (IHC)

PWScr^{m+/p-} and PWScr^{m+/p+} mice were transcardially perfused with 10 ml of PBS before infusion of 4% PFA in PBS. Perfused brains were postfixed for 24-hour in 4% PFA at 4°C before immersion in 30% sucrose. To quantify lateral hypothalamic neurons expressing OX and MCH neurons, serial cryosections were cut coronally at 40 μ m intervals to include

brain regions within -1.10/-1.90 mm of the bregma. Before IHC staining, the sections were washed three times with PBS for 10 min each and then blocked in 5% of the appropriate serum (normal goat serum or normal donkey serum) in 0.1% Triton X-100 in PBS for 1-hour. The sections were incubated with rabbit PPOX polyclonal (1:20; Millipore) and pro-melanin-concentrating hormone (PMCH; 1:50; Invitrogen) primary antibodies in 1% serum in 1% Triton X-100/PBS at room temperature overnight. The sections were then washed three times in PBS for 5 min each. They were incubated with appropriate secondary antibodies (1:1000) (goat anti-rabbit IgG, Alexa Fluor 488) in 1% serum in 1% Triton X-100/PBS for 2-hour at room temperature in the dark, washed three times in PBS for 5 min each, and counterstained with Hoechst (1:400 in PBS; Sigma-Aldrich). Finally, the sections were washed in PBS and mounted on glass slides using ProLong gold antifade reagent (Invitrogen). The sections were imaged with an upright Widefield Epifluorescence Olympus BX51 microscope equipped with a 4x UPLFLN N.A objective. The microscope was controlled by Neurolucida software.

The percentage of OX- and MCH-positive cells was manually scored using NIH ImageJ software. A total of 3-5 sections were evaluated for each mouse (n= 4 for genotype), and the neuron counts were normalized to the total number of DAPI-stained nuclei (approximately 300 nuclei per microscopic field). All digital images were processed in the same way between experimental conditions to avoid artificial manipulation between different data sets. An unpaired t-test was used to compare differences between the two genotypes. The experiment and the analysis of this part were done in collaboration with my colleagues (Marta Pace and Andrea Freschi) of the Genetics and Epigenetics of Behaviour (GEB).

Chromatin immunoprecipitation (ChIP)

For the analysis of PEG3 binding, H3K4me2/3 and H3K27me3, ChIP was performed on formaldehyde cross-linked chromatin isolated from the hypothalamus of 28 PWScr^{m+/p-} and PWScr^{m+/p+} mice. Briefly, the tissue of seven different hypothalamic was minced. Formaldehyde was added to the tissue, which was resuspended in PBS at a final concentration of 1% and incubated at room temperature for 15 min while shaking. The reaction was stopped by the addition of glycine to a final concentration of 0.125 M. The tissue was washed twice with ice-cold PBS, centrifuged and resuspended in lysis buffer 1

(50 mM HEPES pH 8, 10 mM NaCl, 1 mM EDTA, 10% glycerol, 0.5% NP-40 and 0.25% Triton X-100) for 90 min at 4°C. Isolated nuclei were lysed in lysis buffer 2 (10 mM Tris-HCl pH 8.0, 200 mM NaCl, 1 mM EDTA and 0.5 mM EGTA) for 60 min at 4°C. The chromatin was sheared in sonication buffer (10 mM Tris-HCl pH 8.0, 100 mM NaCl, 1 mM EDTA, 0.5 mM EGTA, 0.1% sodium deoxycholate and 0.5% N-lauroylsarcosine) to an average size of 100–400 bp using the Sonifier 150 (Branson).

For each IP, 100 µg of sonicated chromatin was diluted in a final volume of 600 µl with sonication buffer and pre-cleared with 30 µl protein A/G agarose beads (Santa Cruz) for 4-hour at 4°C on a rotating wheel. Anti-PEG3 antibody (7 µg, Abcam Ab99252), anti-histone H3K4me3 (7 µg, Abcam Ab8895), and anti_Histone H3K27me3 (7 µg, Abcam Ab195477) or rabbit IgG were added to the pre-cleared chromatin and incubated overnight at 4°C on a rotating wheel. Chromatin was precipitated with 30 µl protein A/G agarose beads for 4-hour at 4°C with rotation. The beads were then washed five times with 500 µl RIPA buffer (10 mM Tris-HCl pH 8.0, 140 mM NaCl, 1 mM EDTA, 0.5 mM EGTA, 0.1% sodium deoxycholate, 1% Triton X-100 and 0.1% SDS) and once with each of the following buffers: WASH buffer (50 mM HEPES, 0.5% sodium deoxycholate, 1% Triton X-100, 1 mM EDTA, 500 mM NaCl and 0.2% NaN₃), LiCl buffer (0.25 M LiCl, 0.5% NP-40, 0.5% sodium deoxycholate, 1 mM EDTA and 10 mM Tris pH 8) and TE buffer (10 mM Tris pH 8, 1 mM EDTA). The bound chromatin was eluted in 100 µl TE buffer. Crosslinks were reversed by incubation with O/N at 65°C after the addition of 1 µl RNAse cocktail (Ambion) and 2 h at 50°C after the addition of 2.5 µl SDS 20% + 2.5 µl 20 mg/ml proteinase K (Sigma). DNA was extracted by using a QIAquick Gel Extraction Kit (Qiagen). Immunoprecipitated or 1% input DNAs were analyzed by real-time PCR using SYBRGreen PCR Master Mix (Bio-Rad) on a 7900HT Fast Real-Time PCR System (Applied Biosystems). Each reaction was performed in triplicate, and experiments were performed twice. The specific primer pairs used for the analysis were designed using Primer3 (see supplementary Table 3). An unpaired t-test was used to compare differences between the two genotypes.

The experiment and the analysis of this part were done in collaboration with my colleagues (Marta Pace and Andrea Freschi) of the Genetics and Epigenetics of Behaviour (GEB).

Hypothalamic cell culture transfected with *Snord116*-siRNA

Embryonic rat hypothalamus cell line R7 (rHypoE-7 – Tebu-bio) cells were cultured in Dulbecco's modified Eagle's medium (Sigma Co. Ltd, St Louis, MO, USA) supplemented with 10% foetal bovine serum, 50 units of penicillin and 50 µg/ml of streptomycin at 37°C under an atmosphere of 5% CO₂. Cells were seeded in six-well plates (Nunc Co., Roskilde, Denmark) at a density of 1 × 10⁵ cells per well. The day after cell seeding, 20 µM of Silencer® *Snord116*-siRNA (Ambion®) was mixed with RNAiMAX Lipofectamine (Life Technologies) reagent, and the mixture was added to each dish. We used MISSION® siRNA universal negative control #1 (Sigma) as a negative control at 20 µM. Cells were incubated for 48-hour after transfection, and RNA was extracted by using the Trizol method for gene expression analysis (see supplementary Table 3). Experiments were conducted in triplicate. An unpaired t-test was used to compare differences between the two genotypes.

The experiment and the analysis of this part were done in collaboration with my colleagues (Marta Pace and Andrea Freschi) of the Genetics and Epigenetics of Behaviour (GEB).

RNA sequencing and analysis

Total RNA was homogenized in Trizol Reagent (Sigma-Aldrich). Libraries were prepared using a TruSeq polyA mRNA kit (Illumina) according to the manufacturer's instructions and sequenced by using the NovaSeq 6000 System (Illumina).

Raw sequence reads were quality controlled through FASTQC (<https://www.bioinformatics.babraham.ac.uk/projects/fastqc/>) and trimmed using Trimmomatic (v0.38) (<http://www.ncbi.nlm.nih.gov/pubmed/24695404>). To quantify the transcript abundances, we used Kallisto (v0.44.0) [139]. Kallisto was also used to build an index from the mouse reference genome (Ensembl.Mmusculus.v79) with default parameters. To import and summarize transcript-level abundance of Kallisto, the R package Tximport was used. Differential expression was assessed using DESeq2 [140]. Adjusted p-values less than 0.05 were selected, and only genes with > 2-fold change were considered in the analyses.

GO analysis was performed using Metascape [141] (<http://metascape.org/>). The identified DEGs are listed in supplementary Tables 5.

The analysis of this part was done in collaboration with Alfonso Urbanucci from the Department of Tumor Biology, Institute for Cancer Research, Oslo University Hospital, Oslo Norway and Marta Pace from the Genetics and Epigenetics of Behaviour (GEB).

Electrophysiological data analysis

Cortical EEG/EMG signals were recorded using Dataquest A.R.T. (Data Science International). Signals were digitized at a sampling rate of 500 Hz with a filter cut-off of 50 Hz. EEG signals were filtered at 0.3 Hz (low-pass filter) and 0.1 KHz (high-pass filter). The polysomnographic recordings were visually scored offline using SleepSign software (Kissei Comtec Co. Ltd, Japan) per four second epoch window to identify wakefulness (W), non-REM or REM sleep stages, as previously described [138], [142]. Scoring was performed by a single observer who was blinded to the mouse groups.

Specifically, W, non-REM and REM states were scored when characteristic EEG/EMG activity occupied 75% of the epochs. EEG epochs determined to have artefact (interference caused by scratching, movement, eating, or drinking) were excluded from the analysis. Artefact comprised <5-8% of all recordings used for analysis.

The percentage of time spent in total sleep, non-REM and REM sleep out of the total recording time was determined. The amount of time spent in each stage was established by counting the types of epochs (W or NR or R) and averaging over 2-hour periods. The spectral characteristics of the EEG were further analyzed. The EEG power densities of the delta (0, 5–4 Hz) and theta (5–9 Hz) frequencies in non-REM and REM sleep were computed for all conditions investigated. To exclude variability due to the implantation, the power density of each animal was normalized to the power density of the last 4-hour of the light period of the 24-hour recording (22°C and 30°C, respectively). The temperature was recorded at a sampling rate of 5 Hz within the range of 34°C – 41°C and averaged over 2-hour periods. A two-way ANOVA with repeated measures (factors of group x time) was used for the statistical analysis of the 2-hour averaged time-course changes in the percentage of each sleep stage (W, non-REM and REM sleep), delta power, theta power and body temperature between the two genotypes (+/+ vs. -/-). The statistical analysis of the cumulative amount of W, non-REM, and REM sleep over the dark and light periods among the groups at BL, after SD and at the TNZ was performed with one-way ANOVA. An unpaired t-test was used to compare differences in the sleep stages

and in the delta and theta power during the first 4-hour of rebound after SD between the two genotypes.

SUA data acquisition was performed using an RX7 system (Tucker Davis Technology, TDT). The synchronization between the behavioral set up and the TDT system was guaranteed with transistor-transistor logic (TTL) from the CHORA feeders to the TDT system. The data were digitally sampled at 12 kHz. To detect spike timestamps, the neural traces were filtered with a bandpass filter (300 – 5000 Hz), and then, the common average reference (CAR) was applied [143]. Spikes were detected using a hard threshold that was computed as previously described [144]. A correlation filter was applied between each detected spike and the corresponding signal chunk in the other recording sites to detect and exclude false positive spikes given by movement artefact.

To specifically identify active neurons in the LH, we imposed two criteria: (i) the refractory period following a spike was set to 1 ms; and (ii) the maximum duration of a waveform was set to 5 ms. Spikes of individual neurons were sorted offline using the noise robust LDA-GMM algorithm based on a linear discriminant analysis [145]. To identify neurons that specifically respond to a particular sleep-wake cycle, the unit activity was subsequently analyzed per 4-s epoch in each sleep-wake stage for the average discharge rate (spikes per second). Classification of units according to the state in which their maximal discharge rate occurred was performed by ANOVA followed by post hoc paired t-tests with the Bonferroni correction, ($P < 0.05$) [63]. This analysis allowed the classification of units into three main neuronal populations that were shown to respond during specific sleep-wake stages (Figure 4B).

Moreover, to identify the neurons related to feeding behaviour in the LH, we assessed the firing rate of neurons that responded after the food was released by aligning the unit firing to the pellet release from the CHORA feeder after a spontaneous nose-poke activity. The mean baseline firing rate of each neuron was determined in the interval of 5 s before the pellet was released. Paired Student's t-tests were used to classify the firing rate differences of the same units before and after the food was released. To motivate the mice to perform more trials, they were food deprived for 12-hour during the dark period, and the recording session started at the beginning of the light period for the following 2-hour. Sessions were videotaped and reviewed to eliminate trials in which the mice performed the nose-poke activity, but the food was not eaten. Video analysis also

demonstrated that grooming rarely occurred and, thus, did not affect SUA. Indeed, grooming has been shown to induce moderate OX neuron activity [146]. Among all sessions, a mean of 3.25 ± 1.49 trials for the PWScr^{m+/p-} mice and 2 ± 0.69 trials for the PWScr^{m+/p-} mice were removed from the analysis because the food was not eaten.

Statistics

Values were tested for a Gaussian distribution with the Kolmogorov–Smirnov test. Data are presented as the mean \pm standard error of the mean (SEM). Two-way repeated-measures analysis of variance (ANOVA) was used to perform group comparisons with multiple measurements. Paired and unpaired t tests were used for single value comparisons. One-way ANOVA was used to compare more than two groups, followed by post hoc Tukey's test. The Bonferroni correction was further applied in the post hoc analysis, as appropriate, to correct for multiple comparisons. Neuronal dynamics of the LH were analyzed by the chi-square test. Phenopy [133] was used for sleep, temperature and SUA analyses, while GraphPad Prism6 (GraphPad Prism Software, Inc.) was used for statistical analysis. Type I error α was set to 0.05 ($p < 0.05$).

For further details of Phenopy system, see appendix A.

3.2 Study II

In vivo study – Animals

Animals utilized in this study were the same used in the Study I. For more details regarding the animal husbandry, breeding, and genotyping see session 3.1 from Study I.

Experimental design

For the study, male mice with paternally inherited *Snord116* deletions (PWScr^{m+/p-}) and wild-type littermate control mice (PWScr^{m+/p+}) aged 15 to 18 weeks were used.

To investigate the impact of *Snord116* in the sleep architecture, we made continuous recordings by electroencephalography combined with electromyography (EEG/EMG) for 24-hour (12-hour:12-hour light/dark cycle). Subsequently, we investigated changes in spindle properties at specific time points across the sleep-wake cycle. Specifically, we recorded sleep spindles during the same time point of SUA recordings (see experimental design session 3.1 of Study I).

EEG/EMG electrode implantation

See Surgery section from Study I.

EEG/EMG analysis

See Electrophysiological data analysis session of Study I.

REM sleep characterization

Additional analyses were performed to characterize the REM sleep alterations observed in the $PWScr^{m+/p-}$ mice. In particular, a more detailed analysis of REM sleep was carried out according to the partition of REM sleep episodes into single and sequential episodes, which has originally been proposed for rat [147]. First, the REM sleep intervals (RSIs), given by the sum of the time spent in wakefulness and in non-REM sleep between two REM sleep episodes, were calculated. Here, the bimodal distribution of RSI length was determined using a kernel density estimation mathematical model, and single REM sleep episodes and sequential REM sleep episodes were discriminated (Figure S1A). A single RSI is defined as one that is both preceded and followed by long RSIs > 60 sec each, while sequential REM sleep episodes are those that are separated by short RSIs ≤ 60 sec each (Figure 8A).

Second, the REM-non-REM cycle, which is defined as the interval between the onset of consecutive REM episodes, was assessed. The following criteria were used: 8 sec was the minimum length of a REM sleep episode; and cycles that were longer than 30 minutes were excluded from the analysis, since it has been already documented in mouse studies that the cycle length is approximately 2-5 minutes [148]. An unpaired t-test was used to assess differences between short and long RSIs and differences in the number of REM-non-REM sleep cycles.

Sleep spindle properties

Individual sleep spindles were detected using a wavelet-based spindle detection method [149]. Briefly, the algorithm estimates the energy of EEG signal within 9-16 Hz range using the continuous wavelet transform, and then applies a threshold ($3 \text{ SD} + \text{Mean}$) to detect candidate spindles. A lower threshold ($1 \text{ SD} + \text{Mean}$) is then applied to find start and end points of the candidate spindles. Detected events that meet these criteria are considered

as spindles; (i) duration between 0.4-2 s, (ii) number of cycles between 5-30 (minimum and maximum number of events for the two hour recording), (iii) increase in power should be specific to the spindle range. Afterward, several properties of the detected spindles are calculated automatically, such as density, duration, central frequency, peak-to-peak amplitude, and symmetry.

Neurochemical analysis

Neurochemical analysis was performed in PWScr^{m+/p-} mice (n = 5) and PWScr^{m+/p+} mice (n = 5). Mice were anaesthetized with isoflurane at the beginning of the dark period to collect cerebrospinal fluid (CSF). We decided to collect samples at this time point because REM sleep alterations were observed at this stage. CSF was sampled as previously described [150]. Mice were anaesthetized using 1.5%–2.5% isoflurane in oxygen and placed on a platform, and the arachnoid membrane covering the cisterna magna was punctured. The positive flow pressure allows the collection of CSF using a glass micropipette with a narrow tip. Three to eight microliters of CSF per mouse was collected and stored at –80 °C in polypropylene tubes.

CSF preparation for ultrahigh-performance liquid chromatography-tandem mass spectrometry (UPLC-MS/MS)

Eighteen microliters of a solution containing 1 µM each of Glu-d5 and GABA-d6 and 50 nM His-d4 in aqueous 0.1% formic acid was added to 2 µL of each thawed sample of CSF and then vortexed and centrifuged for 10 minutes at 14,000 rpm. The resulting supernatants were moved to glass vials for injection. Calibration standards were prepared by spiking artificial CSF (150 mM Na, 3 mM K, 1.4 mM Ca, 0.8 mM Mg, 1 mM P, 155 mM Cl, 10 mM glucose, 0.5 mg/mL albumin) with stock standard solutions. These calibrators were further diluted 1:10 with the internal standard solution, vortexed and centrifuged before injection.

UPLC-MS/MS

Chromatographic separation was performed with an Acquity UPLC system (Waters, Milford, MA, USA) using an ACE C18-Ar column (2 µm particle size, 2.1x150 mm (purchased from Advanced Chromatography Technologies Ltd, Aberdeen, Scotland, UK).

Separation was carried out at a flow rate of 0.5 mL/min. The eluents were as follows: A, aqueous 0.1% formic acid with 5 mM n-perfluoropentanoic acid (NFPA); B, acetonitrile with 0.1% formic acid. The gradient used starts with 1 minute at 1% B, increasing linearly from 1% to 50% B in 2.5 minutes, and then remaining at 50% B for 30 sec before the column was equilibrated with the initial conditions for 2 additional minutes, adding up to a run time of 6 minutes. The column and autosampler temperatures were set to 45 and 10 °C, respectively. The injection volume was set to 4 µL. Analysis was performed on a XEVO TQ-S triple quadrupole mass spectrometer (Waters) equipped with an electrospray source operated in positive mode. Nitrogen was used as the desolvation (800 L/h, 450 °C) and collision gas. Data were acquired in the multiple reaction monitoring (MRM) mode, with the settings of the precursors, fragments, cone voltages and collision energies for each compound. Waters MassLynx 4.1 and TargetLynx 4.1 software were used for data acquisition and processing, respectively. A paired t-test was used to compare the levels of each neurotransmitter between the two genotypes.

This analysis was done in collaboration with Andrea Armirotti from Facility Analytical Chemistry and in vivo Pharmacology at Italian Institute of Technology.

Statistical analysis

The normality of the distribution of values was tested with the Kolmogorov–Smirnov test. Data are presented as the mean \pm standard error of the mean (SEM). As detailed above for the in vivo experiment, most data were analyzed using two-way ANOVA and Student's t-test as appropriate for the experimental design. If the P values reached statistical significance, Bonferroni adjustment was further applied for post hoc analysis. For the sleep analysis, Phenopy was used [133] while GraphPad Prism6 (GraphPad Prism Software, Inc.) was used for statistical analysis. Type I error (α) was set at 0.05 ($p < 0.05$). For MEA recordings, belonging to the in vitro experiment, data were analyzed using two-way repeated-measures ANOVA (factors=genotype x treatment) followed by Tukey's post hoc test. SigmaPlot software (Systat Software Inc.) was used for statistical analysis to compare data from two different populations, we performed the Mann-Whitney test, since data were not normally distributed.

3.3 Study III

Animals utilized in this study were the same used in the Study I and II. For more details regarding the animal husbandry, breeding, and genotyping see session 3.1 from Study I.

Experimental design and drug administration

For the study, mice with paternally inherited *Snord116* deletions (PWScr^{m+/p-}; n=20) and wild-type littermate control mice (PWScr^{m+/p+}; n=20) of 12 to 15 weeks of age were randomly assigned to two experimental groups:

- i. vehicle-placebo treatment
- ii. Pitolisant treatment.

To investigate the effect of Pitolisant in the sleep-wake cycle, PWScr^{m+/p+} mice (n=10) and PWScr^{m+/p-} mice (n=10) were implanted with electroencephalogram combined with electromyogram (EEG/EMG). EEG/EMG were recorded continuously for 24-hour for a baseline value (12-hour:12-hour dark-light cycle) and for the following 24-hour after either placebo or Pitolisant administration. The placebo (vehicle) consisted of 0.05 ml of NaCl at 0.9% containing dimethyl sulfoxide (DMSO; Sigma Aldrich) at 1%. Pitolisant (BF2.649, 1-[33]piperidine, hydrochloride) was provided by Pr. Stark H. (University of Düsseldorf, Germany) [131] the dosage used was 20 mg/kg as previously described [151]. Pitolisant was freshly dissolved in the vehicle, before each administration, and was administered orally using a mouse gavage probe (20G, Phymep, Paris) placebo/Pitolisant was administered at the beginning of the dark period (active phase for mice, Figure S1B), to preserve the homeostatic and circadian process of sleep. The order of administration was randomized. After a period of 7 days (washout-period) Pitolisant/placebo was again administered, to perform the neurochemistry analysis (Figure S1C).

Surgery and electrophysiological data analysis

To investigate the effect of Pitolisant in the sleep wake-cycle we implanted all animals with EEG/EMG electrodes. For more details regarding the surgical procedure and the electrophysiological data acquisition and analysis see the session 3.1 of the Study I.

Regarding the statistical analysis in this study, a two-way ANOVA with repeated measures on both factors (group x time) was used for the statistical analysis of two-hours averaged

time-course changes in the amount of each sleep stages (W, non-REM and REM sleep) and physical activity of the baseline together with the day when the two genotypes (+/+ vs -/-) received either Pitolisant or placebo. The statistical analysis of the cumulative amount of W, non-REM, and REM sleep over the dark and light periods among groups who received placebo or Pitolisant was carried out with two-tailed t-test. The cumulative amount of physical activity of both genotypes over the dark and light period at the BL and after treatment was assessed by one-way ANOVA. A paired t-test was used to compare the delta temperature for each genotype before and after treatment. A two-way ANOVA with repeated measures on both factors (group x Hz) was used for the statistical analysis of EEG power for REM and non-REM sleep in the corresponding light or dark periods at the BL and after administered Pitolisant.

Electrophysiological data analysis

See Electrophysiological data analysis session of Study I for the analysis of cortical EEG/EMG signals.

A two-way ANOVA with repeated measures on both factors (group x time) was used for the statistical analysis of two-hours averaged time-course changes in the amount of each sleep stages (W, non-REM and REM sleep) and physical activity of the baseline together with the day when the two genotypes (+/+ vs. -/-) received either Pitolisant or placebo. The statistical analysis of the cumulative amount of W, non-REM, and REM sleep over the dark and light periods among groups who received placebo or Pitolisant was carried out with two-tailed t-test. The cumulative amount of physical activity of both genotypes over the dark and light period at the BL and after treatment was assessed by one-way ANOVA. A paired t-test was used to compare the delta temperature for each genotype before and after treatment. A two-way ANOVA with repeated measures on both factors (group x Hz) was used for the statistical analysis of EEG power for REM and non-REM sleep in the corresponding light or dark periods at the BL and after administered Pitolisant.

Statistical analysis

Gaussian distribution of values was tested with the Kolmogorov–Smirnov test. Data was presented as mean \pm standard error of the mean (SEM). As detailed above, the majority of the data was analyzed using two-way ANOVA and t-test as appropriate for the

experimental design. If the F values reached statistical significance, Turkey adjustment or least significant differences (LSDs) were further applied for post-hoc analysis, as appropriate for the number of comparisons. For the sleep, temperature and physical activity analysis Phenopy was used [133], while GraphPad Prism6 (GraphPad Prism Software, Inc) was used for statistical analysis. Type I error α was set at 0.05 ($p < 0.05$).

Chapter 4

Results

4.1 In the **Study I**, we investigated whether *Snord116* may play a role in the hypothalamic formation and in the regulation of the biological and homeostatic control of sleep.

4.1.1 Loss of paternal *Snord116* alters neuronal dynamics in the LH associated with sleep homeostasis

To investigate whether the firing pattern of neurons within the LH manifests signs of paternal-dependent subcortical regulation throughout different arousal states of the brain, we studied mice with paternal deletion of the *Snord116* gene [97], PWScr^{m+/p-} mice, and their wild-type littermate controls, PWScr^{m+/p+} mice. We identified neurons in the LH that are time-locked (see Methods and Figure 4A-F for full details on the procedure) to sleep (S-max) and to wake (W-max) states and to food intake (Type I, II and III). Strikingly, we observed a significant increase in S-max and a reduction in W-max neurons in PWScr^{m+/p-} mutant mice compared with controls at baseline (Figure 4G and supplementary Table 2). A more detailed analysis of B1 and B2 confirmed this distribution of the classes of LH neurons according to EEG states (Figure S2B and supplementary Table 2). Moreover, when the pressure of sleep is low (i.e., B1), mutant mice exhibit more REM sleep than their littermate controls (Figure S2A). This finding suggests that the pressure/need of sleep may be either a permissive or a blocking mechanism with respect to excess REM sleep due to the lack of *Snord116*. This phenomenon is confirmed by the profile of the power densities in REM sleep (Figure S2C). Indeed, in PWScr^{m+/p-} mutant mice, the theta (4.5-9 Hz) band, which is characteristic of REM sleep, is higher in both B1 and B2, but at B2, the EEG frequency phenotype is not accompanied by longer REM sleep duration, implying that the overall higher sleep pressure masks differences in microstructural aspects of electrophysiological sleep. Moreover, the delta (0.5-4.5 Hz) band presents an opposite trend in the two groups of animals; counterintuitively, reduced power is observed in mutant mice as the pressure of sleep increases (Figure S2C). Again, this phenomenon suggests abnormal homeostatic control of sleep in mutant mice.

Thus, we sought to explore the physiological responses of mice following 6-hour of total sleep deprivation (SD) by investigating the distributions of the neuronal classes at different time points during 18-hour of recovery (i.e., SD1, SD2 and SD3, Figure 4B). We observed that SD induced an increase in S-max neurons in wild-type $PWScr^{m+/p+}$ mice, while in mutant $PWScr^{m+/p-}$ mice, the distribution of classes of neurons remained unaltered compared with baseline (Figure 4G). This result indicates that control mice homeostatically respond to SD by modulating LH neuronal dynamics, as previously reported in the literature [152], while mutant mice lack this hypothalamic modulatory process.

Across different conditions, neurons may continue responding to the same state, may respond to different state, or may become aspecific in their activity. Within the rearrangements of neuronal modulation across different phases, an interesting observation in this study is represented by the behavior of the non-responding neurons following SD (Figure S2A, supplementary Table 2). In wild-type mice after SD, the number of neurons of this latter class increases three times compared with the previous baseline, a phenomenon that is gradually recovered over the following 18-hour after deprivation. This change comes with a cost for wake-dependent neurons in wild-type animals. In $PWScr^{m+/p-}$ mutants, this SD effect is missing, reinforcing the observation of a lack of neuromodulation caused by the paternally derived genetic defect.

Finally, the dramatic drop in delta and theta power densities in $PWScr^{m+/p-}$ mutant mice compared with controls at SD2 (Figure S2C) coincides with the permissive role of sleep pressure at this time of the day for the sleep defects in mutants.

4.1.2 OX putative neurons are reduced in $PWScr^{m+/p-}$ mutants compared with controls

The LH is made by a heterogeneous group of cells that express various neuropeptides, such as OX and MCH neurons. To gain insight about the heterogeneous nature of these recording units, we plotted the mean firing rate versus the mean logarithm of the EMG signals across three groups of putative neurons (W-max; S-max and ws neurons) of the whole sleep experiment (Figure S2D). The graphical representation of these neurons within the 2D scatter plot enables us to distinguish between MCH putative and OX putative neurons. MCH putative neurons fire maximally during REM sleep and are thought to present a low EMG amplitude and a low average discharge rate of 1.1 ± 0.26 Hz, while

OX putative neurons fire maximally during wake and are characterized by a high firing rate, 3.17 ± 0.79 Hz, as both classes of neurons were previously described [153]. Based on these criteria, we assessed MCH putative and OX putative neurons between PWScr^{m+/p+} wild-type and PWScr^{m+/p-} mutant mice. The percentage of recorded MCH putative neurons was unchanged between the two genotypes; although non-statistically significant, a total of 211 OX putative neurons were identified in PWScr^{m+/p-} mutant mice compared with 315 OX putative neurons identified in control mice. This observation suggested that PWS mutants may express a reduced number of OX neurons in the LH (Figure S2D).

4.1.3 A high proportion of neurons in the LH do not respond to food intake in PWScr^{m+/p-} mutant mice

Mice underwent food deprivation (FD) during the dark period/resting phase (Figure 4B) to increase their drive for food intake. When food was made available again, pellets were automatically provided in the home cages of each mouse (see Methods). The frequency of nose-poke activity to gain food was similar between the two genotypes (PWScr^{m+/p-}: 107 trials; PWScr^{m+/p+}: 116 trials), indicating no obvious behavioural differences between the two genotypes, as previously described [154], [155]. As for the sleep experiment, the attention fell on the distribution of neuronal modulation between the two genotypes.

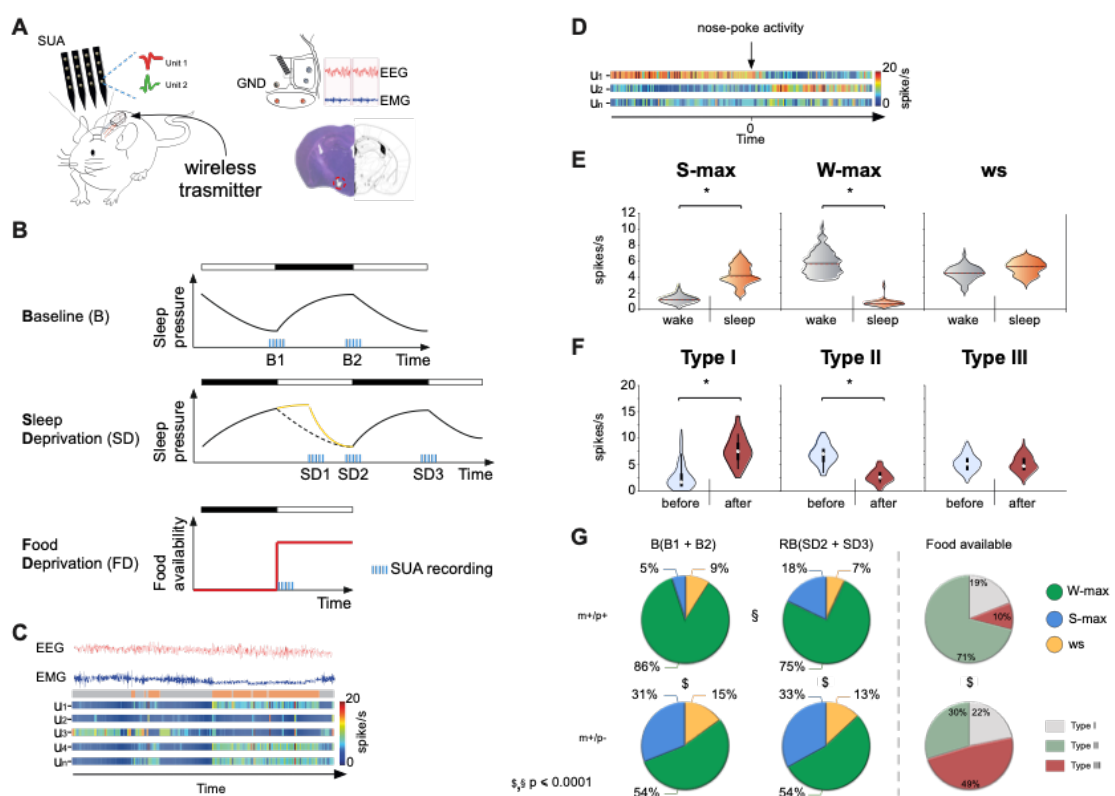


Figure 4, Loss of paternal Snord116 alters neuronal dynamics in the LH associated with sleep and food.

A) The cartoon on the left shows mice chronically implanted with a microwire array of 16 channels with an EEG-EMG wireless transmitter to record the sleep-wake cycle. On the right, a schematic representation of the mouse skull depicting EEG, EMG (red circle) and single unit activity (SUA) in the contralateral hemisphere is shown. The correct placement of the SUA electrode was histologically verified by 40- μ m Nissl-stained coronal brain sections (bregma $-1.10/-1.90$). **B)** The panel shows a schematic representation of the experimental design used to record SUA and the sleep-wake cycle in relation to sleep pressure depicted by EEG/EMG. Recordings were performed at two different baseline (BL) time points (B1 and B2) over the first hour of the rebound period (SD1) following 6-hour of total sleep deprivation (SD) and at other two time points over the 18-hour recovery period (SD2 and SD3). Each recording is 2-h, except for SD1 (1-hour). Each recording is represented by cyan bars. After 5 days of recovery from the previous SD, the animals were fasted for 12-hour during the dark period and fed at the beginning of the light period. Food pellets were provided only after a nose-poke activity. SUA was continuously recorded for 2-hour after being fed. The black bar indicates the dark period of the light/dark cycle, while the white bar indicates the light period of the cycle. **C)** The panel shows an example of EEG/EMG traces with the sleep stages identified (wakefulness is represented in grey, while sleep, including both NREM and REM sleep stages, is shown in orange) aligned with the firing rate recorded in the LH. The heatmaps at the bottom show the response firing rate in spikes/second from 0 Hz (blue) to 20 Hz (red). **D)** The heatmaps show the response firing rate used to classify neurons before and after food consumption (firing rate in spikes/second from 0 Hz [blue] to 20 Hz [red]). **E)** Violin plots of classified units according to the sleep-wake states in which they maximally fired according to ANOVA followed by post hoc Bonferroni correction ($p < .05$) see Methods. **F)** Violin plots of classified units according to their discharge related to food consumption (paired Student's t-test of the firing rate between before and after the pellet was released, binned at 50 ms, $p < 0.05$). See Methods. **G)** The pie chart represents the distribution of recorded neurons according sleep-wake stage: wake (W-max), sleep (both NREM and REM sleep, S-max) and not responding (ws). The rows show the two genotypes (PWScr^{m+/p+} on the top and PWScr^{m+/p-} on the bottom), while the columns show the different recording time points, B, RB and food. According to the neuronal classification (see Methods), W-max neurons are shown in green, S-max neurons are shown in blue, and ws neurons are shown in yellow. Type I, neurons that fire maximally immediately after nose-poke activity and during feeding shown in grey; Type II, neurons that show a sharp increase in firing rate at the beginning of feeding shown in green; Type III, neurons that do not respond to food shown in red. Differences between the two genotypes are indicated by \$, while differences within groups across time points are indicated by §. Significance was computed with the chi-square test; for details on the statistical analysis, see Table S2, S3 and S4. The two genotypes investigated were PWScr^{m+/p-} mice (n=4) and PWScr^{m+/p+} mice (n=4).

We found that PWScr^{m+/p-} mutant mice had less than half the number of type II neurons, which have reduced firing during food intake, of control mice (Figure 4G). This reduction

may be explained by the fact that mutant mice had twice as many non-responding neurons as control mice. Indeed, type I neurons were almost identical in the two groups (supplementary Table 2). These results also suggest for an abnormal distribution of OX neurons in the LH of mutants, as OX neurons drive food intake.

4.1.4 Sleep homeostasis is disrupted in PWS mutant mice

We explored the 24-hour EEG profile of sleep (see Methods) and the responses to sleep loss in a different cohort of animals.

The results confirmed our previous observations that sleep is altered in the PWS mutants [100]. In particular, REM sleep is increased in $PWScr^{m+/p-}$ mutants compared with controls, showing a peak increase at ZT (Zeitgeber Time) 20 and an overall increase in theta power (Figure 5A). These experiments were conducted at standard room temperature of 22°C. Interestingly, the theta profile in mutants did not show circadian rhythm (Figure 5A); $PWScr^{m+/p-}$ mutants had an increase in theta power during the transition between light and dark, when the pressure of sleep is low. Overall, REM sleep abnormalities remained a selective phenotype in these mutants, while the other EEG-determined arousal states were unchanged between the two genotypes (Figure S3A).

Moreover, we tested for the first time the homeostatic EEG response following SD in $PWScr^{m+/p-}$ mutant mice compared with littermate controls. Compared with control mice, $PWScr^{m+/p-}$ mice showed reduced delta activity during non-REM sleep rebound following SD (Figure 5B), although the total amount of non-REM sleep was unaltered over the long-term recovery process (Figure S3A). Notably, delta power is the best electrophysiological marker of sleep propensity, although the temporal distribution of its rebound following SD is less characterized. The behavior of delta sleep in mutant mice suggests a dysregulation in the daily distribution of sleep pressure in these mice.

These results also showed a significant decrease in REM sleep during the first 2-hour of rebound in mutants compared with controls (Figure 5A), confirming both the alteration of homeostatic control in mutants and the alteration of REM sleep.

4.1.5 Thermoneutrality does not increase REM sleep in mutants

REM sleep is an evolutionarily recent physiological state of sleep that, in mammals, is largely dependent on the environmental temperature [156], [157]. The maximum REM

sleep expression in mice is attained when the environmental temperature is near 29°C. The latter represents a thermoneutral zone (TNZ) for this species [158].

In a new set of experiments, we modified the temperature environment of the animals to allow the duration of REM sleep to reach a maximum [158]. Mice were housed for 5 weeks at 30°C, and then, EEG/EMG were recorded for 24-hour at the TNZ. Mutant mice showed a significant increase in all sleep stages (Figure S3A-B) compared with wild-type mice, but REM sleep did not significantly increase in the mutant mice, perhaps due to the high REM sleep percentage at baseline (Figures 5A, S3C and S3D). However, PWScr^{m+/p-} mutant mice maintained a significant increase in REM sleep compared with controls at ZT 20 (Figures 5A and S3A).

4.1.6 Peripheral thermoregulatory responses are absent in PWS mutants

We tested whether loss of paternally expressed *Snord116* affects peripheral responses and whether these changes impact the overall body temperature and body weight of the animals. We monitored the peripheral and cutaneous body temperature at the head (T-head) and tail (T-tail), and consequently, we derived the heat loss index (HLI) (see Methods). Recordings were made at room temperatures of both 22°C and 29-30°C (TNZ). The TNZ imposes body temperature adjustments by changing the vasomotor tone in specialized heat exchange organs, such as the tail, in mice [159]. We observed an increase in the vasculature tail skin tone at the TNZ in both genotypes compared with 22°C (Figure 5C, upper panel). However, greater tail vasodilatation was observed in control mice, particularly between the switch from light to dark periods. These results indicate that while at TNZ, wild-type control mice present a proper peripheral thermoregulatory response when the pressure of sleep is low, which is instrumental in maintaining the core body temperature of the animal at this time of the day, mutant mice lack such an important physiological response. A significant increase in the HLI was recorded in both genotypes, but a greater increase was found in PWScr^{m+/p+} wild-type mice than in mutant mice (Figure 5C, middle panel). We also observed that the peripheral body temperature recorded at 22°C increased in PWScr^{m+/p-} mutant mice compared with control mice during the light period (Figure 5C, bottom panel), suggesting a lack of homeostatic control when sleep is physiologically facilitated in mice. Moreover, mutant mice failed to show the circadian oscillatory profile of temperature at RT that is present in PWScr^{m+/p+} mice.

However, at TNZ, the difference between the two genotypes during the light period was no longer observed. Furthermore, in agreement with previous reports [155], we observed that $PWScr^{m+/-}$ mutant mice had a smaller body size when kept at 22°C (Figure S4). Interestingly, the smaller body size was observed both when the mutant mice were exposed to 30°C later in their development (e.g., for only 5 weeks) and when they were exposed to the TNZ from birth and kept at the TNZ for up to 20 weeks of age (Figure S4). However, while the former 5-week experimental strategy resulted in an increase in body weight in both cohorts of animals, which was more pronounced in wild-type animals than in mutants, the latter (birth) strategy resulted in no changes over time according to temperature (Figure S4). Notably, maintaining at the TNZ from birth resulted in an overall body weight in mutants that was comparable to the body weight at RT. The latter observation suggests that the TNZ is a condition that permits an increase in body weight in PWS animals, although this cannot neutralize the differences with wild type animals under the same conditions.

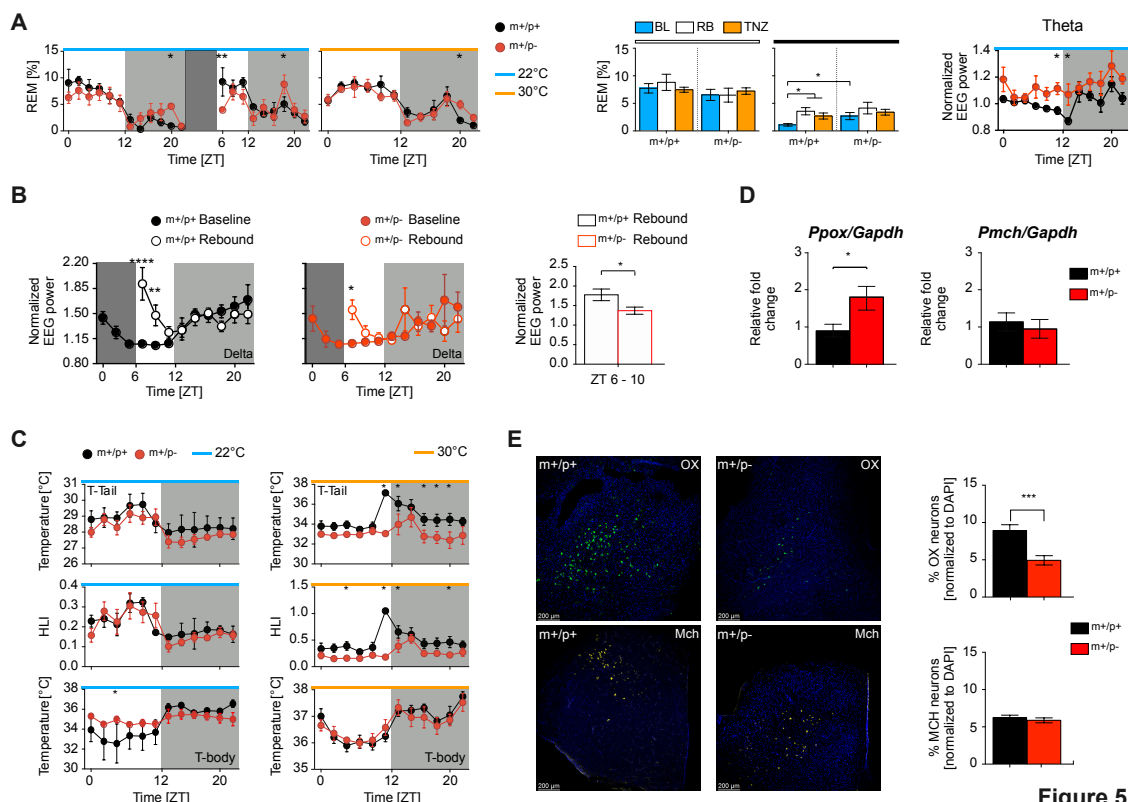


Figure 5

Figure 5, Snord116 influenced REM sleep and its homeostatic regulation, thermoregulatory response via the orexin system. A) Left panel, REM sleep distribution over an uninterrupted 24-hour period over a 12-h light/dark cycle as baseline values and the following 18-hour after total SD. Recordings were made with animals maintained at 22°C (cyan bar in the graph) or at 30°C (orange bar in the graph).

REM sleep was significantly altered in mutant mice relative to control mice at baseline and over the recovery period following 6-h of SD (two-way ANOVA: $F(20, 160) = 8.66$ $p < 0.0001$; “time”; $F(8, 160) = 3.33$; $p < 0.001$; “genotypes”). REM sleep was also altered in mutant mice relative to control mice when the sleep-wake cycle was recorded at the TNZ (two-way ANOVA: $F(11, 88) = 11.61$ $p < 0.0001$; “time”). Data are reported as the percentage in 2-hour bins, averaged within genotypes (mean \pm SEM; $n = 5$ PWScr^{m+/p+} and $n = 5$ PWScr^{m+/p-} mice). PWScr^{m+/p-} mice are represented by red circles, while control mice are represented by black circles.

Middle panel, the cumulative amount (mean \pm SEM) of REM sleep during the 12-hour of the light period (white bar above the bars) and during the 12-hour of the dark period (black bar above the bars) for the three groups investigated (recordings at 22°C are shown in blue, after 6-h of SD in white and at 30°C in orange). The within-group statistical analysis was performed by one-way ANOVA, followed by a post hoc analysis with the Bonferroni multiple comparison test. During the dark period, PWScr^{m+/p-} mice showed an increase in REM sleep ($F(1.85, 4.74) = 18.06$, $p = .0082$). Student’s unpaired t-test between genotypes indicates an increase in REM sleep in PWScr^{m+/p-} mutant mice relative to PWScr^{m+/p+} mice ($t(8) = 2.30$, $p = .04$). The right panel shows the spectral analysis. Theta power at 22°C between genotypes. The theta power of each subject was normalized by the mean of the last 4-hour of the light period. Theta power during REM sleep was increased in PWScr^{m+/p-} mice (two-way ANOVA: $F(11, 88) = 3.08$, $p < .001$ “time”; $F(1, 8) = 8.04$, $p = .02$ “genotypes”). Data are reported in 2-hour bins and are shown as the mean \pm SEM. **B**) The panel shows the delta power at 22°C between baseline vs rebound for PWScr^{m+/p+} and PWScr^{m+/p-} mice. The delta power of each subject was normalized by the mean of the last 4-hour of the light period. Wild-type mice displayed a significant increase in delta power following SD from ZT 6 to ZT 10 (two-way ANOVA: $F(11, 88) = 28.77$ $p < 0.0001$ “interaction”), while mutant mice showed a mild increase only at ZT 6 (two-way ANOVA: $F(11, 88) = 12.25$ $p < 0.0001$ “interaction”). Data are reported in 2-hour bins and are shown as the mean \pm SEM. Right panel, the average of the first 4-h of recovery after SD between the two genotypes for the delta power. PWScr^{m+/p-} mice showed lower delta than PWScr^{m+/p+} mice (unpaired t-test: $t(8) = 2.31$, $p = .04$). Values are reported as the mean \pm SEM. Asterisks (*) indicate a significant difference between genotypes: * $P \leq .05$; ** $p \leq .01$; *** $p \leq .001$; **** $p \leq .0001$. Two genotypes were investigated: PWScr^{m+/p-} mice ($n = 10$, 5 mice at 22°C and 5 mice at 30°C) and PWScr^{m+/p+} mice ($n = 10$, 5 mice at 22°C and 5 mice at 30°C). **C**) Temperature profile for PWScr^{m+/p+} and PWScr^{m+/p-}. The top panel shows the T-tail profile recorded with an infrared thermocamera over 24-hour. Recordings were performed under two different environmental conditions: at 22°C (cyan bar over the graph, shown on the left) and at 30°C, corresponding to the thermoneutrality zone (TNZ) (orange bar over the graph, shown on the right). Middle panel, the heat loss index (HLI) was calculated according to the following formula: $\frac{(T_{-brain}) - (T_a)}{(T_{-tail}) - (T_a)}$ (see Methods) and assessed at 22°C (left) and at the TNZ (right). Bottom panel, the core body temperature profile recorded simultaneously with EEG over 24-hour was recorded using a telemetric system in which the probe was subcutaneously implanted. PWScr^{m+/p-} mice are represented by red circles, while PWScr^{m+/p+} mice are represented by black circles. Values are expressed as a 2-hour mean \pm SEM. At 22°C, no differences were observed between the two genotypes for T-tail and HLI.

PWScr^{m+/p-} mice showed an increase in body temperature during the light period at ZT 6 at 22°C (two-way ANOVA: $F(11,88) = 3.53$, $p = .0004$ “time”; $F(11,88) = 7.86$, $p = <.0001$ “genotypes”). At 30°C, T-tail (two-way ANOVA: $F(11,88) = 2.68$, $p = <.0001$; “interaction”) and HLI (two-way ANOVA: main effect of time-of-day, $F(11,88) = 4.72$, $p = <.0001$ “interaction”) were increased in PWScr^{m+/p-} mice relative to mutant mice. No differences in body temperature were observed at 30°C. Asterisks (*) indicate a significant difference between genotypes (* $P \leq .05$). Two genotypes were investigated: PWScr^{m+/p-} mice ($n = 10$, 5 mice at 22°C and 5 mice at 30°C) and PWScr^{m+/p+} mice ($n = 10$, 5 mice at 22°C and 5 mice at 30°C). **D)** Ppox and Pmch gene expression analysis in PWScr^{m+/p-} mice versus controls. PWScr^{m+/p-} mice (red bar) showed an increase in Ppox (unpaired t-test: $t(8) = 2.49$, $p = .03$) compared with PWScr^{m+/p+} mice (black bar).

No differences in the mRNA Pmch level was observed between the two genotypes. Values are reported as the mean \pm SEM. Asterisks (*) indicate a significant difference between genotypes: * $P \leq .05$. **E)** Cell count distribution of orexin (OX) immunoreactive neurons (upper) and melanin concentrate hormone (MCH) immunoreactive neurons (below) in the lateral hypothalamus of PWScr^{m+/p-} mice (right) versus controls (left). Coronal sections were stained with OX- and MCH-specific antibodies, counterstained with DAPI and scored. Values are expressed as the percentage of positive neurons relative to all stained nuclei (mean \pm SEM). The number of OX⁺ neurons was reduced in the PWScr^{m+/p-} mouse group (unpaired t-test: $t(33) = 3.85$, $p = .0005$). No differences were found in the number of MCH⁺ neurons. Asterisks (*) indicate a significant difference between genotypes: *** $p \leq .001$. Two genotypes were investigated: PWScr^{m+/p-} mice ($n=4$) and PWScr^{m+/p+} mice ($n = 4$).

4.1.7 Lack of Snord116 impairs the OX system in the LH

To assess the regulation of the main neuropeptides in the LH, we examined the expression of OX and MCH. Thus, we assessed the precursor of MCH (Pmch) and the prepro-OX (Ppox). I examined three conditions (Figure S5A): at ZT 6, we tested both the baseline condition (T0) and the effects of SD (T1); and at ZT 7, 1-hour after SD (T2), we tested the effects during the recovery from the loss of sleep.

We observed that PWScr^{m+/p-} mutant mice showed a significant increase in Ppox at T0 baseline compared with control mice, while Pmch was unchanged in both genotypes at T0 (Figure 5D). At T1, both Ppox and Pmch were significantly reduced in PWScr^{m+/p-} mice compared with control mice (Figure S5B), confirming that the homeostatic response in mutants is reduced and that these two systems are dysregulated in mutant mice. At T2, the difference between the two genotypes for Ppox and Pmch was reestablished (Figure S5B), confirming that the effects of SD in mutants are only acute and follow the immediate response after sleep deprivation.

Then, we evaluated the receptors. We assessed mRNA levels of OX receptor-1 (Ox1R) OX receptor-2 (Ox2R) and MCH receptor 1 (Mch1R) in the hypothalamus and in other brain areas as control measures. The expression levels were overall unchanged between the two genotypes, except for Ox2R in the parietal cortex (Figure S5C).

The overall contrast between neuropeptides and the mRNA levels of their receptors prompted us to quantify whether these chemical changes within the OX and MCH systems had consequences for the organization of the neuronal populations of the LH. We observed a significant reduction in OX neurons in the LH of PWScr^{m+/p-} mutant mice (PWScr^{m+/p+} mice 95 ± 9; PWScr^{m+/p-} mice 53 ± 10; p = .0005; Figure 5E), while MCH neurons, which are located near the OX neurons, were unaffected (PWScr^{m+/p+} mice 66 ± 5; PWScr^{m+/p-} mice 63 ± 5; Figure 5E). The discrepancy between the increased Ppox and the reduced neuronal population may be due to a mechanism to compensate for the low number of neurons with an overproduction of the peptide.

4.1.8 Loss of *Snord116* leads to transcriptional reprogramming in the hypothalamus

Next, we investigated whether the loss of *Snord116* affects overall gene expression in the hypothalamus of PWScr^{m+/p-} mutant mice compared with PWScr^{m+/p+} control mice by performing RNA sequencing (RNA-seq). The mice were investigated at the beginning of the light period ZT 0 (group 1, G1), 6-hour later at ZT 6 (group 2, G2) and at ZT 6 but following 6-hour of SD (group 3, G3). First, we sought to identify the differentially expressed genes (DEGs) between the two genotypes in the G1 group. We identified 4777 downregulated genes and 4271 upregulated genes between genotypes (adjusted p < 0.05; see Methods) and a minimum fold change of 2 (supplementary Table 4). Next, we compared the down- and upregulated DEGs (Figure 6A-B) in G1 PWScr^{m+/p-} mutant mice with DEGs derived from post-mortem hypothalamic data from PWS patients vs normal patients [160]. More than 40% of human DEGs overlapped with mouse DEGs, suggesting that loss of *Snord116* recapitulates approximately 40% of the transcriptional changes found in the human hypothalamus. To more closely evaluate the functional importance of these overlapping DEGs, we performed gene ontology (GO) enrichment analysis using Metascape [161]. We found enrichment of several biological processes important for normal neural functions among the downregulated DEG genes, while inflammatory

systems were the processes significantly enriched among the upregulated DEGs (Figure 6A-B).

Interestingly, we found that *Ppox* was significantly downregulated in *PWScr^{m+/p-}* mutant mice and in human PWS patients (Figure 6C), confirming that OX is involved in the abnormal regulation of REM sleep in PWS.

Then, we focused on how SD affects gene expression in the hypothalamus in both normal and *PWScr^{m+/p-}* mutant mice. We compared DEGs in G2 versus G3 of each genotype (Figure 6D). We found that 6-hour of SD largely influenced the transcriptome of mutant mice (i.e., 833 DEGs) compared with control mice (i.e., 30 DEGs). Surprisingly, in the mutant dataset, most of the DEGs were downregulated (804 genes downregulated vs 29 upregulated). GO analysis of all 833 DEGs revealed enrichment of cell organization, development and growth-related processes (Figure 6E), indicating that poor sleep negatively impacts the hypothalamus in PWS subjects. Finally, we investigated the RNA-seq dataset to determine whether *Snord116* loss significantly affects the expression of imprinted genes in humans and mice (refer to supplementary Table 4). Maternally expressed imprinted genes, such as *Meg3*, *Gnas*, and *H19*, as well as paternally expressed imprinted genes, such as *Nap115* and *Peg3*, were differentially expressed in mutant mice before and after SD (Figure 6F).

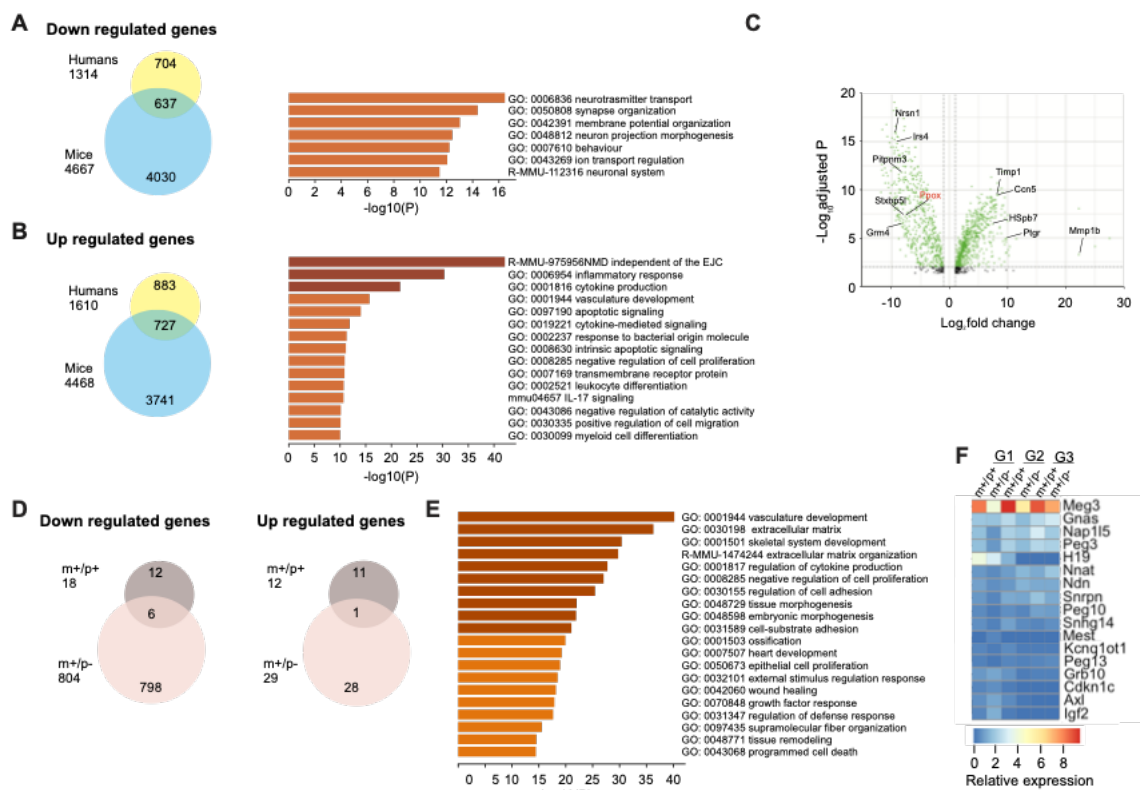


Figure 6

Figure 6, Snord116 loss significantly impacts molecular machinery in the hypothalamus. A-B) Venn diagrams illustrating the number of differentially expressed genes (DEGs) that are down- (A) and upregulated (B) in the hypothalamus of Prader–Willi syndrome (PWS) $PWScr^{m+/p-}$ mice relative to control mice and that overlap in human patients (according to [160]). The results of gene ontology (GO) enrichment analysis of biological processes for the overlapping DEGs are also shown in both A and B. **C)** Volcano plots of 637 and 727 DEGs in $PWScr^{m+/p-}$ mice in group 1 (G1; non-sleep deprived). **D)** Significantly down- and upregulated genes in the hypothalamus of $PWScr^{m+/p-}$ mutant mice compared with $PWScr^{m+/p+}$ control mice affected by sleep deprivation (G2 vs G3). **E)** GO enrichment analysis of biological processes for 833 (804 down- and 29 upregulated genes in panel D) DEGs in $PWScr^{m+/p-}$ mutant mice that are significantly affected by sleep deprivation. **F)** Heatmap of the relative expression of imprinted genes common in humans and mice assessed in $PWScr^{m+/p-}$ mutant mice compared with the $PWScr^{m+/p+}$ mice in G1, G2 and G3. See also Tables S5.

4.1.9 OX regulation in the hypothalamus depends on two paternally expressed genes, *Snord116* and *Peg3*

We next sought to confirm selected physiologically relevant DEGs identified within the RNA sequencing dataset by qRT-PCR. Among maternally and paternally imprinted genes that were altered in the hypothalamus of $PWScr^{m+/p-}$ mutant mice, *Peg3* was the only confirmed gene, showing a remarkable increase in expression in $PWScr^{m+/p-}$ mice (Figure 7A) compared with the control mice (Figure S6A). *Peg3* binds to DNA based on its multiple zinc finger motifs and nuclear localization [162], [163]. Interestingly, a recent study found an association between *Peg3* and OX expression [164]. However, whether *Peg3* is able to bind and regulate the expression of OX in living mice remains unclear. We noticed that two conserved promoter regions within a 3.2-kb fragment located upstream of the *Ppox* gene (Figure S6F) target specific expression within the LH [165]. We showed that PEG3 binds one of these regions. Specifically, chromatin immunoprecipitation analysis (ChIP) [166] followed by quantitative real-time PCR (ChIP qRT-PCR, and Figure 7A) revealed that PEG3 binds the 2.5 kb OX regulatory element region in the hypothalamic mouse brain. Interestingly, a significant reduction in PEG3 binding was observed in $PWScr^{m+/p-}$ mice (Figure 7A), which may be associated with a significant reduction in OX-expressing neurons in mutant mice. These results show that PEG3 positively regulates the expression of *Ppox* by enhancing its expression, as indicated by the presence of a strong enrichment of the H3K4me2/3 in the same region (Figure 7A). Conversely, H3K27me3, which is a

marker of condensed chromatin [167], showed no enrichment in either genotype. The GAPDH promoter was used as a negative control for the ChIP experiment (Figure S6E). These data reinforce the evidence that PEG3 contributes to the regulation of Ppox by enhancing its expression (Figure 7A).

Then, we sought to investigate whether *Peg3* or *Snord116* plays any causal role in the regulation and formation of OX neurons, and we assessed the expression of these two genes in OX-deficient mice. Specifically, we used two genetic mouse models of OX deficiency, Ppox knockout (KO) mice [130] and OX neuron-ablated (ataxin-3 [Atx]) mice [168] (Figure 7B).

Atx mice selectively degenerate postnatally, and a loss of 99% of neurons or more occurs by the age of 4 months [168]. Therefore, in Atx mice, not only are OX neurons ablated, but co-transmitters are also eliminated [169]. Conversely, KO mice are only deficient in Ppox (Figure 7B).

Interestingly, we observed that *Peg3* was significantly increased in Atx mice compared with KO mice ($p = .03$). Moreover, *Snord116* was also increased in Atx mice compared with KO mice and control mice ($p = .03$; Figure 7B). Other imprinted genes tested were unchanged between genotypes (Figure S6B). These data suggest that dysregulation of both *Snord116* and *Peg3* are important and associated with the physiological maintenance of OX neurons. Indeed, we observed that both genes were significantly altered only in narcoleptic mice, in which OX neurons and their co-transmitters were ablated, but not in narcoleptic mice lacking only Ppox.

Finally, to test whether the alteration of *Peg3* observed in the *PWScr^{m+/p-}* mice and in the Atx mice is linked to the absence of *Snord116* and whether *Snord116* modulates the expression of *Peg3*, we used an RNA-interfering approach aimed at silencing *Snord116* in immortalized embryonic rat hypothalamus cells (embryonic rat hypothalamus cell line R7).

Specifically, cells transfected with a *Snord116*-specific siRNA showed significant *Snord116* inhibition of approximately 80% at 48-hour after transfection (Figure 7C). However, the levels of *Peg3* were unchanged (Figure 7C), indicating that *Snord116* does not regulate the expression of the *Peg3* gene. *Pmch* and *Snurp* were also unchanged (Figure S6).

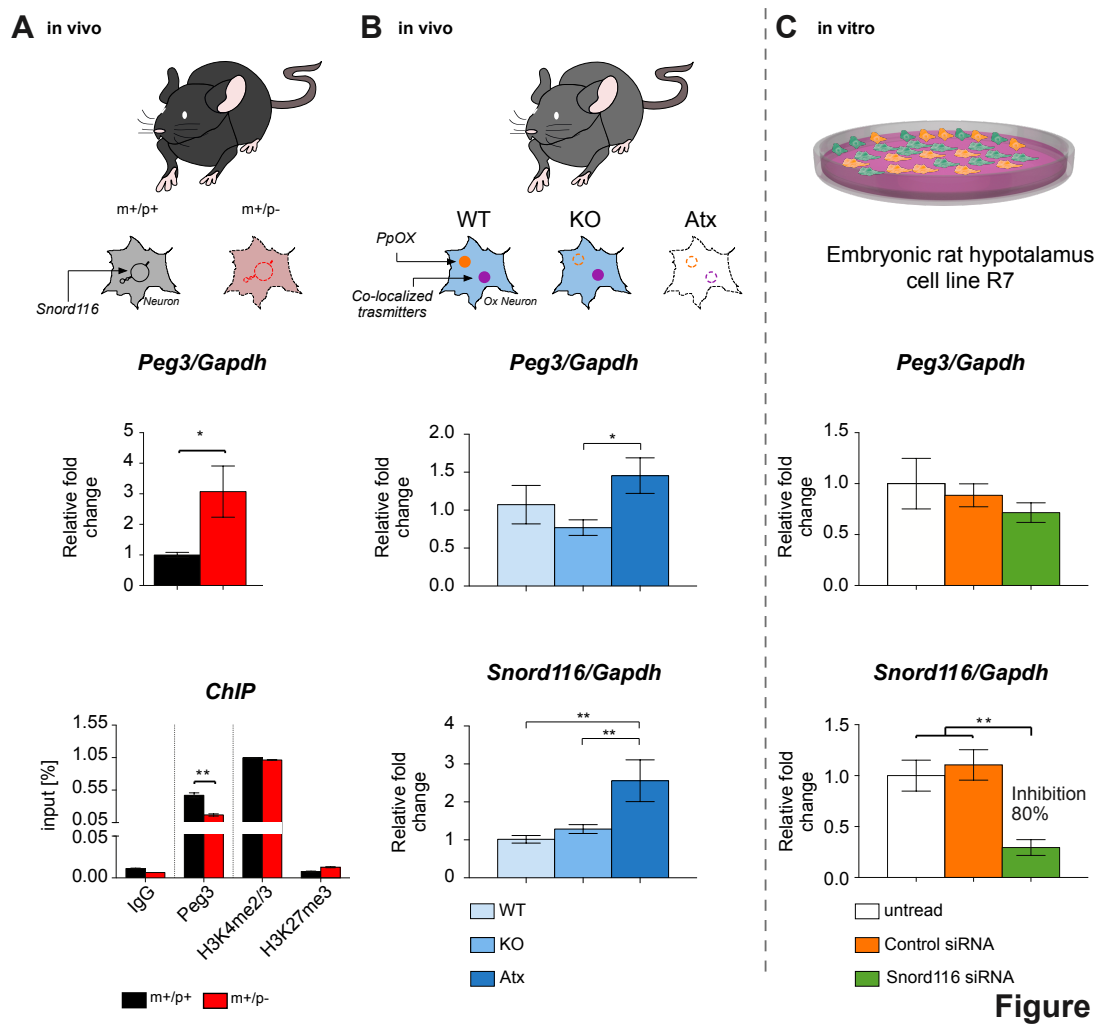


Figure 7

Figure 7, Snord116 and Peg3 play roles in the formation and maintenance of OX neurons.

Peg3 regulates orexin expression in an independent manner from paternal *Snord116*. **A)** Upper panel, the gene expression analysis of *Peg3* in *PWScr^{m+/p-}* mice (red) versus controls (black). *Peg3* mRNA assessed by qRT-PCR was significantly increased in *PWScr^{m+/p-}* mice compared with *PWScr^{m+/p+}* mice (unpaired t-test: $t(6) = 2.45$, $p = .04$). Values expressed are relative to the wild-type control mean \pm SEM. *Gapdh* was used as a housekeeping gene; see Methods. Asterisks (*) indicate a significant difference between genotypes. Bottom panel, ChIP analysis of PEG3 binding to the *Ppox* promoter region in *PWScr^{m+/p-}* mice (red) versus controls (black). PEG3 binding was lower in *PWScr^{m+/p-}* mice than in *PWScr^{m+/p+}* mice (unpaired t-test: $t(2) = 7.11$, $p = .01$). Values are expressed as the mean of the input \pm standard deviation. Asterisks (*) indicate a significant difference between genotypes. Figure 7

B) *Peg3* gene expression (upper panel) and *Snord116* gene expression (bottom panel) in *Ppox* knockout (KO) and orexin neuron-ablated (ataxin-3 [Atx] mice). One-way ANOVA indicated that *Peg3* was significantly increased in Atx mice relative to KO mice, ($F(2,16) = 0.02$, Bonferroni post hoc test $p = .03$). *Snord116* was increased in Atx mice relative to KO and control mice (WT) (one-way ANOVA $F(2,16) = 3.50$, Bonferroni post hoc test $p = .002$). Values are reported as the mean \pm SEM. Asterisks (*) indicate a significant difference between genotypes.

The following genotypes of narcoleptic mice were investigated: WT (n=4), KO (n= 12) and Atx (n=4). **C)** *Snord116* and *Peg3* gene expression analysis in the *Snord116*-siRNA-treated immortalised hypothalamic rat cell line. *Snord116*-siRNA (green bars) reduced the expression of the *Snord116* gene compared with untreated cells or scrambled siRNA-treated cells (white and orange bars) (one-way ANOVA: $F(2, 6)= 11.36$, Bonferroni post hoc test $p = .009$). *Peg3* mRNA levels were unchanged, similar to *Snord116*-SiRNA, in untreated cells and scrambled siRNA-treated cells. The experiment was conducted in triplicate. Data are presented as the mean \pm SEM. Asterisks (*) indicate a significant difference between genotypes: * $P \leq .05$; ** $p \leq .01$.

4.2 In the **Study II**, we investigated the role of *Snord116* in the regulation of the macrostructural sleep aspects and in the brain-circuits involved such as the thalamic reticular nucleus (TRN)/ thalamus circuits or in corticothalamic afferents.

4.2.1 Paternal *Snord116* deletion impacts the macrostructural sleep aspects in mice

Since the EEG analysis in the Study I highlighted an alteration of REM sleep, which reflects a change in the distribution of REM periods with no effects on total sleep or wakefulness, we further explored the duration of REM sleep episodes in detail. These results show, for the first time, the presence of a bimodal distribution of RSI in mice. RSI was bimodally distributed in both genotypes of mice over the 24-hour circadian period, with the two clusters separated at 55 sec, which accounts for the minimum frequency (Figure 8A). Based on these parameters, the two subpopulations of RSI detected were used to distinguish single REM sleep episodes (long RSI >60 sec) and sequential REM sleep episodes (short RSI \leq 60 sec). Although a bimodal distribution was observed in both genotypes of mice, the frequency of short RSIs was significantly higher in the $PWScr^{m+/p-}$ mice than in the $PWScr^{m+/p+}$ mice ($PWScr^{m+/p+}$ 3.40 ± 0.99 vs $PWScr^{m+/p-}$ 7.6 ± 1.6 , $t(18)= 2.21$, $p=0.03$; Figure 8A), suggesting a high REM sleep propensity in the mutant mice. Conversely, the numbers of long RSIs were unchanged between the two genotypes (Figure 8A). In addition, the REM-non-REM cycle was analyzed as an identifier of sleep propensity [170]. These data showed that the cycle length was approximately 2-5 minutes in both genotypes of mice, as already described [148]. However, in the $PWScr^{m+/p-}$ mice, a large increase in REM-non-REM cycles was observed over the 24-hour of the sleep-wake cycle ($PWScr^{m+/p+}$ 9.00 ± 2.06 vs $PWScr^{m+/p-}$ 15.15 ± 1.51 , $t(18)= 2.40$, $p=0.02$; Figure 8A).

4.2.2 Paternal deletion of *Snord116* alters sleep spindles in PWS mice

Sleep spindle properties were explored in relation to the circadian and homeostatic components of sleep (Figure 8D). Sleep spindles are the best-characterized source of EEG power in the 9–16 Hz range during non-REM sleep (see Figure 8B). We calculated these spindle properties for each genotype at different time points and found that the density of spindles was unchanged between the two genotypes in all conditions investigated (Figure 8C). However, we observed that spindle duration ($t(1988)= 3.04, p=0.002$; Figure 8D), central frequency ($t(1988)= 2.70, p=0.006$; Figure 8D), and the number of spindle cycles ($t(1988)= 3.47, p=0.005$; Figure 8D) were significantly increased in the $PWScr^{m+/p-}$ mutants compared to the control mice. Conversely, spindle amplitude was significantly lower in the $PWScr^{m+/p-}$ mutants compared to the $PWScr^{m+/p-}$ mice ($t(1988)= 18.59, p<0.0001$; Figure 8D).

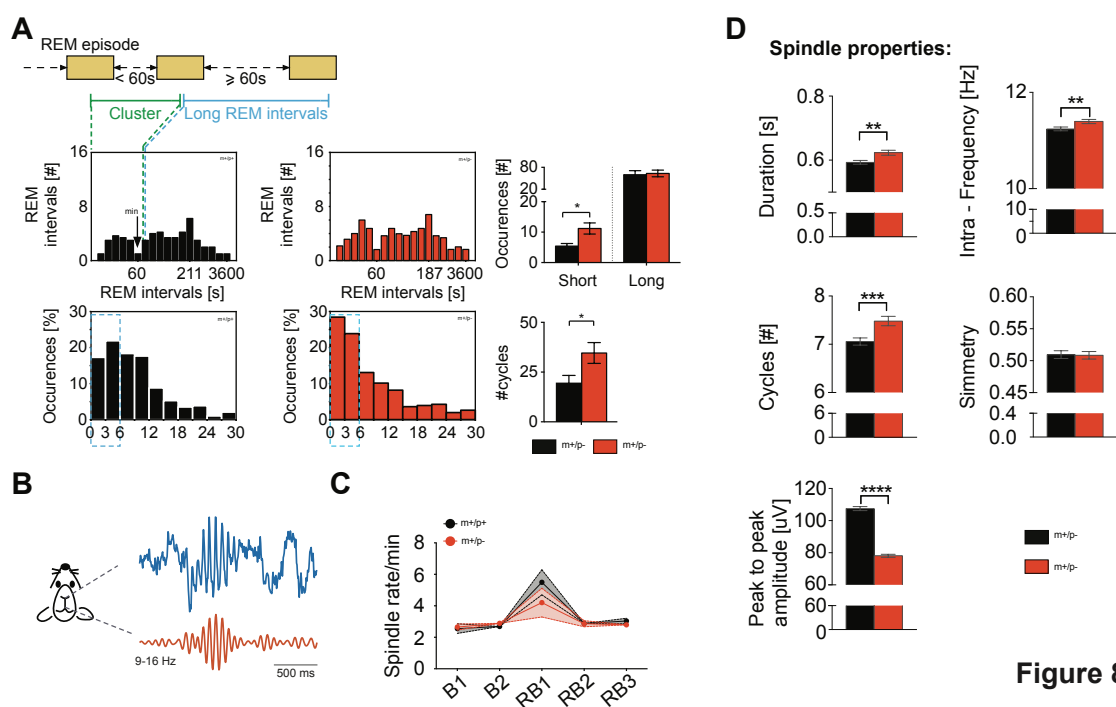


Figure 8

Figure 8, Paternal *Snord116* deletion impacts REM sleep and NREM sleep spindles:

A) On the top, schematic representation of the criteria for the recognition of short-RSI and long-RSI. On the middle average frequency distribution of the duration of the interval from the end of one REM sleep episode to the beginning of the next REM sleep episode (REM sleep interval, RSI) recorded over the 24-hour of the sleep-wake cycles in $PWScr^{m+/p+}$ ($n= 10$ in black) and $PWScr^{m+/p-}$ mice ($n= 10$ in red). The frequency class which was taken as the boundary separating short and long-interval populations (minimum) is at 55-sec. Right, average value of the occurrence of the short and long-RSI for each genotype, values are expressed as mean \pm SEM.

On the bottom, histograms of sleep cycle length during the 24-hour of the sleep-wake cycle in $PWScrm^{+/p+}$ ($n=10$ in black) and $PWScrm^{+/p-}$ mice ($n=10$ in red). Sleep cycles are plotted for 3-hour bins. Only data up to 30 min are shown. Four combinations of criteria (see Method section). Cycles containing wake sequences >64 s were discarded from the analysis. On the right the average value of the number of the cycle length around 2-5 minutes in both genotypes of mice. **B)** Schematic representation of the spindles signal; **C)** The number of the spindles estimated over the 24-hour of the sleep-wake cycles in both genotypes, $PWScrm^{+/p+}$ ($n=10$ in black) and $PWScrm^{+/p-}$ mice ($n=10$ in red). **D)** Sleep spindles properties: duration between 0.4-2 s, central frequency, peak-to-peak amplitude, number of cycles between 5-30 and symmetry. Values are expressed as mean \pm SEM. * $p < 0.05$; ** $p < 0.01$; *** $p < 0.001$

4.2.3 PWS mutants show increased spontaneous physical activity over the circadian cycle

Physical activity was assessed in awake mice without any motor constraints. During the 24-hour of the circadian period, both genotypes showed an increase in physical activity during the night and a decrease in motility during the day. Interestingly, mutant mice displayed an increase in spontaneous physical activity during the subjective night (light phase, resting phase for mice) compared to control mice ($PWScrm^{m+/p+}$ 2.48 ± 0.44 vs $PWScrm^{m+/p-}$ 3.96 ± 0.33 , $t(18) = 2.6$, $p = 0.01$; Figure 9A). Moreover, physical activity was also increased in the mutant mice during the first hours of the dark period compared to the motor activity of control mice (two-way ANOVA: $F(11,99) = 9.318$, $p < 0.0001$, “time of day”, and $F(1,9) = 5.23$, $p = 0.04$, “groups”; Figure 9A).

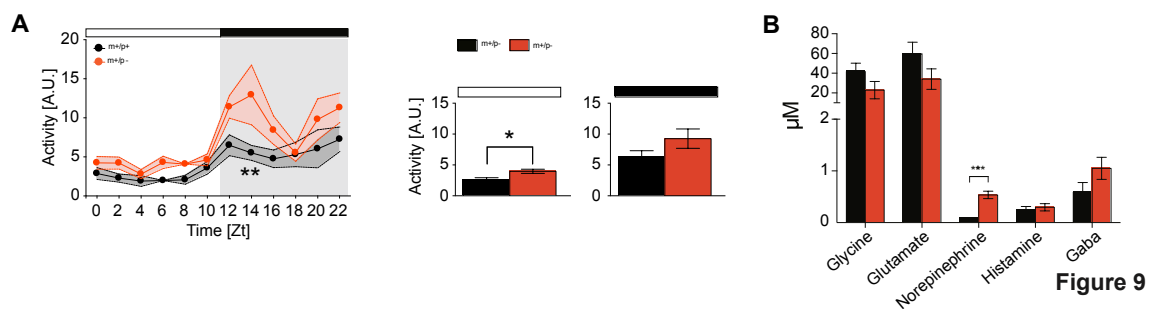


Figure 9, Paternal Snord116 deletion increases physical activity and norepinephrine levels.

A) On the left, telemetry measurements of daily activity in home cages monitored 24-hour per day in $PWScrm^{m+/p+}$ ($n=10$ in black) and $PWScrm^{m+/p-}$ mice ($n=10$ in red). On the right the spontaneous physical activity averaged during the 12-hour light and dark period. Values are the 12-hour means \pm SEM.

B) Levels of neurotransmitters (Glycine, glutamate, norepinephrine, histamine and GABA) assessed in the CSF of PWScr^{m+/p+} (n= 10 in black) and PWScr^{m+/p-} mice (n= 10 in red). Mice were sacrificed at the beginning of the dark period. Values are expressed as mean ± SEM. *p < 0.05; **p < 0.01; ***p < 0.001

4.2.4 Paternal *Snord116* deletion leads to dysregulation of norepinephrine

Neuromodulators are fundamental players in the regulation of sleep-wake cycles. Here, we reported an assessment of the levels of glycine, glutamate, norepinephrine, histamine and GABA in the CSF of both genotypes. Notably, among all the investigated neuropeptides, it was found that the levels of norepinephrine, a neurotransmitter that is involved in arousal and is also important for the regulation of REM sleep [41], [171], was significantly increased in the PWScr^{m+/p-} mice relative to the control (PWScr^{m+/p+} 0.53 ± 0.07 vs PWScr^{m+/p+} 0.08 ± 0.01, t(8)= 6.22, p=0.0003; Figure 9B).

4.3 In the **Study III**, we investigated a new alternative pharmacological approach for PWS aimed at ameliorating the sleep disturbances that significantly comprise the quality of life of these patients by using Pitolisant in mice carrying the deletion of the *Snord116* gene.

4.3.1 Effect of Pitolisant on the Sleep-wake cycle

To assess the effect of Pitolisant on the sleep-wake cycle EEG/EMG was recorded over a 24-hour period (12-hour:12-hour dark-light cycle) as a baseline condition (BL) where mice were left undisturbed, and for the following 24-hour after placebo/Pitolisant administration. There was no mortality in animals randomized into the placebo (n = 10) and Pitolisant (n= 10) groups. To maintain, the within-subjects nature of the protocol the 24-hour of baseline values were always plotted with its corresponding 24-hour treatments (placebo/Pitolisant) for each mouse (Figure 10A). To demonstrate that the effect of Pitolisant is not given by chance, manipulation or confounding factors the changes in the sleep patterns over the 12-hour dark and 12-hour light were plotted in comparison to placebo groups (Figure 10B).

At the BL both genotypes exhibited circadian changes in sleep-wake cycle, showing a high amount of wakefulness during the night and low amount during the 12-hour of the day (Figure 10A), typical of nocturnal rodents. The distribution of all sleep stages (total sleep, REM and non-REM sleep) in both genotypes mice similarly varied across the 24-hour of BL with less time spent in sleep during the dark period (Figure 10A). However, only the percentage of REM sleep during the dark period ($p = .045$, Figure 10B), were significantly increased in the $PWScr^{m+/p-}$ mutants compared to their littermate controls as previously shown [100], while the percentage of total sleep and non-REM sleep was unchanged between the two genotypes of mice over the dark and light periods (Figure 10B).

Overall, mutant mice only present at the BL an alteration of REM sleep during the active phase of mice (dark period), which reflects a change in the microstructure of sleep without affecting the daily amount of wakefulness, total sleep, non-REM sleep.

Pitolisant, which is a wake-promoting drug, was administrated orally at the beginning of the dark period. The placebo was administered at the same time as the Pitolisant in $PWScr^{m+/p+}$ mice and $PWScr^{m+/p-}$ mice and no effect was observed for all sleep parameters measured compared to the BL condition (Figure 10A).

Pitolisant, as expected, enhanced wakefulness in the PWScr^{m+/p+} mice during the night compared to the placebo group ($p < .0001$, Figure 10B). Conversely, in the PWScr^{m+/p-} mice only a slight and not significant increase of wakefulness was observed relative to placebo. Consequently, this increase in wakefulness during the night reflects a significant reduction in the total amount of sleep, only for the PWScr^{m+/p+} mice relative to the placebo group ($p < .0001$, Figure 10B), while as observed for the wake state, also the total amount of sleep during the night was unchanged in the mutant mice compared to placebo.

However, although Pitolisant did not significantly affect wake and total sleep in the mutant mice, but significantly impact the microstructure of sleep, particularly the REM sleep. Indeed, REM sleep was the only stage of sleep that was significantly reduced in both genotypes of mice during the night relative to placebo groups (PWScr^{m+/p+}: $p = .020$; PWScr^{m+/p-}: $p = .019$, Figure 10B).

The response of non-REM sleep to Pitolisant treatment displayed by both genotypes of mice was reminiscent of the same response observed for their respective patterns; wakefulness, and total sleep. Specifically, PWScr^{m+/p+} mice exhibited a significant reduction of non-REM sleep during the night ($p < .0001$, Figure 10B) compared to the placebo group, given by Pitolisant treatment. No significant effect of Pitolisant was observed on non-REM sleep in the PWScr^{m+/p-} mice during the night relative to the placebo group.

During the day the total amount of wake, total sleep, and non-REM sleep were unaffected by Pitolisant in both genotypes of mice (Figure 10B). However, when I looked at their distribution significant differences were observed only in the control mice over the first 4-hour of light period. Specifically, decreases of wakefulness, which reflects a reduction in the total sleep and non-REM sleep were observed ($p < .0001$, Figure 10A). This increase of sleep over the first 4-hour of the day observed in the control mice, as a sort of rebound given by a significant reduction of sleep during the night was not observed in the mutant mice (Figure 10A). Although, Pitolisant did not impact the sleep architecture 12-hour after its administration suggesting that its effect vanishes during the day, however, the only stage of sleep that remained altered compared to placebo group even through the light period is the REM sleep, and this reduction was observed only in the control mice ($p = .040$ vs placebo group, Figure 10B), Conversely, the mutant mice recovered faster reaching the value observed in the placebo group (Figure 10A,B).

Moreover, dynamics of EEG activity during REM and non-REM sleep were computed over the 12-hour of dark and light periods at the BL and after Pitolisant administration.

At the BL REM sleep power densities in the theta activity (6 – 9 Hz) were unchanged between the two genotypes of mice over the dark and light period, although during light period, a decrease in the power of theta activity was observed in both mouse lines. After administering Pitolisant the power of theta activity in the control mice was flattened in the frequency ranges of 1-10 Hz (Figure 10C and Figure S7A), which reflects a marked reduction of REM sleep observed in these mice during the dark period. Conversely, the REM sleep power densities in mutant mice showed the same distribution as observed in the BL (Figure 10C) and was unaltered compared to placebo except in the frequency ranges of 3-3.5 Hz (Figure S7A), although REM sleep was significantly reduced at this stage. During the light period, no differences were observed for the power during REM sleep between the two genotypes of mice suggesting as even observed for the sleep architecture that the effect of Pitolisant vanishes during the day and its action is limited to the 12-hour of the dark period.

As observed for the EEG power in REM sleep also the power during non-REM sleep, which is characterized by high values in the delta frequency band (0.5–5 Hz), was unchanged between the two genotypes at the BL during the light and dark period (Figure 10D). After administering Pitolisant an increase in delta power was more apparent in the control mice, which reached significance in the range of 2–4.5 Hz when compared with mutant mice ($p < .0001$, Figure 10D). Interestingly, although the $PWScr^{m+/p-}$ mice did not show a significant reduction of non-REM sleep during the dark period, as observed in the $PWScr^{m+/p+}$ mice, however the latter showed a higher EEG power during non-REM sleep, which may be explained by a significant increase in the sleep fragmentation after Pitolisant administration in mutant mice. No differences were observed between the two genotypes of mice during the light period, as observed for the EEG power in REM sleep.

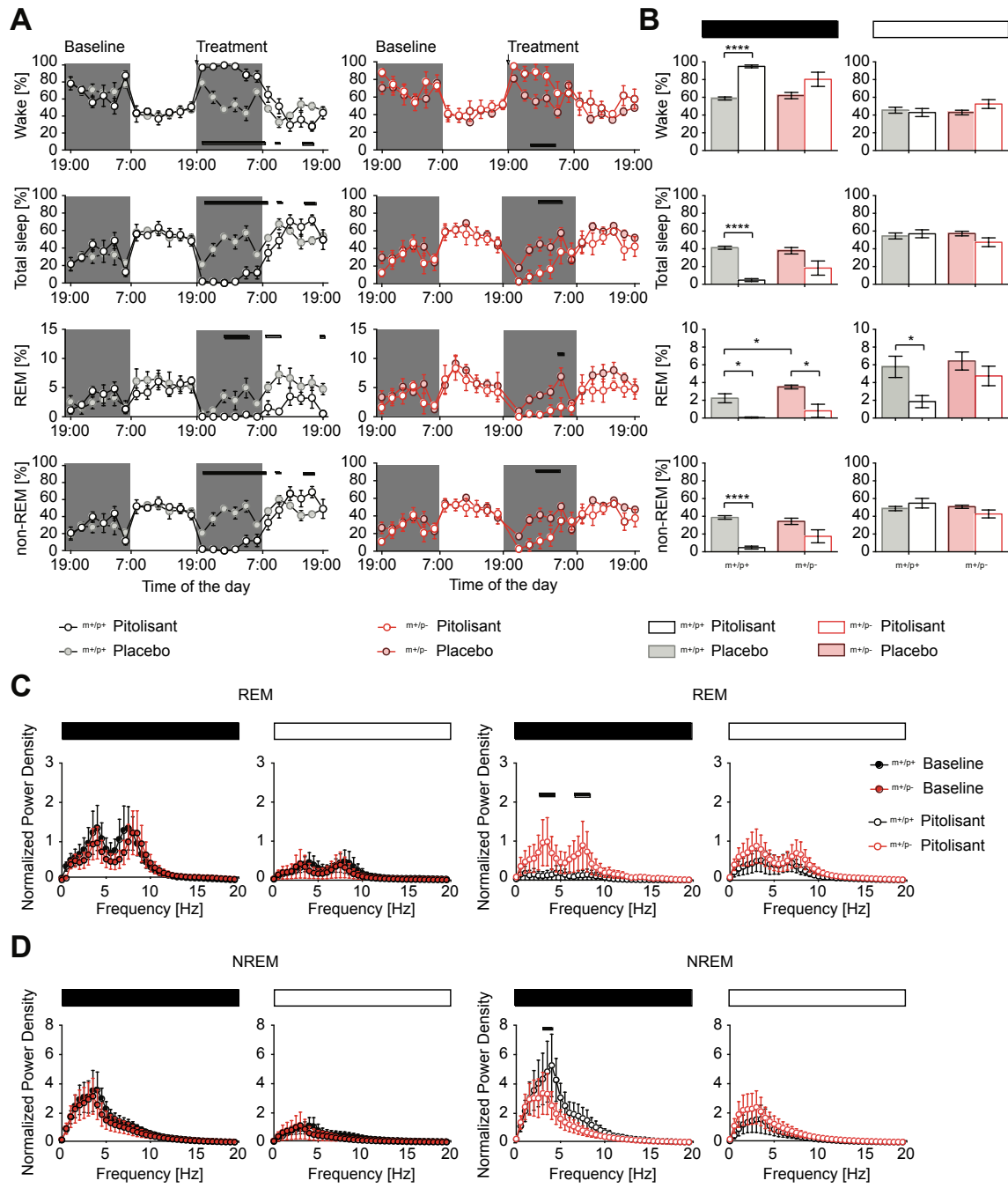


Figure 10, Effect of Pitolisant on the Sleep-wake cycle

A) Wake-sleep distribution over an uninterrupted 48-hour period over a 12-hour light/dark cycle as baseline values and the following 24-hour after Pitolisant/vehicle treatment for control mice (left column in black line and grey and white dots for vehicle and Pitolisant treatment respectively) and mutant mice (right column in red line and pink and white dots for vehicle and Pitolisant treatment respectively). Recordings were made with animals maintained at 22°C. Data are reported as the percentage in 2-hour bins, averaged within genotypes (mean ± SEM; $n = 5$ $PWScr^{m+/p+}$ and $n = 5$ $PWScr^{m+/-}$ mice for both conditions). **B)** The cumulative amount (mean ± SEM) of all sleep-wake stages during the 12-hour of the dark period (black bar above the bars) and during the 12-hour of the light period (white bar above the bars) for the two groups investigated.

C) The normalized power density of the whole spectrum during REM sleep during baseline (left) and Pitolisant treatment (right) for both genotypes; red lines depict $PWScr^{m+/p-}$ mice, and black lines depict $PWScr^{m+/p+}$ mice. **D)** The normalized power density of the whole spectrum during non-REM sleep during baseline (left) and Pitolisant treatment (right) for both genotypes; red lines depict $PWScr^{m+/p-}$ mice, and black lines depict $PWScr^{m+/p+}$ mice.

Finally, the DNE during sleep for the neck muscle was calculated, which is a marker of RSWA to evaluate whether mutant mice characterized by REM sleep alteration also presents RSWA, and also to evaluate the effect of Pitolisant on DNE in both mice lines [172], [173]. The whole distribution of the neck EMGnorm for $PWScr^{m+/p+}$ mice who received placebo was higher during wakefulness and shifted downward during the two sleep stages, REM and non-REM, from the 75th to 99th centiles ($p = .0002$, Figure 11). The same distribution of the EMGnorm, as observed in the control mice was observed in the $PWScr^{m+/p-}$ mice which underwent placebo from the 50th to 99th centiles ($p = .034$, Figure 11). Both genotypes at the BL showed the same distribution of EMGnorm as observed in the mice who received placebo (Figure S7B).

Interestingly, after Pitolisant was administered the distribution of the EMGnorm during wakefulness and the two sleep stages did not differ in the $PWScr^{m+/p+}$ mice, except for 97th and 99th centiles ($p = .0001$, Figure 11). On the contrary, in the mutant mice significant differences in the EMGnorm between wakefulness and the two sleep stages (non-REM and REM sleep) was still observed from the 75th to 99th centiles ($p < .0001$, Figure 11) after Pitolisant administration. Since in the control mice after Pitolisant administration the EMGnorm did not show a net difference between the sleep stages, this

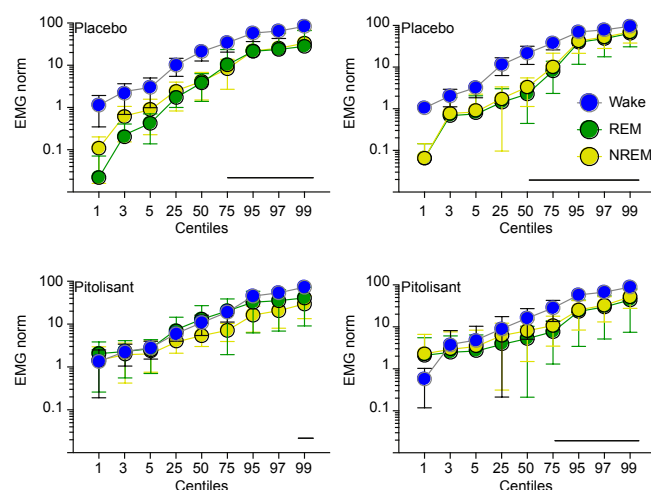


Figure 11, DNE

Comparative physiology of muscle activity during sleep. The panels show the distributions of normalized electromyographic activity (EMG_{NORM}) of neck muscles for $PWScr^{m+/p+}$ (left column) and $PWScr^{m+/p-}$ (right column) for both conditions, upper panel vehicle, lower panel mice treated with Pitolisant

may suggest that Pitolisant increases phasic or tonic muscle activity seen on polysomnographic electromyogram channels only in control mice and not in mutant mice.

4.3.2 Effect of Pitolisant on physical activity

Physical activity was assessed in awake mice, without any motor constraints, to determine whether Pitolisant is associated with side effects such as sedation and depression-like symptoms. Wild-type mice over the 24-hour of BL showed, as expected, an increase in physical activity during the night, while during the day their motility was reduced. In the same mice, Pitolisant did not modify the physical activity over the 24-hour compared to the previous BL (Figure 12). Conversely, in the mutant mice, an increase in physical activity was observed during the night (p. 006, Figure 12), in particular over the first 6-hour of the dark period (p= .002, Figure 12). Interestingly, in the PWScr^{m+/p-} mice after Pitolisant was administered physical activity was significantly reduced during the dark period decreasing to the same level observed in the control mice.

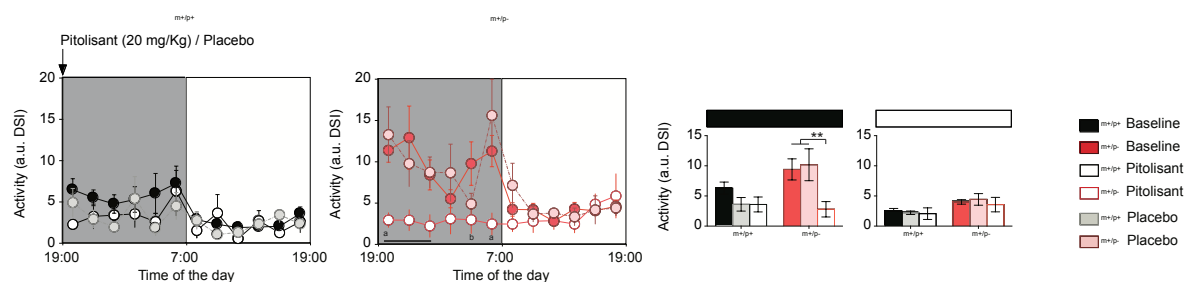


Figure 12, Effect of Pitolisant on physical activity

On the left, telemetry measurements of daily activity in home cages monitored 24-hour per day in PWScr^{m+/p+} (n= 10 in black) and PWScr^{m+/p-} mice (n= 10 in red). With Pink and Gray are reported the two groups treated with the vehicle PWScr^{m+/p-} and PWScr^{m+/p+} respectively. The black or red line of with dots represent the group treated with Pitolisant. On the right the spontaneous physical activity averaged during the 12-hour light and dark period. Values are the 12-hour means \pm SEM

Chapter 5

Discussion

Overall, the main results of this thesis reinforce the evidence that loss of *Snord116* plays a crucial role in the regulation of REM sleep and thermoregulation, both phenotypes being dysregulated in PWS^{cr^{m+/p-}} mutant mice and patients [100], [174]. In particular, we repeatedly observed REM sleep alterations in all studies performed in different experimental groups, at a particular time of the day when the pressure of sleep was increased [175], [176]; in mice, this occurs at a time in the sleep-wake cycle that corresponds to the “siesta time” [175], [176]. Moreover, we also observed that *Snord116* play a crucial role in the hypothalamic functions, primarily affecting the OX neurons. Next we observed that sleep spindle properties were found to be altered in the PWS^{cr^{m+/p-}} mice, while their numbers were unchanged between the two genotypes, suggesting dysfunctions in the cortex where sleep spindles are amplified and not in the thalamus where they are generated. This data implies a dysfunction in the primary cortical neurons observed in PWS^{cr^{m+/p-}} mice, reinforcing our results obtained on sleep spindles (The primary cortical neurons data refers to the MEA experiment, see the following link for more details <https://doi.org/10.1101/809822>).

Taken together first two studies performed in this thesis strongly support that *Snord116* mouse model remarkably recapitulates all the sleep deficits of human PWS, but only incompletely mimics the metabolic alterations. Indeed, both PWS mice and human patients show an alteration of body weight, but the two species show opposite phenotypes; indeed, PWS patients exhibit increased body weight, while mouse models across different studies show reduced weight [99], [155], displaying at least only the first stage (Stage I) of the PWS clinical features, the infancy stage [101].

Finally, in the third part of this thesis we observed that Pitolisant ameliorates the REM sleep alteration in these mice, although other studies are needed to investigate whether Pitolisant may also modulate the sleep-wake cycle via temperature.

5.1 The paternally imprinted gene *Snord116* gene regulate hypothalamic orexin neurons, Study I

In the Study I, we reported for the first time a lack of neuromodulation of the LH in *Snord116* mutant mice, which is accompanied by an imbalance between OX and MCH neurons, causing a 60% reduction in OX neurons in the LH. Within the same 15q11-q13 region, it was previously reported that *Magel2* KO mice lose 40% of OX neurons [177]. These results suggest that multiple paternally expressed genes within the PWS region regulate the OX system in the LH, most likely in a dose-dependent manner. At baseline, we observed that fire discharge of neurons associated with sleep (i.e., S-max neurons) are higher in mutant mice than in controls, suggesting that the role of *Snord116* that originates from the LH is important in the determination of abnormal sleep in PWS. Indeed, several lines of evidence indicate that LH exerts pivotal control of cortical sleep, including REM sleep [178]. Furthermore, while we observed that the proportion of S-max and W-max neurons significantly changed after 6-hour of SD with an increase in sleep neurons of approximately 13% in wild-type control mice, PWS mutants lack this neuronal response by the LH to sleep loss. In the LH, OX and MCH systems exert opposing effects on REM sleep [179]: OX suppresses while MCH promotes REM sleep. Therefore, the imbalance between OX and MCH systems in PWS mutants is in agreement with an increase in REM sleep.

Additionally, OX and MCH neurons in the LH regulate food intake and metabolism [180], [181]. We found that mutant mice displayed a higher proportion of neurons, which were classified as non-responding neurons (type III), relative to food intake than controls. In contrast, type II neurons, which are downregulated in the LH during eating, were significantly reduced in mutants. It has been demonstrated that OX neurons decrease their firing during eating and remain in a depressed state throughout the entire eating phase [182]. These findings suggest a lack of regulatory feedback mechanisms mediated by the OX system in relation to food intake in the LH of PWS model mice, a phenomenon that can relate to the hyperphagia and obesity phenotype observed in PWS patients. This evidence of neuromodulatory dysregulation of the LH is in agreement with previous results [154], which describe that a late onset of mild hyperphagia and obesity in mice can be induced only when *Snord116* is selectively disrupted in the hypothalamus in adult mice.

Dysregulation of the OX system has been reported in a few clinical studies, although to date, the results remain contradictory. One study described an increase in the OX-A level in PWS subjects [183], while another showed a decrease in the peptide in the cerebrospinal fluid [184]. Taken together, these findings call for an alteration of the OX system in PWS, although the contrasting results may also suggest that the loss of function of paternal alleles within the PWS region results in an increased phenotypic variance.

These data suggest that *Snord116* is essential for the regulation, formation and maintenance of the OX system in the LH. We assessed *Snord116* expression in two different strains with OX deficiency, OX/ataxin-3 (Atx) mice and OX peptide knockout (KO) mice [130], [168], and we found that only Atx mice showed a significant increase in *Snord116*. This line selectively loses OX neurons and their co-transmitters. In contrast, in KO mice that do not display a loss of OX neurons but are lacking OX peptides, the level of *Snord116* was unaffected. The increase in *Snord116* in mice with depletion of OX neurons is probably a compensatory mechanism. My conclusions are supported by a recent study [164] that described the role of Peg3 in the development and expression of OX and MCH neurons. The study demonstrates for the first time that PEG3 is able to bind OX promoters by increasing the expression of OX. However, a reduced binding of PEG3 was observed in mutant mice relative to control mice, which may be explained by a reduction in OX neurons. Thus, Peg3 was selectively altered in PWScr^{m+/p-} mutant mice as well as in narcoleptic mice. In particular, Peg3 was found to be altered only in Atx narcoleptic mice, while it was unchanged in Ppox KO mice. This may be explained by the fact that PEG3 binds the OX promoter, which is not altered in KO mice because they have a null mutation. This study reveals that these two paternally imprinted genes, *Snord116* and Peg3, are unlikely to interact with each other, but both contribute to the development and functions of OX neurons. Indeed, in our in vitro experiment with immortalized hypothalamic cells, knockdown of *Snord116* did not change the levels of Peg3.

All these evidences are in line with the pioneering evidence in androgenetic mice [125] that paternally imprinted genes are important for the formation of the hypothalamus. In particular, this study implies that *Snord116* and Peg3 plays a crucial role in the formation of OX neurons.

We observed that PWScr^{m+/p-} mutant mice present a high body temperature coupled with an increase and lack of appropriate thermoregulatory responses. Thermoregulation is

tightly integrated with the regulation of sleep and is also controlled by OX neuromodulation [169], [185]. For example, narcoleptic subjects exhibit a paradoxical lower core body temperature while awake [186] and a higher body temperature during sleep [187], [188]. In mammals, in physiological conditions, peripheral vasodilatation helps decrease the core body temperature during sleep initiation. Mutant mice displayed a high body temperature during the light period, which corresponded to their resting phase/subjective sleep. Interestingly, narcoleptic mice show body similar temperature abnormalities [189]. Moreover, when PWS mutant mice were kept at the TNZ, where resting metabolic rate remains stable and where REM sleep is preferentially increased [190], [191], we observed a surprising thermoregulatory response coupled with an altered homeostatic REM sleep response. REM sleep did not increase, and the peripheral thermoregulatory response of the mutant mice resembled what would be expected in a sub-neutrality (e.g., 22°C) environment. REM sleep is a stage of sleep in which thermoregulation is suspended; for this reason, REM sleep expression is more sensitive to ambient temperature manipulation than non-REM sleep [190], [191].

A recent study [192] described that endotherms have evolved neural circuits to opportunistically promote REM sleep when the need for thermoregulatory defense is minimized, such as in TNZ conditions, suggesting a tight link between thermoregulation and REM sleep. In this study, the increase in body weight observed at the TNZ suggests that thermoneutrality is a permissive condition that induces body weight gain but does not compensate for the metabolic abnormality in these mice. Indeed, the differences with wild-type mice remained unchanged. Mutants showed growth retardation at both environmental conditions investigated, namely, at both 22°C and 30°C.

The transcriptomic analysis in the hypothalamus suggests that loss of *Snord116* might negatively affect synaptic organization while promoting inflammatory responses in the hypothalamus, as previously observed in post-mortem hypothalamic brain tissue from PWS patients [160]. GO analysis of all 833 DEGs in the mutant hypothalamus following SD suggested, instead, that loss of *Snord116* leads to a homeostatic response that relies on several cellular growth processes of the hypothalamus (Figure 5E). This result indicates that defects in sleep homeostasis in PWS can be derived from development processes of the hypothalamus, as has been described in other neurodevelopmental disorders [193]–

[195]. This data has a clinical implication because up to 76% of PWS patients exhibit abnormal and poor sleep [8], [196] that may negatively impact the normal function of the hypothalamus.

In conclusion, this study demonstrates for the first time that paternally expressed genetic elements in the LH affect the dynamics between neuronal activity in the LH and cortical EEG sleep states. This new evidence reinforces the recent hypothesis that genomic imprinting plays a crucial role in mammalian sleep [197] and confirms original studies in androgenetic chimeric mice [125], suggesting that the paternal genome may account for regulatory mechanisms in the hypothalamus.

5.2 The paternally imprinted gene *Snord116* regulates macrostructural sleep aspects and cortical neuronal activity, Study II

In the Study I, we observed that mice lacking the *Snord116* had an increase in REM sleep during the dark period, when mice are most active, and may resemble the EDS observed in humans PWS [108]. Since it has already been reported that REM sleep is precisely regulated in terms of its duration, while non-REM is substantially regulated in terms of intensity [36], [157], we decided in the study to analyze the succession of REM sleep episodes and the period of time intervening between the end of one REM sleep episode and the beginning of the next (REM sleep interval, RSI). RSI follows a bimodal distribution characterized by short and long periods. The presence of a bimodal distribution has already been described [156] in many species, such as rats [198], cats [199] and humans [200], but, at the best of my knowledge, no data are yet available on the RSI distribution in mice. For the first time, these data reveal a bimodal RSI distribution in mice, with the minimum frequency at 55 sec, while in rats, the minimum between the two peaks has been identified at 3 min [156]. A bimodal distribution of RSI was observed in both genotypes of mice. However, mutant mice showed a significant increase in short RSI. Short RSI has been described as an indicator of the capacity to produce REM sleep in accordance to the homeostatic drive under favorable ambient conditions and associated with the capacity to produce REM sleep proportionally to the homeostatic drive under favorable ambient conditions [156], [201]. Indeed, the amount of REM sleep with short RSIs has been shown:

- I. to be increased during a REM sleep rebound in proportion to the degree of previous REM deprivation induced by low ambient temperature [147];
- II. to be depressed when animals are kept under an uncomfortable ambient condition, such as during the exposure to a low Ta [156], and concomitantly with a reduced capacity of cAMP accumulation at hypothalamic-preoptic level [202], [203].

This observation may reflect a strengthened drive for REM sleep and/or a distorted and more favorable perception of the ambient conditions, in terms of the thermal comfort, in the mutant mice. Therefore, since sleep propensity also affects the non-REM-REM cycle, I also assessed the number of these cycles over the 24-hour of the BL in both genotypes of mice. As expected, mutant mice presented a significant increase in the non-REM-REM cycle (approximately 2-5 minutes) [148] compared to the control group, suggesting, once again, that the mutant mice have a strong tendency to fall asleep easily. Overall, these data imply that the loss of *Snord116* significantly compromised sleep microstructure, mainly affecting REM sleep.

We found that PWScr^{m+/p-} mice showed alterations in REM sleep without affecting non-REM sleep. An exception, however, was found in the sleep spindles, hallmarks of non-REM sleep that reflect the activity of complementary thalamocortical circuits. The thalamic reticular nucleus (TRN) is the spindle pacemaker, and TRN/thalamus circuits can generate spindles in isolation, although cortical inputs may contribute by initiating or amplifying spindle oscillations [71], [72]. Here, we show that the duration, amplitude and frequency of sleep spindles are significantly altered in PWScr^{m+/p-} mice, while their numbers are unchanged between the two genotypes. This data suggests that TRN/thalamus circuits or in corticothalamic afferents to these intra-thalamic circuits may probably not be affected in the mutant mice, while, an impairment of cortical amplification may explain the alterations of sleep spindle properties. Since it has been shown that sleep spindles facilitate neuroplasticity and support learning, memory consolidation, and intellectual performance [204], and since sleep spindle alterations have been documented in children with neurodevelopmental disorders [204], [205], I speculate that the neurodevelopmental and cognitive alterations observed in these mice [206] may also arise from altered thalamocortical input. Thus, I believe that sleep spindle alterations may

either reflect the severity of the underlying disorder or directly exacerbate the severity of impairments. Evidence also indicates that alterations in sleep spindle properties have a very early association with an increased risk of cognitive impairment [207]; These results imply that sleep spindles may also represent reliable sleep EEG biomarkers associated with PWS disorder, although a better characterization of these findings in PWS subjects is needed.

Additionally, we observed that PWS^{Scr^{m+/p-}} mice have dysregulated norepinephrine levels in the CSF collected at the beginning of the dark period. Norepinephrine is a neurotransmitter important for maintaining normal sleep states, and dysregulated norepinephrine signaling is responsible for cataplexy attacks, which, together with narcolepsy, represent common features of PWS [208].

Thus, the activity of norepinephrine neurons in the locus coeruleus is important in modulating cortical activity during non-REM sleep [209]. Norepinephrine not only influences general arousal but also affects locomotor activity. Indeed, it has been observed that intraventricular infusion of norepinephrine increases motor activity [210]. Interestingly, we observed that norepinephrine was significantly higher in the mutant mice than in the controls, suggesting that norepinephrine may also have a role in controlling motor activity in these mice. Overall, these data imply that mutant mice may also have a dysregulated norepinephrine system. The extent to which norepinephrine alterations may affect the sleep-wake cycle and locomotor activity should be further investigated and may have therapeutic relevance.

These data imply a dysfunction of cortical amplification, manifested by the altered sleep spindles properties not affecting their numbers observed in the mutant mice. Based on these results, we investigated whether cortical neurons isolated from thalamocortical projections showed an altered intrinsic mechanism of sleep comparable to the sleep endophenotypes observed in living mice. To address this question, I worked in collaboration with Ilaria Colombi on her doctoral project, for the results see link <https://doi.org/10.1101/809822>. There we used an in vitro model. Previous studies have demonstrated that embryonic cortical neurons on MEA are able to recapitulate some essential features of sleep in a controllable way [211]–[213]. Here, we treated cortical cultures with Carbachol to change the synchronized default sleep-like state, characterized by slow-wave oscillations typical of non-REM sleep, into a theta-predominant state, which

is typical of REM sleep. Because of this EEG feature of REM, the shorthand definition of REM sleep is a highly activated brain in a paralyzed body [214]. The LFP analysis of MEA cortical neurons revealed abnormalities in the theta waves in the PWScr^{m+/p-} neurons similar to those observed in living mice. Carbachol administration caused evident desynchronization of the activity of both genotypes, but mutant cultures showed different response profiles after Carbachol treatment compared to control cultures. Overall, these results suggested that PWS cultures displayed alterations in neuronal activity patterns during spontaneous activity and when external stimulation was applied. Taken together, these data imply that *Snord116* may either directly influence the neuronal synchronization of cortical neurons or affect it indirectly via norepinephrine, which we found to be altered in our study in living mice. Indeed, norepinephrine is a neurotransmitter that decreases network synchrony both in vivo [215], [216] and in vitro [215], consistent with our results, in which PWScr^{m+/p-} cultures showed an increased level of this neurotransmitter that may be responsible for the increased desynchronization level of activity in the MEA recording.

Finally, we also assessed the expression of IEGs in both in vitro and in vivo models, and we observed that our in vitro model exactly recapitulates the transcriptional alteration observed in living mice. This finding also suggests that cortical cultures coupled to MEA represent a promising tool to identify novel therapeutic targets, such as sleep feature alterations and network synchronization defects. Moreover, these data suggest, in agreement with a recent publication [217], that the *Snord116* gene affects the transcriptional profiles of circadian genes in the cortex (*Per2* and *Bmal1*), which are involved in development outside the suprachiasmatic nucleus and contribute to brain plasticity [218]. Indeed, we also found that the PWScr^{m+/p-} mice had low levels of *Bdnf* mRNA, which is extremely important in the regulation of synapses and the plasticity process. This latter evidence may pave the way for new interventional approaches for PWS by using TrkB agonists or by using compounds that increase the BDNF level [219].

Overall, the results suggest once again that *Snord116* is important in controlling REM sleep. Additionally, here I provide the first evidence supporting the role of *Snord116* in regulating cortical neuronal activity, opening avenues for new interventions in PWS. The dysregulation of sleep spindles in mutant mice raises the possibility that this phenomenon can be a clinically useful marker to assess PWS symptoms in humans.

5.3 Effect of Pitolisant on REM sleep alteration in the *Snord116* mice as model of Prader Willi Syndrome, Study III

In the Study I and II, we systematically observed that mice carrying the paternal deletion of the *Snord116* gene have a REM sleep alteration, supporting the hypothesis that REM sleep, its propensity and regulation is linked to genomic imprinting [197]. Additionally, the Study I describe that paternally expressed imprinted genes are essential for hypothalamic function, in regulating the homeostatic and circadian sleep process. This process may be mediated via the regulation of orexin levels, which was found significantly reduced in these mice. Based on this latter evidence we decided to administer Pitolisant to PWScr^{m+/p-} mice, with the aim of ameliorating the sleep phenotypes. Pitolisant, is a wake promoting drug that enhances wakefulness by acting not only on the histaminergic system, which should not be compromised in these mice, but also by modulating other ascending waking pathways [131].

Overall these data shows that the control mice adequately respond to Pitolisant by increasing wakefulness and reducing total sleep, with both non-REM and REM sleep stages being decreased, during the dark period, immediately after administration. Conversely, the response of Pitolisant in mutant mice was much less marked. Indeed, mutant mice after being administered Pitolisant did not show a significant change in wakefulness, total sleep and non-REM sleep during the 12-hour of the dark period compared to PWScr^{m+/p-} mice who received a placebo. This suggests a high propensity to sleep and an inability to maintain wakefulness in these mice. Interestingly, we observed that the only stage of sleep significantly affected by Pitolisanat in the mutant mice was the REM sleep, which was significantly reduced after its administration during the night. This reduction of REM sleep is fully recovered over the following day in the mutant mice, while in the control group REM sleep was still reduced, suggesting a higher propensity in these mice to enter into REM sleep.

Overall this data highlights that Pitolisant ameliorates the REM sleep alteration in these mice, although other studies are needed to investigate whether Pitolisant may also modulate the sleep-wake cycle via temperature.

5.4 Limitations of the thesis and suggestions for future experiment

Although in this thesis several methodological approaches have been used to understand the role of the *Snord116* gene in the regulation of the hypothalamus and sleep functions in these mutant mice, I believe that two crucial experiments are needed to clarify whether *Snord116* may recapitulate some of the endophenotypes observed in the mutant mice and discussed in this study.

Specifically, could be interesting to clarify the effect of:

- I. *Snord116* deletion in specific neurons versus the KO deletion affecting all brain;
- II. *Snord116* congenital deletion versus deletion induced in adult mice.

In this thesis, we showed that mice lacking the *Snord116* in the whole brain has REM sleep alteration and OX dysfunction. However, would be extremely interesting to know whether the conditional deletion of the *Snord116* gene in specific cell/neuron (i.e Orexin) could be enough to recapitulate the alteration observed in these mutant mice. To perform this experiment, I should have used transgenic line mice that drive Cre-gene expression under the control of the OX promotor ($OX^{cre/+}$). Specifically, these mutant mice $PWScr^{m+/p-}$ should be crossed with a transgenic $OX^{cre/+}$ mouse to generate double heterozygous mice ($PWScr^{m+/p-}/OX^{cre/+}$).

Next, it could be useful to understand whether the deletion of the *Snord116* induced in adult mice may negatively affect the orexin neurons. This experiment may help to understand the role of the *Snord116* in the neurodevelopmental deficit affecting the used mutant mice and described by several research groups [220] that is something beyond the reduction of the OX neurons. Thus, may help to clarify whether *Snord116* is extremely important for the formation maintenance and regulation of the OX neurons, as I hypothesized in the study I or rather is related to the neurodevelopmental deficit affecting these mice. This study should have been performed by using transgenic $OX^{cre/+}$ mice where *Snord116* should be selectively KO in the LH by using a specific siRNA for *Snord116* that is already commercially available.

Chapter 6

Conclusions

Overall in all three studies I observed that *Snord116* play a crucial role in the regulation of REM sleep and its propensity and for the fine regulatory cortical process that controls sleep architecture. The REM sleep alterations may be compatible with a loss of OX-expressing neurons in the LH, while MCH-expressing neurons remained unaffected, thereby creating an imbalance between the two systems. I also report, for the first time, a link between *Snord116* and a different paternally imprinted gene, *Peg3*, which plays a pivotal role in the control of the hypothalamic OX neuromodulator system. Finally, here I also provide a new pharmacological approach for PWS to ameliorate the sleep alteration that significantly affect the PWS patients, although clinical trials are needed to confirm my results to validate the use Pitolisant in PWS patients.

An approach to monitoring home-cage behavior in mice that facilitates data sharing

Edoardo Balzani^{1,5}, Matteo Falappa^{1,2,5}, Fuat Balci^{3,4} & Valter Tucci¹

¹Department of Neuroscience and Brain Technologies, Istituto Italiano di Tecnologia, Genova, Italy. ²Dipartimento di Neuroscienze, Riabilitazione, Oftalmologia, Genetica e Scienze Materno-Infantili (DINOgMI), Università degli Studi di Genova, Genova, Italy. ³Department of Psychology, Koç University, Istanbul, Turkey. ⁴Research Center for Translational Medicine, Koç University, Istanbul, Turkey. ⁵These authors contributed equally to this work. Correspondence should be addressed to V.T. (valter.tucci@iit.it).

Published online 17 May 2018; doi:10.1038/nprot.2018.031

Genetically modified mice are used as models for a variety of human behavioral conditions. However, behavioral phenotyping can be a major bottleneck in mouse genetics because many of the classic protocols are too long and/or are vulnerable to unaccountable sources of variance, leading to inconsistent results between centers. We developed a home-cage approach using a Chora feeder that is controlled by—and sends data to—software. In this approach, mice are tested in the standard cages in which they are held for husbandry, which removes confounding variables such as the stress induced by out-of-cage testing. This system increases the throughput of data gathering from individual animals and facilitates data mining by offering new opportunities for multimodal data comparisons. In this protocol, we use a simple work-for-food testing strategy as an example application, but the approach can be adapted for other experiments looking at, e.g., attention, decision-making or memory. The spontaneous behavioral activity of mice in performing the behavioral task can be monitored 24 h a day for several days, providing an integrated assessment of the circadian profiles of different behaviors. We developed a Python-based open-source analytical platform (Phenopy) that is accessible to scientists with no programming background and can be used to design and control such experiments, as well as to collect and share data. This approach is suitable for large-scale studies involving multiple laboratories.

INTRODUCTION

Behavior is a noisy phenomenon to study in animal models. The resultant difficulty in investigating behavior is coupled with the limitations of traditional behavioral phenotyping procedures in mice, which are often inefficient (low-throughput) and can lead to inconsistent results. Disparate behavioral findings from ‘identical assays’ caused by exogenous factors have been demonstrated by cross-laboratory studies in different mouse strains and mutants, suggesting that findings regarding many behavioral measures may in fact be specific to individual laboratories. For instance, despite all the efforts to equate the testing conditions among three different testing sites and cocaine-induced locomotor activity, as well as activity and the time spent in open arms of an elevated plus maze (as an index of anxiety), results differed between sites¹.

Nevertheless, the investigation and characterization of behavior remain a fundamental part of the analysis of many biological systems and, therefore, are of great interest to the life sciences. Mouse is a widely used animal model, not only to map mammalian genes, but also to determine the function of each of these genes, including its association with behavioral and cognitive traits. There are now several large-scale projects creating collections of mutant mice for the study of ~20,000 mouse genes. All these projects are rigorously producing extensive archives of mouse lines, which are available for use by the wider scientific community. However, behavioral phenotyping with traditional methods constitutes a limiting factor in the evaluation of these lines due to their low-throughput and the data not being suitable for computational analytical approaches. For instance, the Morris water maze, which is typically used to test spatial memory performance, requires the testing of animals out of the cage over multiple trials and sessions (i.e., days). The critical unit of analysis in this task is the latency to locate a hidden platform upon the placement of the animal in a circular pool by the experimenter, which is not ideal for modeling the data for elucidating the generative processes

that underlie performance. Consequently, the next critical step that would add substantial value to the field is the annotation of precise phenotypes for each of these models.

To capture the complexity of mouse behavior, neurogeneticists adopt a reductionist strategy, focusing on intermediate phenotypes (endophenotypes).

Conventionally, endophenotypes have been conceptualized as heritable behavioral symptoms that can be measured in affected and unaffected subjects in order to identify the genes linked to a given disease^{2–4}. The so-called ‘dissecting complex phenotypes’ model⁵ has been extensively adopted in translational research because it reduces the burden of analyzing intricate behaviors, which are often difficult to define and parameterize in animal models. This approach has partially shifted interest in genetic psychiatry from targeting psychiatric diseases as a whole toward mapping the genetic basis of the endophenotypes that independently characterize the symptomatology of the psychiatric diseases. It is believed that the complexity of phenotypes depends on the complexity of the underlying genetics. As a consequence, in experimental practice, it is assumed that by reducing the complexity of the targeted phenotypes, a smaller genetic network will be captured and this will progressively lead to the identification of individual readouts of the isolated single genes.

The effect size observed in relation to a given endophenotype serves as an operational measure of the phenotypic variance associated with a genetic locus³; hence, it is informative of the risk of disease manifestation. For example, specific genetic variants within the 22q11.2 region, coding for the enzyme catechol O-methyltransferase (COMT), which is fundamental for the catabolism of dopamine, are widely studied to account for a range of behavioral and physiological endophenotypes that depend on the function of the prefrontal cortex, as well as occurring in combination with schizophrenia^{6–8}. Interestingly, meta-analyses

Appendix B

Paper as first author, shared authorship

Paternally expressed imprinted Snord116 and Peg3 regulate hypothalamic orexin neurons

P Marta, [F Matteo](#), F Andrea, B Edoardo, B Chiara... - bioRxiv, 2019 - biorxiv.org

Imprinted genes are highly expressed in the hypothalamus; however, whether specific imprinted genes affect hypothalamic neuromodulators and their functions is unknown. It has been suggested that Prader-Willi syndrome (PWS), a neurodevelopmental disorder caused by lack of paternal expression at chromosome 15q11-q13, is characterised by hypothalamic insufficiency. Here, we investigate the role of the paternally expressed Snord116 gene within the context of sleep and metabolic abnormalities of PWS, and we report a novel role ...

The paternally imprinted gene Snord116 regulates cortical neuronal activity

P Marta, C Ilaria, [F Matteo](#), A Freschi, M Bandarabadi... - bioRxiv, 2019 - biorxiv.org

Prader-Willi syndrome (PWS) is a neurodevelopmental disorder that is characterized by rapid eye movement (REM) sleep abnormalities. The disease is caused by genomic imprinting defects that are inherited through the paternal line. Among the genes located in the PWS region on chromosome 15 (15q11-q13), small nucleolar RNA 116 (Snord116) has been previously associated with intrusions of REM sleep into wakefulness in both humans and mice. Here, we further explore the processes of sleep regulation by studying the ...

Bibliography

- [1] I. Tobler, "Is sleep fundamentally different between mammalian species?," *Behav. Brain Res.*, vol. 69, no. 1–2, pp. 35–41, 1995.
- [2] A. A. Borb and P. Achermann, "Sleep homeostasis and models of sleep regulation," *J. Biol. Rhythms*, vol. 14, no. 6, pp. 559–570, 1999.
- [3] R. Huber, M. F. Ghilardi, M. Massimini, and G. Tononi, "Local sleep and learning," *Nature*, vol. 430, no. 6995, p. 78, 2004.
- [4] C. Cirelli and G. Tononi, "Is sleep essential?," *PLoS Biol.*, vol. 6, no. 8, p. e216, 2008.
- [5] A. P. A. Vorster, H. C. Krishnan, C. Cirelli, and L. C. Lyons, "Characterization of sleep in *Aplysia californica*," *Sleep*, vol. 37, no. 9, pp. 1453–1463, 2014.
- [6] W. F. Flanigan Jr, "Sleep and Wakefulness in Iguanid Lizards, *Ctenosaura pectinata* and *Iguana iguana*; pp. 417–436," *Brain. Behav. Evol.*, vol. 8, no. 6, pp. 417–436, 1973.
- [7] B. Rasch and J. Born, "About sleep's role in memory," *Physiol. Rev.*, vol. 93, no. 2, pp. 681–766, 2013.
- [8] K. Williams, A. Scheimann, V. Sutton, E. Hayslett, and D. G. Glaze, "Sleepiness and sleep disordered breathing in Prader-Willi syndrome: relationship to genotype, growth hormone therapy, and body composition," *J Clin Sleep Med*, vol. 4, no. 2, pp. 111–118, 2008.
- [9] M. Massimini, R. Huber, F. Ferrarelli, S. Hill, and G. Tononi, "The sleep slow oscillation as a traveling wave," *J. Neurosci.*, vol. 24, no. 31, pp. 6862–6870, 2004.
- [10] V. V Vyazovskiy and K. D. Harris, "Sleep and the single neuron: the role of global slow oscillations in individual cell rest," *Nat. Rev. Neurosci.*, vol. 14, no. 6, p. 443, 2013.
- [11] C. S. Nayak and A. C. Anilkumar, "EEG Normal Sleep," in *StatPearls [Internet]*, StatPearls Publishing, 2019.
- [12] S. M. Purcell *et al.*, "Characterizing sleep spindles in 11,630 individuals from the National Sleep Research Resource," *Nat. Commun.*, 2017.
- [13] A. Krol, R. D. Wimmer, M. M. Halassa, and G. Feng, "Thalamic Reticular Dysfunction as a Circuit Endophenotype in Neurodevelopmental Disorders," *Neuron*. 2018.
- [14] M. Steriade, "Active neocortical processes during quiescent sleep.," *Arch. Ital. Biol.*, vol. 139, no. 1, pp. 37–51, 2001.
- [15] G. Tononi and C. Cirelli, "Sleep function and synaptic homeostasis," *Sleep Med. Rev.*, vol. 10, no. 1, pp. 49–62, 2006.
- [16] P. Achermann and A. A. Borbély, "Mathematical models of sleep regulation," *Front Biosci*, vol. 8, no. Suppl., pp. S683–S693, 2003.
- [17] T. T. Dang-Vu, M. Desseilles, D. Petit, S. Mazza, J. Montplaisir, and P. Maquet, "Neuroimaging in sleep medicine," *Sleep Med.*, vol. 8, no. 4, pp. 349–372, 2007.
- [18] V. Vyazovskiy, A. A. Borbély, and I. Tobler, "Fast track: Unilateral vibrissae stimulation during

- waking induces interhemispheric EEG asymmetry during subsequent sleep in the rat," *J. Sleep Res.*, vol. 9, no. 4, pp. 367–371, 2000.
- [19] M. Kalia, "Neurobiology of sleep," *Metabolism*, vol. 55, pp. S2–S6, 2006.
- [20] S. Scarpelli, A. D'Atri, M. Gorgoni, M. Ferrara, and L. De Gennaro, "EEG oscillations during sleep and dream recall: state-or trait-like individual differences?," *Front. Psychol.*, vol. 6, p. 605, 2015.
- [21] M. Solms, "Dreaming and REM sleep are controlled by different brain mechanisms," *Behav. Brain Sci.*, vol. 23, no. 6, pp. 843–850, 2000.
- [22] M. H. Schmidt, "The energy allocation function of sleep: a unifying theory of sleep, torpor, and continuous wakefulness," *Neurosci. Biobehav. Rev.*, vol. 47, pp. 122–153, 2014.
- [23] M. W. O'Malley and S. Datta, "REM sleep regulating mechanisms in the cholinergic cell compartment of the brainstem," *Indian J. sleep Med.*, vol. 8, no. 2, p. 58, 2013.
- [24] G. Buzsáki, "Theta oscillations in the hippocampus," *Neuron*, vol. 33, no. 3, pp. 325–340, 2002.
- [25] P. A. Blissitt, "Sleep, memory, and learning," *J. Neurosci. Nurs.*, vol. 33, no. 4, p. 208, 2001.
- [26] W. Fishbein and B. M. Gutwein, "Paradoxical sleep and memory storage processes," *Behav. Biol.*, vol. 19, no. 4, pp. 425–464, 1977.
- [27] M. G. Frank and J. H. Benington, "The role of sleep in memory consolidation and brain plasticity: dream or reality?," *Neurosci.*, vol. 12, no. 6, pp. 477–488, 2006.
- [28] R. E. Brown, R. Basheer, J. T. McKenna, R. E. Strecker, and R. W. McCarley, "Control of sleep and wakefulness," *Physiol. Rev.*, vol. 92, no. 3, pp. 1087–1187, 2012.
- [29] J. M. Walker and R. J. Berger, "Sleep as an adaptation for energy conservation functionally related to hibernation and shallow torpor," in *Progress in brain research*, vol. 53, Elsevier, 1980, pp. 255–278.
- [30] J. M. Krueger, F. Obál, J. Fang, T. Kubota, and P. Taishi, "The role of cytokines in physiological sleep regulation," *Ann. N. Y. Acad. Sci.*, vol. 933, no. 1, pp. 211–221, 2001.
- [31] J. M. Krueger and J. F. Obal, "Sleep function.," *Front. Biosci. a J. virtual Libr.*, vol. 8, pp. d511-9, 2003.
- [32] J. M. Krueger, F. Obál Jr, L. Kapás, and J. Fang, "Brain organization and sleep function," *Behav. Brain Res.*, vol. 69, no. 1–2, pp. 177–185, 1995.
- [33] J. L. McGaugh, "Time-dependent processes in memory storage," *Science (80-.)*, vol. 153, no. 3742, pp. 1351–1358, 1966.
- [34] C. A. Everson, B. M. Bergmann, and A. Rechtschaffen, "Sleep deprivation in the rat: III. Total sleep deprivation," *Sleep*, 1989.
- [35] J. H. Benington and H. C. Heller, "Restoration of brain energy metabolism as the function of sleep," *Prog. Neurobiol.*, vol. 45, no. 4, pp. 347–360, 1995.
- [36] A. A. Borbely and P. Achermann, "Sleep homeostasis and models of sleep regulation," *J Biol Rhythm.*, vol. 14, no. 6, pp. 557–568, 1999.
- [37] P. L. Madsen *et al.*, "Cerebral O₂ metabolism and cerebral blood flow in humans during deep and rapid-eye-movement sleep," *J. Appl. Physiol.*, 1991.

- [38] P. L. Madsen, S. Holm, S. Vorstrup, L. Friberg, N. A. Lassen, and G. Wildschjødtz, "Human regional cerebral blood flow during rapid-eye-movement sleep," *J. Cereb. Blood Flow Metab.*, 1991.
- [39] M. Hirshkowitz and M. H. Schmidt, "Sleep-related erections: clinical perspectives and neural mechanisms," *Sleep Med. Rev.*, vol. 9, no. 4, pp. 311–329, 2005.
- [40] S. F. Glotzbach and H. C. Heller, "Central nervous regulation of body temperature during sleep," *Science (80-.)*, vol. 194, no. 4264, pp. 537–539, 1976.
- [41] H. N. Mallick and V. M. Kumar, "Basal forebrain thermoregulatory mechanism modulates auto-regulated sleep," *Front. Neurol.*, vol. 3, p. 102, 2012.
- [42] T. T. Dang-Vu, M. Desseilles, P. Peigneux, and P. Maquet, "A role for sleep in brain plasticity," *Pediatr. Rehabil.*, vol. 9, no. 2, pp. 98–118, 2006.
- [43] A. Pascual-Leone *et al.*, "Characterizing brain cortical plasticity and network dynamics across the age-span in health and disease with TMS-EEG and TMS-fMRI," *Brain Topogr.*, vol. 24, no. 3–4, p. 302, 2011.
- [44] R. W. McCarley, "Neurobiology of REM and NREM sleep," *Sleep Med.*, vol. 8, no. 4, pp. 302–330, 2007.
- [45] G. Tononi and C. Cirelli, "Sleep and synaptic homeostasis: a hypothesis," *Brain Res. Bull.*, vol. 62, no. 2, pp. 143–150, 2003.
- [46] G. Tononi and C. Cirelli, "Time to be SHY? Some comments on sleep and synaptic homeostasis," *Neural Plast.*, vol. 2012, 2012.
- [47] M. G. Frank, "Erasing synapses in sleep: is it time to be SHY?," *Neural Plast.*, vol. 2012, 2012.
- [48] J. H. Benington and M. G. Frank, "Cellular and molecular connections between sleep and synaptic plasticity," *Prog. Neurobiol.*, vol. 69, no. 2, pp. 71–101, 2003.
- [49] W. Plihal and J. Born, "Effects of early and late nocturnal sleep on declarative and procedural memory," *J. Cogn. Neurosci.*, vol. 9, no. 4, pp. 534–547, 1997.
- [50] P. Peigneux, S. Laureys, X. Delbeuck, and P. Maquet, "Sleeping brain, learning brain. The role of sleep for memory systems," *Neuroreport*, vol. 12, no. 18, pp. A111–A124, 2001.
- [51] A. Giuditta *et al.*, "The sequential hypothesis of the function of sleep," *Behav. Brain Res.*, vol. 69, no. 1–2, pp. 157–166, 1995.
- [52] J. M. Siegel, "The REM sleep-memory consolidation hypothesis," *Science (80-.)*, vol. 294, no. 5544, pp. 1058–1063, 2001.
- [53] A. A. Borbély, S. Daan, A. Wirz-Justice, and T. Deboer, "The two-process model of sleep regulation: a reappraisal," *J. Sleep Res.*, vol. 25, no. 2, pp. 131–143, 2016.
- [54] A. R. Braun *et al.*, "Regional cerebral blood flow throughout the sleep-wake cycle. An H215O PET study," *Brain*, 1997.
- [55] G. S. Richardson, "The human circadian system in normal and disordered sleep.," *J. Clin. Psychiatry*, vol. 66, pp. 3–9, 2005.
- [56] S. M. Reppert and D. R. Weaver, "Coordination of circadian timing in mammals," *Nature*, vol. 418, no. 6901, p. 935, 2002.

- [57] V. Pilonis *et al.*, “Melanopsin regulates both sleep-promoting and arousal-promoting responses to light,” *PLoS Biol.*, vol. 14, no. 6, p. e1002482, 2016.
- [58] D. M. Edgar, W. C. Dement, and C. A. Fuller, “Effect of SCN lesions on sleep in squirrel monkeys: Evidence for opponent processes in sleep-wake regulation,” *J. Neurosci.*, 1993.
- [59] D.-J. Dijk and S. W. Lockley, “Invited Review: Integration of human sleep-wake regulation and circadian rhythmicity,” *J. Appl. Physiol.*, vol. 92, no. 2, pp. 852–862, 2002.
- [60] C. B. Saper, T. E. Scammell, and J. Lu, “Hypothalamic regulation of sleep and circadian rhythms,” *Nature*, vol. 437, no. 7063, p. 1257, 2005.
- [61] L. Verret *et al.*, “A role of melanin-concentrating hormone producing neurons in the central regulation of paradoxical sleep,” *BMC Neurosci.*, vol. 4, no. 1, p. 19, 2003.
- [62] I. V Estabrooke *et al.*, “Fos expression in orexin neurons varies with behavioral state,” *J. Neurosci.*, vol. 21, no. 5, pp. 1656–1662, 2001.
- [63] M. G. Lee, O. K. Hassani, and B. E. Jones, “Discharge of identified orexin/hypocretin neurons across the sleep-waking cycle,” *J. Neurosci.*, vol. 25, no. 28, pp. 6716–6720, 2005.
- [64] C. B. Saper, P. M. Fuller, N. P. Pedersen, J. Lu, and T. E. Scammell, “Sleep state switching,” *Neuron*, vol. 68, no. 6, pp. 1023–1042, 2010.
- [65] J. A. Hobson and E. F. Pace-Schott, “The Neurobiology of Sleep: Genetics, cellular physiology and subcortical networks,” *Nat. Rev. Neurosci.*, 2002.
- [66] M. Steriade, “Arousal: Revisiting the reticular activating system,” *Science*. 1996.
- [67] K. Spiegel, R. Leproult, and E. Van Cauter, “Impact of sleep debt on metabolic and endocrine function,” *Lancet*, 1999.
- [68] A. Bollimunta, J. Mo, C. E. Schroeder, and M. Ding, “Neuronal mechanisms and attentional modulation of corticothalamic alpha oscillations,” *J. Neurosci.*, 2011.
- [69] R. T. Canolty *et al.*, “Oscillatory phase coupling coordinates anatomically dispersed functional cell assemblies,” *Proc. Natl. Acad. Sci.*, vol. 107, no. 40, pp. 17356–17361, 2010.
- [70] I. Timofeev and M. Bazhenov, *Mechanisms and biological role of thalamocortical oscillations*. 2005.
- [71] F. Ferrarelli and G. Tononi, “Reduced sleep spindle activity point to a TRN-MD thalamus-PFC circuit dysfunction in schizophrenia,” *Schizophr. Res.*, vol. 180, pp. 36–43, 2017.
- [72] P. Fuentealba and M. Steriade, “The reticular nucleus revisited: intrinsic and network properties of a thalamic pacemaker,” *Prog. Neurobiol.*, vol. 75, no. 2, pp. 125–141, 2005.
- [73] S. M. Sherman, “Thalamocortical interactions,” *Curr. Opin. Neurobiol.*, vol. 22, no. 4, pp. 575–579, 2012.
- [74] I. D. Manns, L. Mainville, and B. E. Jones, “Evidence for glutamate, in addition to acetylcholine and GABA, neurotransmitter synthesis in basal forebrain neurons projecting to the entorhinal cortex,” *Neuroscience*, vol. 107, no. 2, pp. 249–263, 2001.
- [75] E. E. Hur and L. Zaborszky, “Vglut2 afferents to the medial prefrontal and primary somatosensory cortices: a combined retrograde tracing in situ hybridization,” *J. Comp. Neurol.*, vol. 483, no. 3, pp.

- 351–373, 2005.
- [76] M. C. Xi, F. R. Morales, and M. H. Chase, “Induction of wakefulness and inhibition of active (REM) sleep by GABAergic processes in the nucleus pontis oralis,” *Arch. Ital. Biol.*, vol. 139, no. 1, pp. 125–145, 2001.
- [77] C. Cirelli, “The genetic and molecular regulation of sleep: From fruit flies to humans,” *Nature Reviews Neuroscience*. 2009.
- [78] I. Tobler *et al.*, “Altered circadian activity rhythms and sleep in mice devoid of prion protein,” *Nature*, 1996.
- [79] J. Zhang, F. Obál Jr, J. Fang, B. J. Collins, and J. M. Krueger, “Non-rapid eye movement sleep is suppressed in transgenic mice with a deficiency in the somatotropic system,” *Neurosci. Lett.*, vol. 220, no. 2, pp. 97–100, 1996.
- [80] C. Peyron *et al.*, “A mutation in a case of early onset narcolepsy and a generalized absence of hypocretin peptides in human narcoleptic brains,” *Nat Med*, vol. 6, no. 9, pp. 991–997, 2000.
- [81] C. Cirelli, “A molecular window on sleep: changes in gene expression between sleep and wakefulness,” *Neurosci.*, vol. 11, no. 1, pp. 63–74, 2005.
- [82] R. Holliday and J. E. Pugh, “DNA modification mechanisms and gene activity during development,” *Science (80-.)*, vol. 187, no. 4173, pp. 226–232, 1975.
- [83] A. D. Riggs, “X inactivation, differentiation, and DNA methylation,” *Cytogenet. Genome Res.*, vol. 14, no. 1, pp. 9–25, 1975.
- [84] M. Okano, D. W. Bell, D. A. Haber, and E. Li, “DNA methyltransferases Dnmt3a and Dnmt3b are essential for de novo methylation and mammalian development,” *Cell*, vol. 99, no. 3, pp. 247–257, 1999.
- [85] E. Li, T. H. Bestor, and R. Jaenisch, “Targeted mutation of the DNA methyltransferase gene results in embryonic lethality,” *Cell*, vol. 69, no. 6, pp. 915–926, 1992.
- [86] M. Okano, S. Xie, and E. Li, “Cloning and characterization of a family of novel mammalian DNA (cytosine-5) methyltransferases,” *Nat. Genet.*, vol. 19, no. 3, p. 219, 1998.
- [87] P. L. Jones *et al.*, “Methylated DNA and MeCP2 recruit histone deacetylase to repress transcription,” *Nat. Genet.*, 1998.
- [88] M. S. Cosgrove, J. D. Boeke, and C. Wolberger, “Regulated nucleosome mobility and the histone code,” *Nat. Struct. Mol. Biol.*, vol. 11, no. 11, p. 1037, 2004.
- [89] B. D. Strahl and C. D. Allis, “The language of covalent histone modifications,” *Nature*, vol. 403, no. 6765, p. 41, 2000.
- [90] L. S. Wilkinson, W. Davies, and A. R. Isles, “Genomic imprinting effects on brain development and function,” *Nat. Rev. Neurosci.*, vol. 8, no. 11, p. 832, 2007.
- [91] S. K. Murphy and R. L. Jirtle, “Imprinting evolution and the price of silence,” *Bioessays*, vol. 25, no. 6, pp. 577–588, 2003.
- [92] S. B. Cassidy, S. Schwartz, J. L. Miller, and D. J. Driscoll, “Prader-Willi syndrome,” *Genet. Med.*, vol. 14, p. 10, Sep. 2011.

- [93] M. A. Angulo, M. G. Butler, and M. E. Cataletto, "Prader-Willi syndrome: A review of clinical, genetic, and endocrine findings," *J. Endocrinol. Invest.*, 2015.
- [94] D. Kanber *et al.*, "A paternal deletion of MKRN3, MAGEL2 and NDN does not result in Prader-Willi syndrome," *Eur. J. Hum. Genet.*, vol. 17, no. 5, p. 582, 2009.
- [95] C. P. Schaaf *et al.*, "Truncating mutations of MAGEL2 cause Prader-Willi phenotypes and autism," *Nat. Genet.*, vol. 45, p. 1405, Sep. 2013.
- [96] A. J. de Smith *et al.*, "A deletion of the HBII-85 class of small nucleolar RNAs (snoRNAs) is associated with hyperphagia, obesity and hypogonadism," *Hum. Mol. Genet.*, vol. 18, no. 17, pp. 3257–3265, 2009.
- [97] B. V. Skryabin *et al.*, "Deletion of the MBII-85 snoRNA gene cluster in mice results in postnatal growth retardation," *PLoS Genet.*, vol. 3, no. 12, p. e235, 2007.
- [98] J. Cavaillé *et al.*, "Identification of brain-specific and imprinted small nucleolar RNA genes exhibiting an unusual genomic organization," *Proc. Natl. Acad. Sci.*, vol. 97, no. 26, pp. 14311–14316, 2000.
- [99] F. Ding *et al.*, "SnoRNA Snord116 (Pwcr1/MBII-85) deletion causes growth deficiency and hyperphagia in mice," *PLoS One*, vol. 3, no. 3, p. e1709, 2008.
- [100] G. Lassi *et al.*, "Deletion of the Snord116/SNORD116 alters sleep in mice and patients with Prader-Willi syndrome," *Sleep*, vol. 39, no. 3, pp. 637–644, 2016.
- [101] J. L. Miller *et al.*, "Nutritional phases in Prader-Willi syndrome," *Am. J. Med. Genet. Part A*, vol. 155, no. 5, pp. 1040–1049, 2011.
- [102] U. Eiholzer, Y. Nordmann, D. L'allemand, M. Schlumpf, S. Schmid, and K. Kromeyer-Hauschild, "Improving body composition and physical activity in Prader-Willi syndrome," *J. Pediatr.*, vol. 142, no. 1, pp. 73–78, 2003.
- [103] A. P. Goldstone, "Prader-Willi syndrome: Advances in genetics, pathophysiology and treatment," *Trends in Endocrinology and Metabolism*. 2004.
- [104] M. G. Butler, "Management of obesity in Prader-Willi syndrome," *Nat. Rev. Endocrinol.*, vol. 2, no. 11, p. 592, 2006.
- [105] C. Bizzarri *et al.*, "Children with Prader-Willi syndrome exhibit more evident meal-induced responses in plasma ghrelin and peptide YY levels than obese and lean children," *Eur. J. Endocrinol.*, vol. 162, no. 3, pp. 499–505, 2010.
- [106] A. Lukoshe, A. C. Hokken-Koelega, A. van der Lugt, and T. White, "Reduced cortical complexity in children with Prader-Willi Syndrome and its association with cognitive impairment and developmental delay," *PLoS One*, vol. 9, no. 9, p. e107320, 2014.
- [107] D. J. Clarke, J. Waters, and J. A. Corbett, "Adults with Prader-Willi syndrome: abnormalities of sleep and behaviour," *J R Soc Med*, vol. 82, no. 1, pp. 21–24, 1989.
- [108] D. Camfferman, R. D. McEvoy, F. O'Donoghue, and K. Lushington, "Prader Willi Syndrome and excessive daytime sleepiness," *Sleep Med. Rev.*, vol. 12, no. 1, pp. 65–75, 2008.
- [109] G. Hertz, M. Cataletto, S. H. Feinsilver, and M. Angulo, "Sleep and breathing patterns in patients

- with Prader Willi syndrome (PWS): effects of age and gender," *Sleep*, vol. 16, no. 4, pp. 366–371, 1993.
- [110] T. Gilboa and V. Gross-Tsur, "Epilepsy in Prader-Willi syndrome: Experience of a national referral centre," *Dev. Med. Child Neurol.*, 2013.
- [111] E. O. Bixler, A. N. Vgontzas, H.-M. Lin, S. L. Calhoun, A. Vela-Bueno, and A. Kales, "Excessive daytime sleepiness in a general population sample: the role of sleep apnea, age, obesity, diabetes, and depression," *J. Clin. Endocrinol. Metab.*, vol. 90, no. 8, pp. 4510–4515, 2005.
- [112] N. Shah and F. Roux, "The relationship of obesity and obstructive sleep apnea," *Clin. Chest Med.*, vol. 30, no. 3, pp. 455–465, 2009.
- [113] G. M. Nixon and R. T. Brouillette, "Sleep and breathing in Prader-Willi syndrome," *Pediatr. Pulmonol.*, vol. 34, no. 3, pp. 209–217, 2002.
- [114] B. J. Yee *et al.*, "Assessment of sleep and breathing in adults with prader-willi syndrome: a case control series," *J. Clin. Sleep Med.*, vol. 3, no. 07, pp. 713–718, 2007.
- [115] S. Nevsimalova, J. Vankova, I. Stepanova, E. Seemanova, E. Mignot, and S. Nishino, "Hypocretin deficiency in Prader-Willi syndrome," *Eur. J. Neurol.*, vol. 12, no. 1, pp. 70–72, 2005.
- [116] Y. Dauvilliers *et al.*, "CSF hypocretin-1 levels in narcolepsy, Kleine-Levin syndrome, and other hypersomnias and neurological conditions," *J. Neurol. Neurosurg. Psychiatry*, vol. 74, no. 12, pp. 1667–1673, 2003.
- [117] R. Ferri *et al.*, "NREM sleep alterations in narcolepsy/cataplexy," *Clin. Neurophysiol.*, vol. 116, no. 11, pp. 2675–2684, 2005.
- [118] A. N. Vgontzas *et al.*, "Daytime Sleepiness and Rem Abnormalities in Prader-Willi Syndrome: Evidence of Generalized Hypoarousal," *Int. J. Neurosci.*, vol. 87, no. 3–4, pp. 127–139, 1996.
- [119] U. Eiholzer *et al.*, "Hypothalamic and gonadal components of hypogonadism in boys with Prader-Labhart-Willi syndrome," *J. Clin. Endocrinol. Metab.*, 2006.
- [120] U. Eiholzer and B. Y. Whitman, "A comprehensive team approach to the management of patients with Prader-Willi syndrome," *Journal of Pediatric Endocrinology and Metabolism*. 2004.
- [121] D. F. Swaab, "Prader-Willi syndrome and the hypothalamus," *Acta Paediatr.*, vol. 86, no. S423, pp. 50–54, 1997.
- [122] R. Arens *et al.*, "Arousal and cardiorespiratory responses to hypoxia in Prader-Willi syndrome," *Am. J. Respir. Crit. Care Med.*, vol. 153, no. 1, pp. 283–287, 1996.
- [123] R. Manni *et al.*, "Hypersomnia in the Prader Willi syndrome: clinical-electrophysiological features and underlying factors," *Clin. Neurophysiol.*, vol. 112, no. 5, pp. 800–805, 2001.
- [124] A. A. Menendez, "Abnormal ventilatory responses in patients with Prader-Willi syndrome," *Eur. J. Pediatr.*, vol. 158, no. 11, pp. 941–942, 1999.
- [125] E. B. Keverne, R. Fundele, M. Narasimha, S. C. Barton, and M. A. Surani, "Genomic imprinting and the differential roles of parental genomes in brain development," *Dev. Brain Res.*, vol. 92, no. 1, pp. 91–100, 1996.
- [126] V. C. De Cock *et al.*, "Efficacy of modafinil on excessive daytime sleepiness in Prader-Willi

- syndrome," *Am. J. Med. Genet. Part A*, 2011.
- [127] C. Inocente *et al.*, "Pitolisant, an inverse agonist of the histamine H3 receptor: an alternative stimulant for narcolepsy-cataplexy in teenagers with refractory sleepiness," *Clin Neuropharmacol*, vol. 35, no. 2, pp. 55–60, 2012.
- [128] D. Lazewska and K. Kiec-Kononowicz, "Recent advances in histamine H3 receptor antagonists/inverse agonists," *Expert Opin Ther Pat*, vol. 20, no. 9, pp. 1147–1169, 2010.
- [129] J. C. Schwartz, "The histamine H3 receptor: from discovery to clinical trials with pitolisant," *Br J Pharmacol*, vol. 163, no. 4, pp. 713–721, 2011.
- [130] R. M. Chemelli *et al.*, "Narcolepsy in orexin knockout mice: molecular genetics of sleep regulation," *Cell*, vol. 98, no. 4, pp. 437–451, 1999.
- [131] X. Ligneau *et al.*, "BF2.649 [1-{3-[3-(4-Chlorophenyl)propoxy]propyl}piperidine, hydrochloride], a nonimidazole inverse agonist/antagonist at the human histamine H3 receptor: Preclinical pharmacology," *J Pharmacol Exp Ther*, vol. 320, no. 1, pp. 365–375, 2007.
- [132] E. Törnqvist, A. Annas, B. Granath, E. Jalkestén, I. Cotgreave, and M. Öberg, "Strategic focus on 3R principles reveals major reductions in the use of animals in pharmaceutical toxicity testing," *PLoS One*, 2014.
- [133] E. Balzani, M. Falappa, F. Balci, and V. Tucci, "An approach to monitoring home-cage behavior in mice that facilitates data sharing," *Nat. Protoc.*, vol. 13, no. 6, pp. 1331–1347, 2018.
- [134] S. J. Swoap, J. M. Overton, and G. Garber, "Effect of ambient temperature on cardiovascular parameters in rats and mice: a comparative approach," *Am J Physiol Regul Integr Comp Physiol*, vol. 287, no. 2, pp. R391–6, 2004.
- [135] J. R. Speakman and J. Keijer, "Not so hot: Optimal housing temperatures for mice to mimic the thermal environment of humans," *Mol Metab*, vol. 2, no. 1, pp. 5–9, 2012.
- [136] A. A. Romanovsky, A. I. Ivanov, and Y. P. Shimansky, "Selected contribution: ambient temperature for experiments in rats: a new method for determining the zone of thermal neutrality," *J Appl Physiol*, vol. 92, no. 6, pp. 2667–2679, 2002.
- [137] P. Chomczynski and K. Mackey, "Short technical reports. Modification of the TRI reagent procedure for isolation of RNA from polysaccharide- and proteoglycan-rich sources," *Biotechniques*, vol. 19, no. 6, pp. 942–945, 1995.
- [138] M. Pace, A. Adamantidis, L. Facchin, and C. Bassetti, "Role of REM Sleep, Melanin Concentrating Hormone and Orexin/Hypocretin Systems in the Sleep Deprivation Pre-Ischemia," *PLoS One*, vol. 12, no. 1, p. e0168430, 2017.
- [139] N. L. Bray, H. Pimentel, P. Melsted, and L. Pachter, "Near-optimal probabilistic RNA-seq quantification," *Nat. Biotechnol.*, vol. 34, no. 5, p. 525, 2016.
- [140] M. I. Love, W. Huber, and S. Anders, "Moderated estimation of fold change and dispersion for RNA-seq data with DESeq2," *Genome Biol.*, vol. 15, no. 12, p. 550, 2014.
- [141] S. Tripathi *et al.*, "Meta-and orthogonal integration of influenza 'OMICS' data defines a role for UBR4 in virus budding," *Cell Host Microbe*, vol. 18, no. 6, pp. 723–735, 2015.

- [142] M. Pace *et al.*, “Rapid eye movements sleep as a predictor of functional outcome after stroke: A translational study,” *Sleep*, 2018.
- [143] K. A. Ludwig, R. M. Miriani, N. B. Langhals, M. D. Joseph, D. J. Anderson, and D. R. Kipke, “Using a common average reference to improve cortical neuron recordings from microelectrode arrays,” *J Neurophysiol*, vol. 101, no. 3, pp. 1679–1689, 2009.
- [144] J. C. Erickson *et al.*, “Falling-edge, variable threshold (FEVT) method for the automated detection of gastric slow wave events in high-resolution serosal electrode recordings,” *Ann Biomed Eng*, vol. 38, no. 4, pp. 1511–1529, 2010.
- [145] M. R. Keshtkaran and Z. Yang, “Noise-robust unsupervised spike sorting based on discriminative subspace learning with outlier handling,” *J Neural Eng*, vol. 14, no. 3, p. 36003, 2017.
- [146] B. Y. Mileykovskiy, L. I. Kiyashchenko, and J. M. Siegel, “Behavioral correlates of activity in identified hypocretin/orexin neurons,” *Neuron*, vol. 46, no. 5, pp. 787–798, 2005.
- [147] G. Zamboni, R. Amici, E. Perez, C. A. Jones, and P. L. Parmeggiani, “Pattern of REM sleep occurrence in continuous darkness following the exposure to low ambient temperature in the rat,” *Behav Brain Res*, vol. 122, no. 1, pp. 25–32, 2001.
- [148] L. A. Toth and P. Bhargava, “Animal models of sleep disorders,” *Comp. Med.*, vol. 63, no. 2, pp. 91–104, 2013.
- [149] M. Bandarabadi, C. G. Herrera, T. C. Gent, C. Bassetti, K. Schindler, and A. R. Adamantidis, “Dissecting local sleep spindles in the thalamocortical system,” in *JOURNAL OF SLEEP RESEARCH*, 2018, vol. 27.
- [150] L. Liu and K. Duff, “A technique for serial collection of cerebrospinal fluid from the cisterna magna in mouse,” *J Vis Exp*, no. 21, 2008.
- [151] J. S. Lin *et al.*, “An inverse agonist of the histamine H(3) receptor improves wakefulness in narcolepsy: studies in orexin-/- mice and patients,” *Neurobiol Dis*, vol. 30, no. 1, pp. 74–83, 2008.
- [152] M. Schoonakker, J. H. Meijer, T. Deboer, and K. Fifel, “Heterogeneity in the circadian and homeostatic modulation of multiunit activity in the lateral hypothalamus,” *Sleep*, vol. 41, no. 6, p. zsy051, 2018.
- [153] O. K. Hassani, M. G. Lee, and B. E. Jones, “Melanin-concentrating hormone neurons discharge in a reciprocal manner to orexin neurons across the sleep-wake cycle,” *Proc Natl Acad Sci U S A*, vol. 106, no. 7, pp. 2418–2422, 2009.
- [154] J. Poley-Wolf *et al.*, “Hypothalamic loss of Snord116 recapitulates the hyperphagia of Prader-Willi syndrome,” *J Clin Invest*, vol. 128, no. 3, pp. 960–969, 2018.
- [155] Y. Qi *et al.*, “Snord116 is critical in the regulation of food intake and body weight,” *Sci Rep*, vol. 6, p. 18614, 2016.
- [156] R. Amici, G. Zamboni, E. Perez, C. A. Jones, and P. L. Parmeggiani, “The influence of a heavy thermal load on REM sleep in the rat,” *Brain Res*, vol. 781, no. 1–2, pp. 252–258, 1998.
- [157] R. Amici *et al.*, “Cold exposure and sleep in the rat: REM sleep homeostasis and body size,” *Sleep*, vol. 31, no. 5, pp. 708–715, 2008.

- [158] R. Szymusiak and E. Satinoff, "Maximal REM sleep time defines a narrower thermoneutral zone than does minimal metabolic rate," *Physiol Behav*, vol. 26, no. 4, pp. 687–690, 1981.
- [159] P. Li, S. H. Sur, R. E. Mistlberger, and M. Morris, "Circadian blood pressure and heart rate rhythms in mice," *Am. J. Physiol. Integr. Comp. Physiol.*, vol. 276, no. 2, pp. R500–R504, 1999.
- [160] E. G. Bochukova *et al.*, "A transcriptomic signature of the hypothalamic response to fasting and BDNF deficiency in Prader-Willi syndrome," *Cell Rep.*, vol. 22, no. 13, pp. 3401–3408, 2018.
- [161] Y. Zhou *et al.*, "Metascape provides a biologist-oriented resource for the analysis of systems-level datasets," *Nat. Commun.*, vol. 10, no. 1, p. 1523, 2019.
- [162] M. M. Thiaville, J. M. Huang, H. Kim, M. B. Ekram, T. Y. Roh, and J. Kim, "DNA-binding motif and target genes of the imprinted transcription factor PEG3," *Gene*, vol. 512, no. 2, pp. 314–320, 2013.
- [163] Y. Kuroiwa *et al.*, "Peg3 imprinted gene on proximal chromosome 7 encodes for a zinc finger protein," *Nat Genet*, vol. 12, no. 2, pp. 186–190, 1996.
- [164] A. Seifinejad *et al.*, "Molecular codes and in vitro generation of hypocretin and melanin concentrating hormone neurons," *Proc. Natl. Acad. Sci.*, vol. 116, no. 34, pp. 17061–17070, 2019.
- [165] T. Moriguchi, T. Sakurai, S. Takahashi, K. Goto, and M. Yamamoto, "The human prepro-orexin gene regulatory region that activates gene expression in the lateral region and represses it in the medial regions of the hypothalamus," *J. Biol. Chem.*, vol. 277, no. 19, pp. 16985–16992, 2002.
- [166] A. Ye, H. He, and J. Kim, "PEG3 binds to H19-ICR as a transcriptional repressor," *Epigenetics*, vol. 11, no. 12, pp. 889–900, 2016.
- [167] Y. S. Bogliotti and P. J. Ross, "Mechanisms of histone H3 lysine 27 trimethylation remodeling during early mammalian development," *Epigenetics*, vol. 7, no. 9, pp. 976–981, 2012.
- [168] J. Hara *et al.*, "Genetic ablation of orexin neurons in mice results in narcolepsy, hypophagia, and obesity," *Neuron*, vol. 30, no. 2, pp. 345–354, 2001.
- [169] T. Kuwaki, "Thermoregulation under pressure: a role for orexin neurons," *Temp.*, vol. 2, no. 3, pp. 379–391, 2015.
- [170] L. Trachsel, I. Tobler, P. Achermann, and A. A. Borbély, "Sleep continuity and the REM-nonREM cycle in the rat under baseline conditions and after sleep deprivation," *Physiol. Behav.*, vol. 49, no. 3, pp. 575–580, 1991.
- [171] H. A. Mitchell and D. Weinshenker, "Good night and good luck: norepinephrine in sleep pharmacology," *Biochem Pharmacol*, vol. 79, no. 6, pp. 801–809, 2010.
- [172] C. H. Schenck, S. R. Bundlie, M. G. Ettinger, and M. W. Mahowald, "Chronic behavioral disorders of human REM sleep: a new category of parasomnia," *Sleep*, vol. 9, no. 2, pp. 293–308, 1986.
- [173] M. J. Sateia, "International classification of sleep disorders-third edition: highlights and modifications," *Chest*, vol. 146, no. 5, pp. 1387–1394, 2014.
- [174] S. McVea, A. J. Thompson, N. Abid, and J. Richardson, "Thermal dysregulation in Prader-Willi syndrome: a potentially fatal complication in adolescence, not just in infancy," *Case Reports*, vol. 2016, p. bcr2016215344, 2016.
- [175] J. C. Ehlen *et al.*, "Maternal Ube3a Loss Disrupts Sleep Homeostasis But Leaves Circadian

- Rhythmicity Largely Intact," *J Neurosci*, vol. 35, no. 40, pp. 13587–13598, 2015.
- [176] R. Huber, T. Deboer, and I. Tobler, "Effects of sleep deprivation on sleep and sleep EEG in three mouse strains: empirical data and simulations," *Brain Res*, vol. 857, no. 1–2, pp. 8–19, 2000.
- [177] S. V Kozlov *et al.*, "The imprinted gene *Magel2* regulates normal circadian output," *Nat Genet*, vol. 39, no. 10, pp. 1266–1272, 2007.
- [178] S. Jegu *et al.*, "Optogenetic identification of a rapid eye movement sleep modulatory circuit in the hypothalamus," *Nat Neurosci*, vol. 16, no. 11, pp. 1637–1643, 2013.
- [179] F. Naganuma, S. S. Bandaru, G. Absi, C. E. Mahoney, T. E. Scammell, and R. Vetrivelan, "Melanin-concentrating hormone neurons contribute to dysregulation of rapid eye movement sleep in narcolepsy," *Neurobiol. Dis.*, vol. 120, pp. 12–20, 2018.
- [180] J. R. Barson, I. Morganstern, and S. F. Leibowitz, "Complementary roles of orexin and melanin-concentrating hormone in feeding behavior," *Int J Endocrinol*, vol. 2013, p. 983964, 2013.
- [181] D. Burdakov, M. M. Karnani, and A. Gonzalez, "Lateral hypothalamus as a sensor-regulator in respiratory and metabolic control," *Physiol Behav*, vol. 121, pp. 117–124, 2013.
- [182] J. A. Gonzalez, P. Iordanidou, M. Strom, A. Adamantidis, and D. Burdakov, "Awake dynamics and brain-wide direct inputs of hypothalamic MCH and orexin networks," *Nat Commun*, vol. 7, p. 11395, 2016.
- [183] A. M. Manzardo, L. Johnson, J. L. Miller, D. J. Driscoll, and M. G. Butler, "Higher plasma orexin a levels in children with Prader-Willi syndrome compared with healthy unrelated sibling controls," *Am J Med Genet A*, vol. 170, no. 9, pp. 2328–2333, 2016.
- [184] M. Omokawa *et al.*, "Decline of CSF orexin (hypocretin) levels in Prader-Willi syndrome," *Am. J. Med. Genet. Part A*, vol. 170, no. 5, pp. 1181–1186, 2016.
- [185] M. Cerri *et al.*, "Enhanced slow-wave EEG activity and thermoregulatory impairment following the inhibition of the lateral hypothalamus in the rat," *PLoS One*, vol. 9, no. 11, p. e112849, 2014.
- [186] R. Fronczek *et al.*, "Manipulation of core body and skin temperature improves vigilance and maintenance of wakefulness in narcolepsy," *Sleep*, vol. 31, no. 2, pp. 233–240, 2008.
- [187] S. S. Mosko, J. B. Holowach, and J. F. Sassin, "The 24-hour rhythm of core temperature in narcolepsy," *Sleep*, vol. 6, no. 2, pp. 137–146, 1983.
- [188] C. P. Pollak and D. R. Wagner, "Core body temperature in narcoleptic and normal subjects living in temporal isolation," *Pharmacol Biochem Behav*, vol. 47, no. 1, pp. 65–71, 1994.
- [189] T. Mochizuki, E. B. Klerman, T. Sakurai, and T. E. Scammell, "Elevated body temperature during sleep in orexin knockout mice," *Am J Physiol Regul Integr Comp Physiol*, vol. 291, no. 3, pp. R533–40, 2006.
- [190] M. Cerri, "The Central Control of Energy Expenditure: Exploiting Torpor for Medical Applications," *Annu Rev Physiol*, vol. 79, pp. 167–186, 2017.
- [191] P. L. Parmeggiani, "Thermoregulation and sleep," *Front Biosci*, vol. 8, pp. s557–67, 2003.
- [192] N. Komagata, B. Latifi, T. Rusterholz, C. L. A. Bassetti, A. Adamantidis, and M. H. Schmidt, "Dynamic REM Sleep Modulation by Ambient Temperature and the Critical Role of the Melanin-

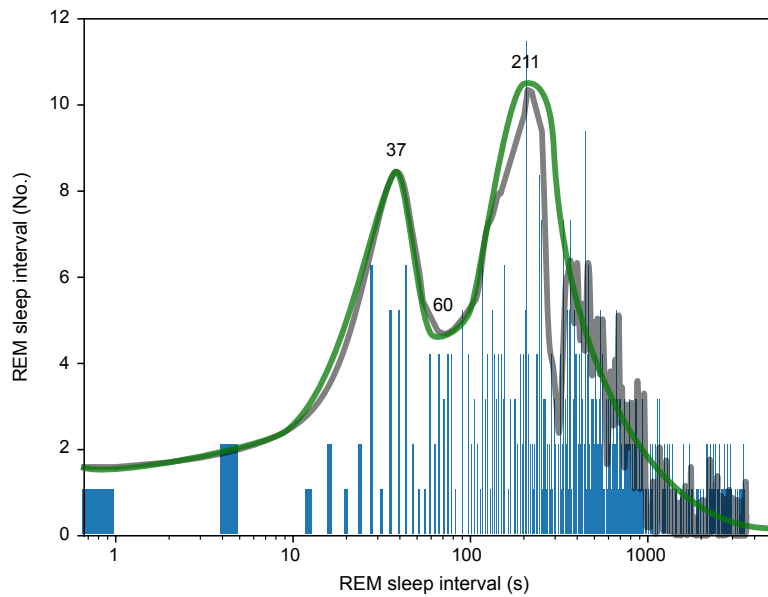
- Concentrating Hormone System," *Curr. Biol.*, 2019.
- [193] A. J. Esbensen and A. J. Schwichtenberg, "Sleep in neurodevelopmental disorders," in *International review of research in developmental disabilities*, vol. 51, Elsevier, 2016, pp. 153–191.
- [194] R. L. Hardiman and A. Bratt, "Hypothalamic-pituitary-adrenal axis function in Fragile X Syndrome and its relationship to behaviour: A systematic review," *Physiol. Behav.*, vol. 167, pp. 341–353, 2016.
- [195] R. Kronk, E. E. Bishop, M. Raspa, J. O. Bickel, D. A. Mandel, and D. B. Bailey Jr, "Prevalence, nature, and correlates of sleep problems among children with fragile X syndrome based on a large scale parent survey," *Sleep*, vol. 33, no. 5, pp. 679–687, 2010.
- [196] M. Gunay-Aygun, S. Schwartz, S. Heeger, M. A. O’Riordan, and S. B. Cassidy, "The changing purpose of Prader-Willi syndrome clinical diagnostic criteria and proposed revised criteria," *Pediatrics*, vol. 108, no. 5, pp. e92–e92, 2001.
- [197] V. Tucci, "Genomic Imprinting: A New Epigenetic Perspective of Sleep Regulation," *PLOS Genet.*, 2016.
- [198] R. Amici *et al.*, "Pattern of desynchronized sleep during deprivation and recovery induced in the rat by changes in ambient temperature," *J Sleep Res*, vol. 3, no. 4, pp. 250–256, 1994.
- [199] R. Ursin, "Sleep stage relations within the sleep cycles of the cat," *Brain Res.*, vol. 20, no. 1, pp. 91–97, 1970.
- [200] H. Merica and J.-M. Gaillard, "A study of the interrupted REM episode," *Physiol. Behav.*, vol. 50, no. 6, pp. 1153–1159, 1991.
- [201] G. Zamboni, E. Perez, R. Amici, C. A. Jones, and P. L. Parmeggiani, "Control of REM sleep: an aspect of the regulation of physiological homeostasis," *Arch Ital Biol*, vol. 137, no. 4, pp. 249–262, 1999.
- [202] C. A. Jones *et al.*, "Lithium affects REM sleep occurrence, autonomic activity and brain second messengers in the rat," *Behav. Brain Res.*, vol. 187, no. 2, pp. 254–261, 2008.
- [203] G. Zamboni *et al.*, "Specific changes in cerebral second messenger accumulation underline REM sleep inhibition induced by the exposure to low ambient temperature," *Brain Res.*, vol. 1022, no. 1–2, pp. 62–70, 2004.
- [204] R. Gruber and M. S. Wise, "Sleep spindle characteristics in children with neurodevelopmental disorders and their relation to cognition," *Neural Plast.*, vol. 2016, 2016.
- [205] L. C. Burnett, G. Hubner, C. A. LeDuc, M. V Morabito, J. F. M. Carli, and R. L. Leibel, "Loss of the imprinted, non-coding Snord116 gene cluster in the interval deleted in the Prader Willi syndrome results in murine neuronal and endocrine pancreatic developmental phenotypes," *Hum Mol Genet*, vol. 26, no. 23, pp. 4606–4616, 2017.
- [206] A. Adhikari *et al.*, "Cognitive deficits in the Snord116 deletion mouse model for Prader-Willi syndrome," *Neurobiol Learn Mem*, 2018.
- [207] J. Taillard *et al.*, "Non-REM sleep characteristics predict early cognitive impairment in an aging population," *Front. Neurol.*, vol. 10, 2019.
- [208] S. V Weselake, J. L. Foulds, R. Couch, M. B. Witmans, D. Rubin, and A. M. Haqq, "Prader-Willi

- syndrome, excessive daytime sleepiness, and narcoleptic symptoms: a case report," *J Med Case Rep*, vol. 8, p. 127, 2014.
- [209] O. Eschenko, C. Magri, S. Panzeri, and S. J. Sara, "Noradrenergic neurons of the locus coeruleus are phase locked to cortical up-down states during sleep," *Cereb. Cortex*, vol. 22, no. 2, pp. 426–435, 2011.
- [210] M. A. Geyer, D. S. Segal, and A. J. Mandell, "Effect of intraventricular infusion of dopamine and norepinephrine on motor activity," *Physiol Behav*, vol. 8, no. 4, pp. 653–658, 1972.
- [211] I. Colombi, F. Tinarelli, V. Pasquale, V. Tucci, and M. Chiappalone, "A simplified in vitro experimental model encompasses the essential features of sleep," *Front. Neurosci.*, vol. 10, p. 315, 2016.
- [212] V. Hinard *et al.*, "Key electrophysiological, molecular, and metabolic signatures of sleep and wakefulness revealed in primary cortical cultures," *J. Neurosci.*, vol. 32, no. 36, pp. 12506–12517, 2012.
- [213] S. Saberi-Moghadam, A. Simi, H. Setareh, C. Mikhail, and M. Tafti, "In vitro cortical network firing is homeostatically regulated: a model for sleep regulation," *Sci. Rep.*, vol. 8, no. 1, p. 6297, 2018.
- [214] M. W. O'Malley and S. Datta, "REM Sleep Regulating Mechanisms in the Cholinergic Cell Compartment of the Brainstem," *Indian J Sleep Med*, vol. 8, no. 2, pp. 58–66, 2013.
- [215] D. E. Bergles, V. A. Doze, D. V. Madison, and S. J. Smith, "Excitatory actions of norepinephrine on multiple classes of hippocampal CA1 interneurons," *J. Neurosci.*, vol. 16, no. 2, pp. 572–585, 1996.
- [216] M. T. Colonnese *et al.*, "A conserved switch in sensory processing prepares developing neocortex for vision," *Neuron*, vol. 67, no. 3, pp. 480–498, 2010.
- [217] R. L. Coulson *et al.*, "Snord116-dependent diurnal rhythm of DNA methylation in mouse cortex," *Nat. Commun.*, vol. 9, no. 1, p. 1616, 2018.
- [218] Y. Kobayashi, Z. Ye, and T. K. Hensch, "Clock genes control cortical critical period timing," *Neuron*, vol. 86, no. 1, pp. 264–275, 2015.
- [219] S. Habtemariam, "The brain-derived neurotrophic factor in neuronal plasticity and neuroregeneration: new pharmacological concepts for old and new drugs," *Neural Regen. Res.*, vol. 13, no. 6, p. 983, 2018.
- [220] E. Bieth *et al.*, "Highly restricted deletion of the SNORD116 region is implicated in Prader-Willi Syndrome," *Eur J Hum Genet*, vol. 23, no. 2, pp. 252–255, 2015.
- [221] L. M. Paterson, D. J. Nutt, and S. J. Wilson, "Sleep and its disorders in translational medicine," *J. Psychopharmacol.*, vol. 25, no. 9, pp. 1226–1234, 2011.
- [222] J. A. Hobson and E. F. Pace-Schott, "The cognitive neuroscience of sleep: neuronal systems, consciousness and learning," *Nat. Rev. Neurosci.*, vol. 3, no. 9, p. 679, 2002.

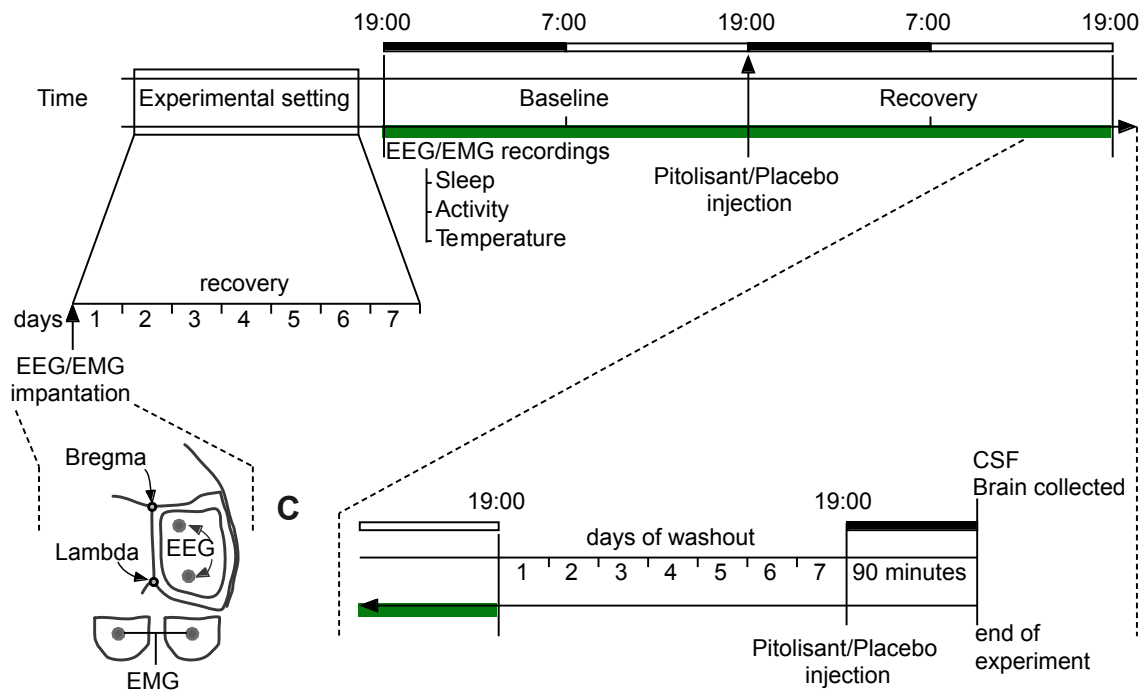
Supplementary materials

Figures

A

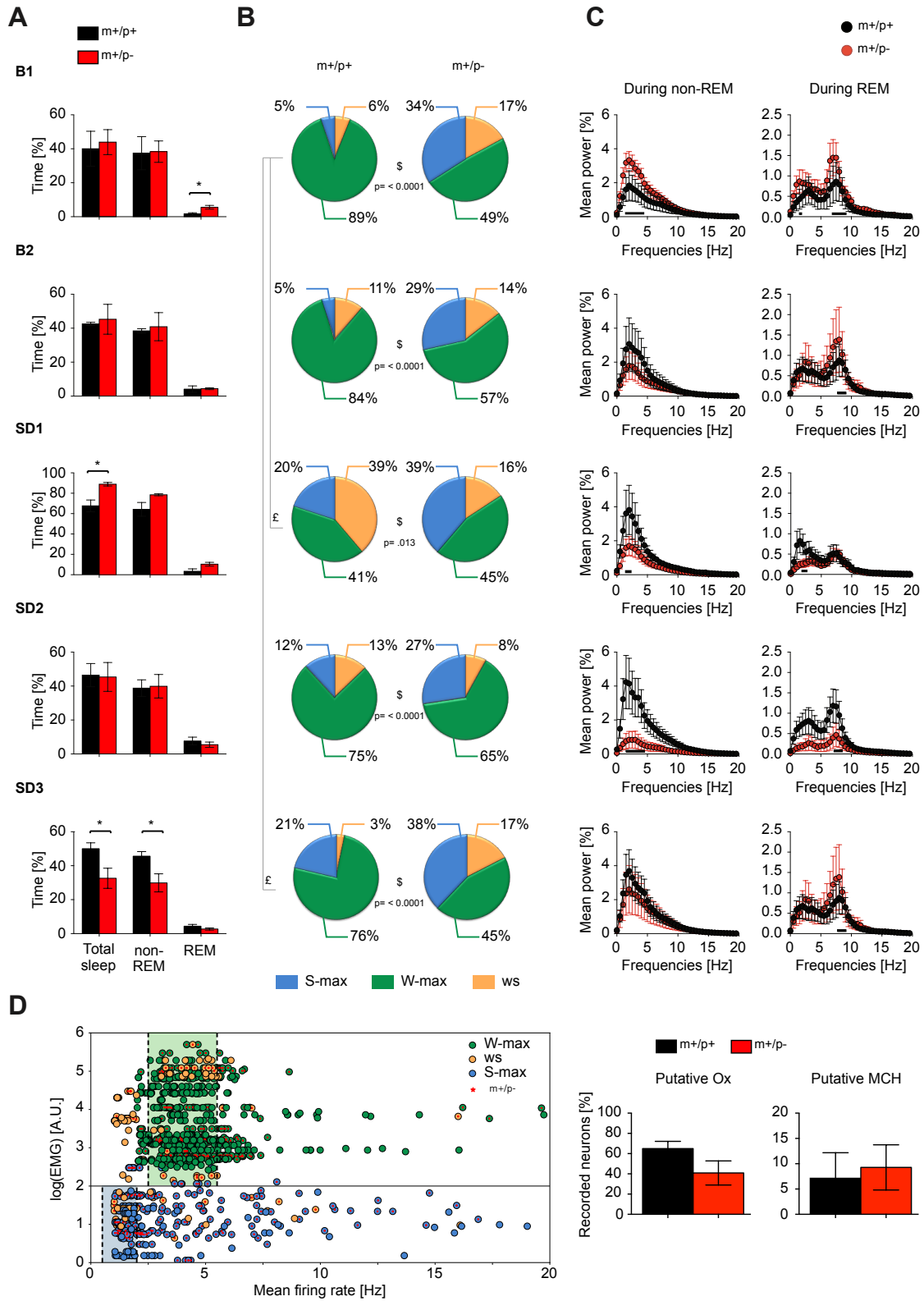


B



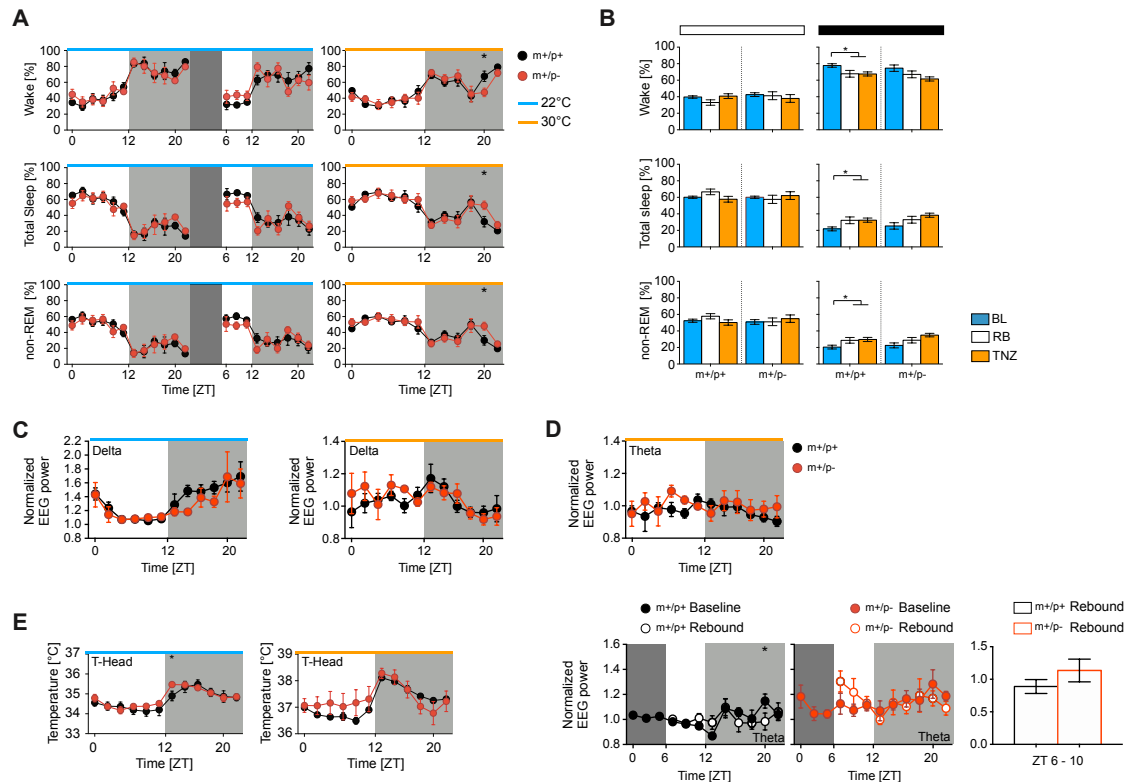
Supplementary 1 **A)** Whit blue bar are reported the frequency distribution of the duration of the interval from the end to one REM sleep episodes to the beginning of the subsequent episodes (REM sleep interval, RSI) during light dark cycle in mice. The grey line is the kernel density estimation constructed with the distribution of the REM sleep episodes. The green line is the smoothing of the grey line using the Savitzky-Golay Filter.

B) Experimental design of Study III



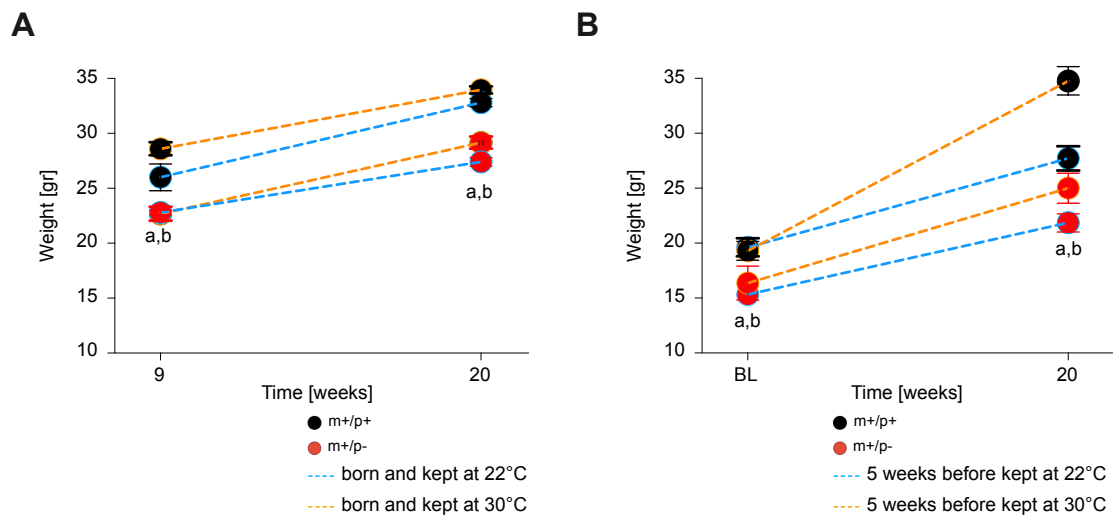
Supplementary 2, *PWScr^{m+/p-}* mice have altered neuronal dynamics of the LH in relation to sleep and food. The results of single unit activity (SUA) combined with EEM/EMG recordings. **A**) The percentage of total time spent in sleep stages (NREM plus REM sleep), NREM sleep and REM sleep, in *PWScr^{m+/p-}* mice (red bar)

compared with control mice (black bar). EEG/EMG/SUA were recorded at different time points and are shown in each row: B1 and B2, baseline; SD1, 1-h immediately after 6 h of SD; and SD2 and SD3, two time points during the 18-h recovery period. At B1, REM sleep was increased in $PWScr^{m+/p-}$ mice (unpaired t-test: $t(6) = 3.06$, $p = .02$) relative to $PWScr^{m+/p+}$ mice. At B2, no differences between the two genotypes were observed in any of the sleep stages investigated. At SD1, total sleep was increased in $PWScr^{m+/p-}$ mice (unpaired t-test: $t(6) = 3.53$, $p = .01$) relative to controls. At SD2, no differences between the two genotypes were observed in any of the sleep stages investigated. At SD3, total sleep (unpaired t-test: $t(6) = 2.52$, $p = .04$) and NREM sleep (unpaired t-test: $t(6) = 2.64$, $p = .03$) were decreased in $PWScr^{m+/p-}$ mice relative to $PWScr^{m+/p+}$ mice. Data are presented as the mean \pm SEM. Asterisks (*) indicate a significant difference between genotypes: * $P \leq .05$. **B)** The panel shows the neuronal distribution of recorded neurons (according to the classification described in the Methods session) in a pie chart for each time point. The percentage is derived from the total number of recorded neurons. W-max neurons are shown in green, S-max neurons are shown in blue, and ws neurons are shown in yellow. Differences between the two genotypes are indicated by \$, while differences within groups across time points are indicated by §. Significance was computed with the chi-square test. **C)** The normalized power density of the whole spectrum during NREM and REM sleep (left and right, respectively) for both genotypes; red circles depict $PWScr^{m+/p-}$ mice, and black circles depict $PWScr^{m+/p+}$ mice. **D)** Neuronal classification in a 2D scatter plot. The x-axis plots the mean firing rate of each cell in the state in which they maximally fire, and the y-axis plots the mean logarithm of EMG signals according to the selected sleep-wake state. W-max neurons are shown in green, S-max neurons in blue, and ws neurons in yellow. Neurons recorded from mutant mice are marked by red dots. Putative OX neurons (green squares) and MCH putative neurons (blue squares) are also shown (see Methods). The two genotypes investigated were $PWScr^{m+/p-}$ mice ($n=4$) and $PWScr^{m+/p+}$ mice ($n= 4$).

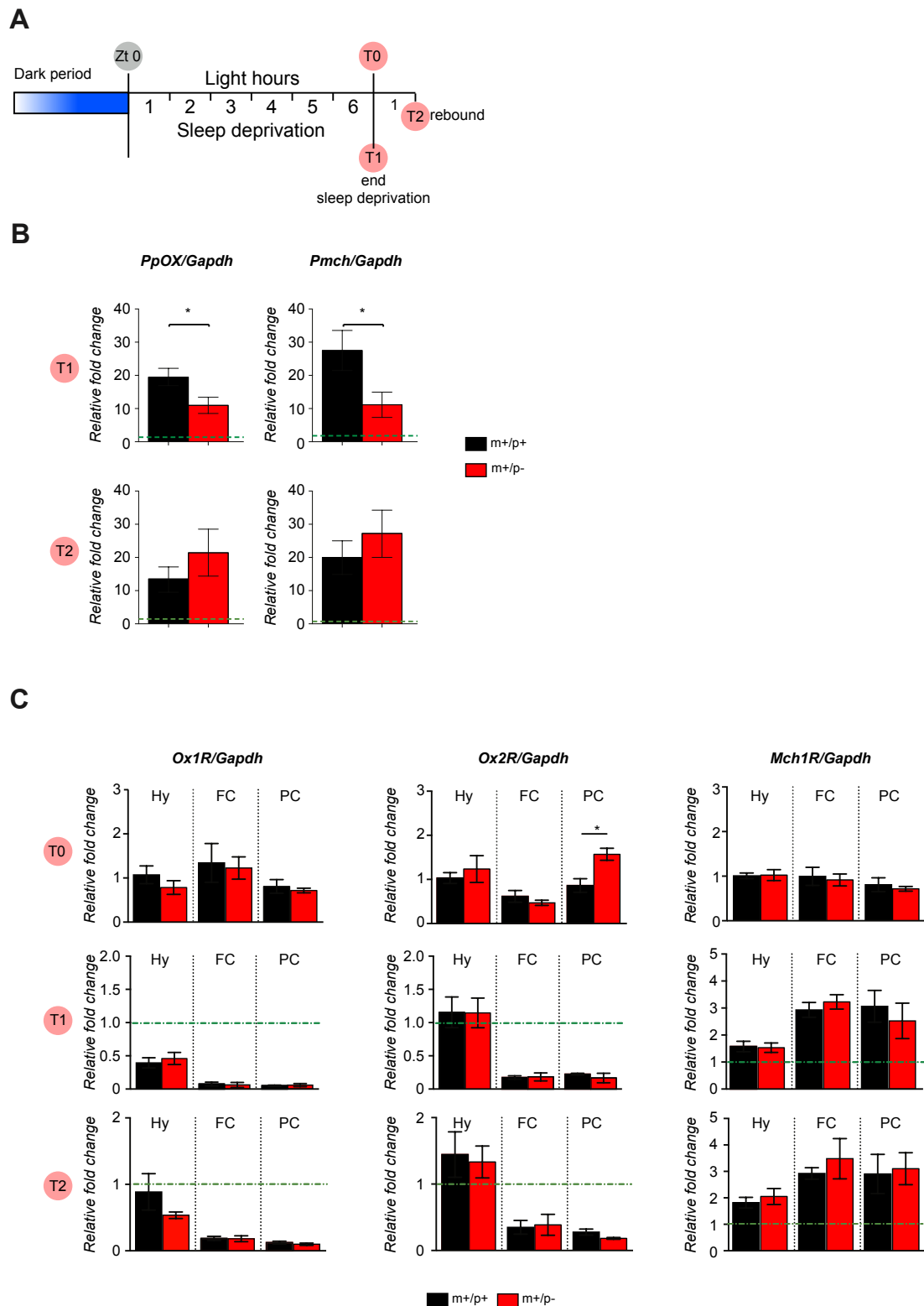


Supplementary 3, Sleep-wake cycle and temperature profile recorded. **A)** The panel shows the hourly percentage of time spent in wakefulness, total sleep (including both NREM sleep and REM sleep), NREM sleep, and REM sleep in $PWScr^{m+/p-}$ mice (red) versus control mice (black), recorded over an uninterrupted 24-h period of the 12-h light/dark cycle for baseline (BL) and during the 18-h after SD. Recordings were conducted in animals maintained at 22°C (cyan bar in each graph) and at 30°C (orange bar in each graph). No significant differences were found at 22°C between genotypes among all sleep stages investigated. At 30°C, a two-way repeated-measures ANOVA revealed significant main effects of time for wakefulness ($F(11,88) = 13.70, p < .0001$ "time"), for total sleep ($F(11,88) = 13.51, p < .0001$ "time") and for NREM sleep ($F(11,88) = 12.50, p < .0001$ "time"). Data are presented as the 2-h mean values \pm SEM. **B)** Cumulative amount of time spent in wakefulness, total sleep and NREM sleep for $PWScr^{m+/p-}$ and $PWScr^{m+/p+}$ mice over the 12-h light period and the 12-h dark period. Cyan bar indicates the baseline (BL) value, the white bar indicates the 18-h recovery (RB) period following 6 h of SD, and the orange bar indicates recordings at 30°C. Statistical analysis was performed by one-way ANOVA followed by post hoc analysis with the Bonferroni multiple comparison test. Dark period: $PWScr^{m+/p+}$ mice showed a difference in the percentage of wakefulness ($F(1.79, 7.19) = 6.85, p = .02$), total sleep ($F(1.80, 7.20) = 7.35, p = .01$) and NREM sleep ($F(1.86, 7.46) = 5.40, p = .03$). Data are presented as the mean \pm SEM. Asterisks (*) indicate a significant difference between genotypes: * $P \leq .05$. **C-D)** Spectral analysis. Normalized delta and theta power during NREM sleep (C-upper) and REM sleep (D-upper) at 22°C (cyan bar above the graph) and at 30°C (orange bar above the graph) and after SD and relative to baseline for $PWScr^{m+/p-}$ mice (D-button) were recorded between genotypes. No substantial differences were observed between genotypes and conditions investigated. Data are presented as the means of 2-h bins \pm SEM. Asterisks (*) indicate a significant difference between

genotypes: * $P \leq .05$; ** $p \leq .01$; *** $p \leq .001$; **** $p \leq .0001$. The bottom right shows the normalised theta power recorded from ZT 6 to ZT 10, and no differences were observed between genotypes. Two genotypes were investigated: $PWScr^{m+/p-}$ mice ($n=10$, 5 mice at 22°C and 5 mice at 30°C) and $PWScr^{m+/p+}$ mice ($n=10$, 5 mice at 22°C and 5 mice at 30°C). **E**) Head temperature (Head-T) profiles for $PWScr^{m+/p+}$ and $PWScr^{m+/p-}$ mice were recorded with an infrared thermocamera over 24 h. Recordings were performed under two different environmental conditions: at 22°C (cyan bar over the graph, shown on the left) and at 30°C, representing the thermoneutrality zone (TNZ) (orange bar over the graph, shown on the right). T-head was slightly increased in $PWScr^{m+/p-}$ mice relative to control mice during the dark period at ZT 14 at 22°C. Asterisks (*) indicate a significant difference between genotypes: * $P \leq .05$.

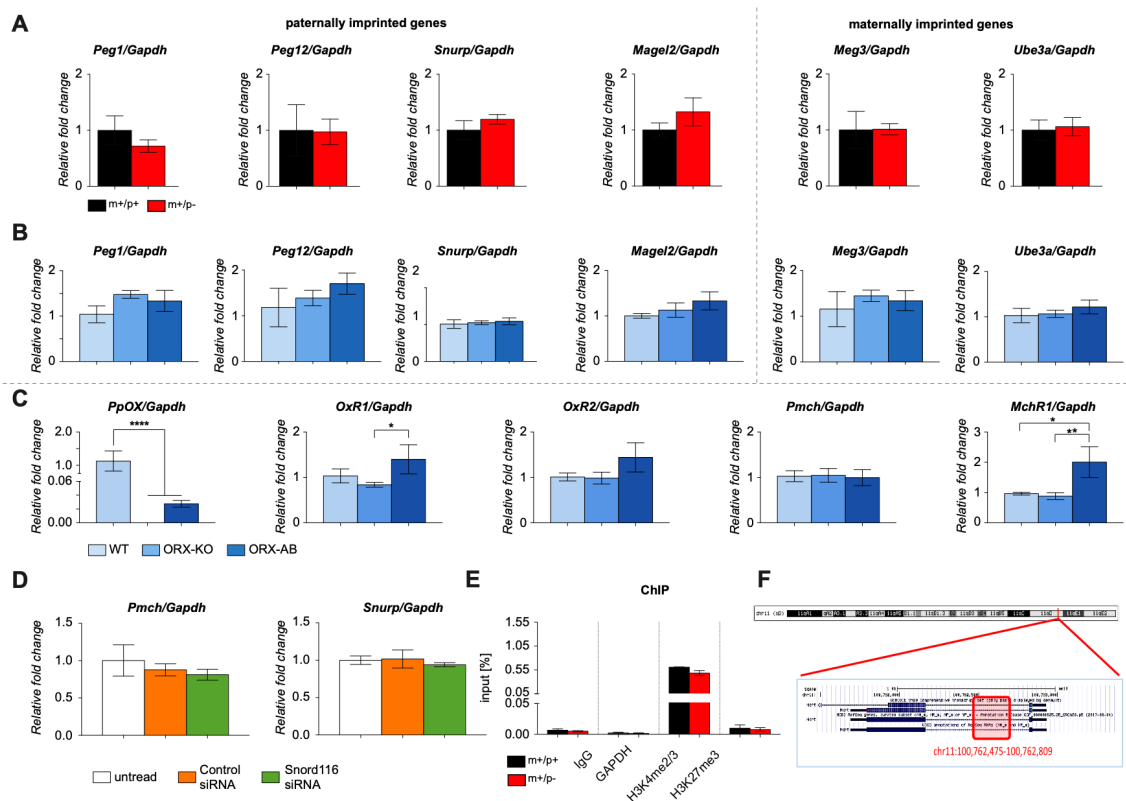


Supplementary 4, Snord116 loss induces growth retardation. Body weight was assessed at 22°C and 30°C (TNZ). **A**) The absolute weekly body weights of mice born at 22°C (cyan connection) and mice born at 30°C (orange connection) were assessed. $PWScr^{m+/p-}$ mice are indicated by red circles, while $PWScr^{m+/p+}$ mice are represented by black circles. Two-way ANOVA revealed that $PWScr^{m+/p-}$ mice had significant growth retardation compared with control mice when raised at either 22°C or 30°C ($F(3, 32)=179.5$, $p < .0001$ “time”; $F(3, 32)=45.07$, $p < .0001$ “genotypes”). a indicates differences between genotypes at 22°C, while b indicates differences between genotypes at 30°C. Two genotypes were investigated: $PWScr^{m+/p-}$ mice ($n=10$, 5 mice at 22°C and 5 mice at 30°C) and $PWScr^{m+/p+}$ mice ($n=10$, 5 mice at 22°C and 5 mice at 30°C). **B**) At 15 to 20 weeks of age (at the time point when the sleep-wake cycle was recorded), the absolute weekly body weight was assessed in mice after housing for 5 weeks either at 22°C or 30°C. Two-way ANOVA revealed that $PWScr^{m+/p-}$ mice had significant growth retardation compared with control mice housed at either 22°C or 30°C ($F(3, 32)=10.58$, $p < .0001$ “interaction”). a indicates differences between genotypes at 22°C, while b indicates differences between genotypes at 30°C. Two genotypes were investigated: $PWScr^{m+/p-}$ mice ($n=10$, 5 mice at 22°C and 5 mice at 30°C) and $PWScr^{m+/p+}$ mice ($n=10$, 5 mice at 22°C and 5 mice at 30°C).



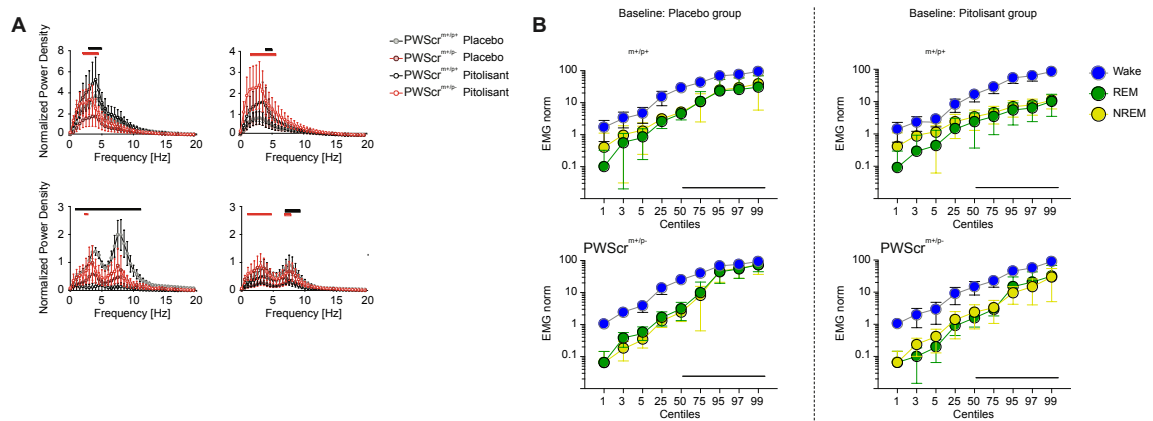
Supplementary 5, **Gene expression analysis of the OX and MCH systems.** **A)** Experimental timeline. *PWScr^{m+/p-}* and *PWScr^{m+/p+}* mice were sacrificed at three different time points to assess the gene expression of prepro-OX (*Ppox*) and the precursor of MCH (*Pmch*). Mice were sacrificed at Zeitgeber 6 (ZT 6; T0), after

6-h of SD at ZT 6 (T1), and after 6-h of SD (ZT 7; T2). **B)** At T1, PWScr^{m+/p-} mice showed reduced Ppox (unpaired t-test: $t(8) = 3.14$, $p = .01$) and Pmch (unpaired t-test: $t(8) = 2.66$, $p = .02$) compared with PWScr^{m+/p+} mice. At T2, no differences were observed between the two genotypes for both genes. **C)** Gene expression analysis of the OX receptor 1 (Ox1R), the OX receptor 2 (Ox2R) and the MCH receptor 1 (Mch1R) in the hypothalamus (Hy), the frontal cortex (FC) and the parietal cortex (PC). The green lines in T1 and T2 represent the baseline value (T0). Only Ox2R in the PC was found to be increased in PWScr^{m+/p-} mice (unpaired t-test: $t(8) = 3.44$, $p = .008$). Gene expression (mean \pm SEM) was assessed by qRT-PCR in mice of the 2 genotypes: PWScr^{m+/p-} mice ($n = 15$, 5 mice for each time point) and PWScr^{m+/p+} mice ($n = 15$, 5 mice for each time point). Gapdh was used as a reference gene.



Supplementary 6, Gene expression analysis of the maternally and paternally imprinted genes in PWScr^{m+/p-} mice and in mice of two narcoleptic models. **A)** Gene expression analysis of Peg1, Peg12, Snurp, Magel2, Meg3 and Ube3a in PWScr^{m+/p-} mice relative to control mice. Unpaired t tests did not reveal any significant changes between the two genotypes. **B)** Gene expression of Peg1, Peg12, Snurp, Magel2, Meg3 and Ube3a in WT, KO and Atx mice. One-way ANOVA did not reveal any significant changes between genotypes. **C)** Gene expression analysis of Ppox, OxR1, OxR2, Pmch and MchR1 in WT, KO and Atx mice. We confirmed a significant reduction in Ppox in both strains of narcoleptic mice relative to WT mice (one-way ANOVA: $F(3,16) = 11.63$, Bonferroni post hoc test $p < .0001$). OxR1 (one-way ANOVA: $F(3,16) = 7.034$, Bonferroni post hoc test $p < .03$) and MchR1 (one-way ANOVA: $F(2,15) = 5.17$, Bonferroni post hoc test $p < .01$) were reduced only in Atx mice relative to WT and KO mice. Gene expression (mean \pm SEM) was assessed by qRT-

PCR in mice of the 2 genotypes: $PWScr^{m+/p-}$ mice ($n=5$) and $PWScr^{m+/p+}$ mice ($n=5$). KO ($n=12$) and Atx ($n=4$) narcoleptic mice were investigated and compared with WT mice ($n=4$). *Gapdh* was used as a reference gene. **D)** Gene expression analysis of *Pmch* and *Snurp* in the *Snord116*-siRNA-treated immortalised hypothalamic rat cell line (green bars). Both genes were unchanged compared with untreated cells or scrambled siRNA-treated cells (white and orange bars). **E)** ChIP analysis of PEG3 binding on the *Gapdh* promoter region in $PWScr^{m+/p-}$ mice (red) versus controls (black). Values are expressed as the mean of the input \pm standard deviation. **F)** A cartoon showing the details and coordinates of the genomic region assessed in the ChIP analysis of PEG3 binding to the *Ppox* promoter region.



Supplementary 7, **A)** The normalized power density of the whole spectrum during non-REM and REM sleep (top and bottom, respectively) for both genotypes in two conditions (vehicle on the left column, Pitolisant on the right column); red lines depict $PWScr^{m+/p-}$ mice, and black lines depict $PWScr^{m+/p+}$ mice; white dots are for the Pitolisant treatment while grey are for the vehicle. **B)** Comparative physiology of muscle activity during sleep. The panels show the distributions of normalized electromyographic activity (EMG_{NORM}) of neck muscles for $PWScr^{m+/p+}$ (top) and $PWScr^{m+/p-}$ (bottom) for both conditions, left panel vehicle, right panel mice treated with Pitolisant

Tables

Supplementary Table 1: Imprinted gene
See attached excel file 1

Supplementary Table 4: RNA sequencing
See attached excel file 2

Supplementary Tables 2:

Phase:	B1		B2		SD		SD1		SD2	
Genotype:	m+/p+	m+/p-	m+/p+	m+/p-	m+/p+	m+/p-	m+/p+	m+/p-	m+/p+	m+/p-
W-max	90	60	104	43	48	55	77	73	96	54
Wake										
NR - max	2	21	1	19	6	27	6	17	24	23
R - max	2	4	2	4	2	17	5	5	2	11
NRR - max	1	5	3	7	15	3	1	9	1	12
Sleep										
wsp	9	11	1	9	14	11	13	5	4	16
WR - max	3	4	6	6	31	8	0	4	0	5
None										
Total	107	105	117	88	116	121	102	113	127	121

Genotype:	m+/p+	m+/p-
W-max	415	285
Wake		
NR - max	39	107
R - max	13	41
NRR - max	21	36
Sleep		
wsp	41	52
WR - max	40	27
None		
Total	569	548

Phase	m+/p+	m+/p-	Totals	p-value
B1	90	60	150	<.0001
W-max	90	60	150	
Others	17	45	62	
Totals	107	105	212	
B2	104	43	147	<.0001
W-max	104	43	147	
Others	13	45	58	
Totals	117	88	205	
SD	48	55	103	ns
W-max	48	55	103	
Others	68	66	134	
Totals	116	121	237	
SD1	77	73	150	ns
W-max	77	73	150	
Others	25	40	65	
Totals	102	113	215	
SD2	96	54	150	<.0001
W-max	96	54	150	
Others	31	67	98	
Totals	127	121	248	

Phase	m+/p+	m+/p-	Totals	p-value
S-max	5	30	35	<.0001
W-max	5	30	35	
Others	102	75	177	
Totals	107	105	212	
S-max	6	30	36	<.0001
W-max	6	30	36	
Others	111	58	169	
Totals	117	88	205	
S-max	23	47	70	.0017
W-max	23	47	70	
Others	93	74	167	
Totals	116	121	237	
S-max	12	31	43	.059
W-max	12	31	43	
Others	90	82	172	
Totals	102	113	215	
S-max	27	46	73	.052
W-max	27	46	73	
Others	100	75	175	
Totals	127	121	248	

Phase	m+/p+	m+/p-	Totals	p-value
ws	12	15	27	ns
W-max	12	15	27	
Others	95	90	185	
Totals	107	105	212	
ws	7	15	22	.02
W-max	7	15	22	
Others	110	73	183	
Totals	117	88	205	
ws	45	19	64	<.0001
W-max	45	19	64	
Others	71	102	173	
Totals	116	121	237	
ws	13	9	22	ns
W-max	13	9	22	
Others	89	104	193	
Totals	102	113	215	
ws	4	21	25	.0002
W-max	4	21	25	
Others	123	100	223	
Totals	127	121	248	

Phase	m+/p+	m+/p-	Totals	p-value
ws	12	7	19	ns
W-max	12	7	19	
Others	90	104	194	
Totals	107	117	224	
ws	12	45	57	<.0001
W-max	12	45	57	
Others	90	48	138	
Totals	107	116	223	
ws	12	13	25	ns
W-max	12	13	25	
Others	90	77	167	
Totals	107	102	209	
ws	12	4	16	.0001
W-max	12	4	16	
Others	90	96	186	
Totals	107	127	234	

Phase	m+/p+	m+/p-	Totals	p-value
ws	15	15	30	ns
W-max	15	15	30	
Others	60	43	103	
Totals	105	88	193	
ws	15	19	34	ns
W-max	15	19	34	
Others	60	55	115	
Totals	105	121	226	
ws	15	9	24	ns
W-max	15	9	24	
Others	60	74	134	
Totals	105	114	219	
ws	15	21	36	ns
W-max	15	21	36	
Others	60	54	114	
Totals	105	121	226	

Phase	m+/p+	m+/p-	Totals	p-value
Type I	28	16	44	ns
Others	119	58	177	
Totals	147	74	221	
Type II	105	22	127	<.0001
Others	42	52	94	
Totals	147	74	221	
Type III	14	36	50	<.0001
Others	133	38	171	
Totals	147	74	221	

Supplementary Tables 3:

OREXIN SYSTEM

GENE	FORWARD	REVERSE
PPHCRT	5'- CAGGCACCATGAACTTTCCTTCTA	5'- CAGCAGCAGCGTCACG
OREXIN R1	5'- CGCCAACCCTATCATCTACAA	5'- GCTCTGCAAGGACAAGGACTT
OREXIN R2	5'- GCTCACCAGCATAAGCACACT	5'- TGGACAGGAGTGAAGATGGTACT

MCH SYSTEM

GENE	FORWARD	REVERSE
PMCH	5'- ATCAAAGAACACAGGCTCCAAAC	5'- CGGATCCTTTCAGAGCAAGGTA
MCH R1	5'- GCCACCTCCTCGCACAA	5'- CTTACCACGGCAAAAATGAC

MATERNAL IMPRINTED GENES

GENE	FORWARD	REVERSE
UBE3A	5'- GCGAGCAGCTGCAAAGCATCTAAT	5'- AGCTTGCTCCTTCTTGGAGGGAT
MEG3	5'- CACAGAAGACGAAGAGCTGGA	5'- GGTAGAGGTGCACAGCAGGT

PATERNAL IMPRINTED GENES

GENE	FORWARD	REVERSE
PEG1	5'- CCATATTTGAGCAGGCCAGC	5'- TCCATTCGAACAGACAGAGACT
PEG3	5'- GACTCGTCCTCACGATCCC	5'- AGTCCAGCTTGCCGAAGAT
PEG12	5'- GGCACAGCTCAGAACTAGGG	5'- AAGTCCTGGGTGAATCCCTT
MAGEL2	5'- AGATTTTTGGCCGCACTCTA	5'- GGCATTTGCGTCCTTGTATT
SNRPN/SNURF	5'- CTGCTCTTCCAACCCAGG	5'- ATGCAAAACAGCCAGAACGT

HOUSEKEEPING GENE

GENE	FORWARD	REVERSE
GAPDH	5'- GAACATCATCCCTGCATCCA	5'- CCAGTGAGCTTCCCGTTCA

CHIP Primers

GENE	FORWARD	REVERSE
PPHCRT	5' – TCCTTTGCTGGGGAAACTGT – 3'	5' – AGAGAGGAGTATGGGTGGGT – 3'
SNRPN	5' – TAACACACCCAAGGAGTCCG – 3'	5' – GACTAGCGCAGAGAGAGGAGAG – 3'
GAPDH	5' – CCCAGCCAAGTTTGAAAGGG – 3'	5' – GCATCTCCCTCACACACCTCTT – 3'

RATS primers

GENE	FORWARD	REVERSE
PPHCRT	5' – AACCTTCTTCTACAAAGGTTCC – 3'	5' – CAGTCCGTGCAACAGTTC – 3'
PMCH	5' – CACAAAGAACACAGGCTCCA – 3'	5' – TTCCCTTTTTCTGTGTGG – 3'
Peg3	5' – GGGGAGTGCTACCTTCTTGA – 3'	5' – CTGTTTTGCTCACACCCAAG – 3'
Snord116	5' – TGCTTGGATCGATGATGATTT – 3'	5' – CTGGACCTCAGTCACGATGAT – 3'
Snrpn/Snurf	5' – CAGCAATCATGACTGTGGGTA – 3'	5' – TCTTTGGCTTGATCTTCTGA – 3'
Gapdh	5' – GAACATCATCCCTGCATCCA – 3'	5' – CCAGTGAGCTTCCCGTTCA – 3'